Design and Simulation of Camless Engine Electro-Mechanical Valve Actuation System for Four Stroke Single Cylinder Engine

YITAYEW LINGEREW MANIE

A Thesis Submitted to the Department of Mechanical Engineering
School Of Mechanical, Chemical and Materials Engineering

Presented in Partial Fulfillment of the Requirement for the Degree of Master's in Automotive Engineering

Office of Graduate Studies
Adama Science and Technology University

June, 2024

Adama, Ethiopia

Design and Simulation of Camless Engine Electro-Mechanical Valve Actuation System for Four Stroke Single Cylinder Engine

Yitayew Lingerew Manie

Advisor: Alemayehu Wakjira Huluka (PhD).

A Thesis Submitted to Department of Mechanical Engineering

School Of Mechanical, Chemical and Materials Engineering

Presented in Partial Fulfillment of the Requirement for the Degree of Master's in Automotive Engineering

Office of Graduate Studies

Adama Science and Technology University

June, 2024

Adama, Ethiopia

DECLARATION

I hereby declare that this Master Thesis entitled **"Design and Simulation of Camless Engine Electromechanical Valve Actuation System for Four Stroke Single Cylinder Engine"** is my original work and that has not been submitted to any other university for similar purpose. The references used in this thesis are duly recognized by proper citation.

<u>Yitayew Lingerew</u>	____________________________	_________________
Name of the Student	Signature	Date

RECOMMENDATION

I, the advisor of this thesis, hereby certify that I have closely advised the student while developing this thesis and read the revised version of the thesis entitled **"Design and Simulation of Camless Engine Electromechanical Valve Actuation System for Four Stroke Single Cylinder Engine"** prepared under my guidance by **Yitayew Lingerew Manie**. Therefore, I recommend the submission of a revised version of the thesis to the department following the applicable procedures.

Alemayehu Wakjira Huluka (PhD)

Major Advisor	Signature	Date

APPROVAL PAGE OF MSc. THESIS

I, the advisor of the thesis entitled **"Design and Simulation of Camless Engine Electromechanical Valve Actuation System for Four Stroke Single Cylinder Engine"** and developed by **Yitayew Lingerew**; hereby certify that the recommendation and suggestions made by the board of examiners are appropriately incorporated into the final version of the thesis.

Alemayehu Wakjira Huluka (PhD)

____________________________	____________________	__________________
Major Advisor/Supervisor	Signature	Date

We, the undersigned, members of the Board of Examiners of the thesis by **Yitayew Lingerew Manie** have read and evaluate the thesis entitled **"Design and Simulation of Camless Engine Electromechanical Valve Actuation System for Four Stroke Single Cylinder Engine"** and examine the candidate during the open defense. This is, therefore, to certify that the thesis accepted for partial fulfillment of the requirement of the degree of Master of Science in Automotive Engineering.

_____________________	____________________	_______________________
Chairperson	Signature	Date
_____________________	_____________________	_______________________
Internal Examiner	Signature	Date
_____________________	_____________________	_______________________
External Examiner	Signature	Date

Finally, approval and acceptance of the thesis are contingent upon the submission of its final copy to the Office of Postgraduate Studies (OPGS) through the Department of Graduate Council (DGC) and School Graduate Committee (SGC).

____________________________	______________________	______________________
Department Head	Signature	Date
_____________________________	______________________	______________________
School Dean	Signature	Date
_____________________________	______________________	_____________________
Office of Postgraduate Studies, Dean	Signature	Date

ACKNOWLEDGMENT

My first and greatest thanks are to almighty God and my wife, for letting me through all difficulties and helped me to complete this thesis. Next, I would like to acknowledge and express my deepest gratitude to my advisor **Alemayehu Wakjira Huluka (PhD)** for his guidance on this thesis work. I am also grateful to the Adama Science and Technology University and Mechanical Engineering Department for providing the resources and opportunities that made this thesis possible. Last but not least, I am grateful for all of the people who have helped to make my thesis a success by providing inspiration, support, and guidance.

TABLE OF CONTENTS

LIST OF TABLES

TABLE PAGE

LIST OF FIGURES

FIGURE PAGE

ACRONYMS

BDC	Bottom Dead Center
BMD	Bending Moment Diagram
CEMF	Counter Electromotive Force
CG	Cash Guarantee
CI	Compression Ignition
CLE	Camless Engine
DC	Direct Current
ECU	Electronic Control Unit
ECV	Electrohydraulic Camless Valve train
ECVAS	Electronically Control Valve Actuation System
EMCV	Electromechanical Camless Valve
EMF	Electromotive Force
EMVA	Electromagnetic Valve Actuators
EMVAs	Electromechanical Valve Actuations
EMVT	Electromechanical Valve Train
EH-CEVA	Electro-Hydraulic Camless Engine Valve Actuator
EVO/C	Exhaust Valve Open/Closed
GEV	Gas Exchange Valve
ICE	Internal Combustion Engine
ILC	Iterative Learning Controller
I/O	Input/ Output
IVO/C	Intake Valve Open/Closed
MOV	Metal Oxide Varistor
PWM	Pulse Width Modules
RPM	Revolution Per Minute
SAE	Society of Automotive Engineer
SI	Spark Ignition
SWG	Standard Wire Gauge
TDC	Top Dead Center
VCT	Variable Camshaft Timing
VTEC	Variable Timing Electronics Control
VVA	Variable Valve Actuation
VVT	Variable Valve Timing

LIST OF CONVERSION FACTORS

1Mpa =1N/mm^2

1m =100cm =1000mm

1bar = 105 Pa = 100 kPa

1ns = 10^{-9} sec

1cc = 1cm^3 = 10^{-6} m^3

1kw =1000 watt

1rev = 2 rad = 360

k=0^0 C+273

g/cm^3 = 1000kg/m^3

LIST OF SYMBOLS

Notation	*Description*	*Unit*
a	Area of the piston	mm^2
α	Minimum speed	rpm
a_p	Area of valve port	mm^2
α_v	Valve face angle	degree
a_w	Area of the wire section	mm^2
B	Magnetic flux density	Tesla
C	Spring index	----
D	Diameter of bore	mm
d_c	Core diameter of the stud	mm
d_p	Pitch circle diameter of the studs	mm
d_p	Valve Port Diameter	mm
d_v	Diameter of the valve head	mm
d_w	Wire diameter	mm
d_0	Valve Stem Diameter	mm
d_2	Valve Head Diameter	mm
E_c	Engine capacity	cc
e m f	electromotive force	volt
F	Force	N
F_{gv}	Gas load on the valve	N
F_s	Initial spring force	N
G	Gravity	m/s^2
G	Modulus of rigidity	Pa
G	Least distance between the solenoid and the armature	mm
H	Valve lift	mm
h_{max}	Maximum Valve Lift	mm
I	Moment of inertia	mm^3
I	Current	A
K	Stress factor	----
L	Inductance of the coil	H
l_c	Length of the winding coil	mm
L_f	Free length of the spring	mm
l_w	Length of the wire in the coil	mm
M	Mass	kg
Mmf	Magneto motive force	AT
M_{bmax}	Maximum bending moment	Nm
N	Engine speed	RPM
N	Number of turns of coil	-----
N	Number of active turns of the coil	----

n_s	Number of studs	mm
P	Power	watt
P_c	Greatest back pressure	Pa
P_s	Greatest suction pressure	Pa
Q	Heat flux	W/m^2
R	Resistance of wire in the coil	Ω
Ro	Conductor resistance at reference temperature	Ω
r_c	Compression ratio	------
S	Stroke	mm
s_c	Compressive strain	mm
T	Time	sec
T	Valve margin thickness	mm
t_d	Thickness of the valve disc	mm
t_{evo}	Total time taken to exhaust valve stays open	sec
t_h	Thickness of cylinder head	mm
t_w	Thickness of the cylinder wall	mm
V	Voltage	v
v_{mp}	Mean piston velocity	m/s
v_p	Velocity of gas through the port	m/s
W	Weight of the valve	N
W	Valve face width	mm
W	Work done	Nm
X	Required degree of valve opening /closing/	degree
Δx	Change in length of the spring	mm
Y	Given degree of valve opening/closing/	degree
Z	Section modulus	mm^3
σ_b	Permissible bending stress	N/mm^2
σ_{bmax}	Maximum bending stress	Pa
σ_c	Allowable circumferential stress	Mpa
δ_{max}	Maximum compression of spring	mm
σ_t	Tensile stress	MPa
τ	Shear stress	Pa
Θ_A	Opening angle after	degree
Θ_B	Opening angle before	degree
Θ_{dvo}	Total duration of valve opening	degree
ρ_w	Resistivity of the wire material	Ω-m
μ	Permeability of free space	-----
Φ	Magnetic flux	weber

ABSTRACT

This thesis presents the design, modeling, and control of new mechatronic valve actuators for the "breathing channels" in automotive engines, specifically focusing on the control of the mechanical valves that regulate the intake and exhaust of gases in internal combustion engines (ICE). Research has demonstrated that implementing variable valve actuation can result in notable improvements to engine efficiency and emissions. The current engine technology relies on mechanically driven camshafts, which lack flexibility and real-time modification capabilities. To overcome this limitation, the thesis proposes integrating individually controlled valves into the ICE, leading to the development of camless engine technology. Electromechanical valve actuators (EMVAs) have been considered one of the most promising technological solutions to develop this novel engine technology. The aim of this thesis research is to experience engineering design science by taking an idea from a concept and then modeling it using software. Existing literature reveals that conventional camless engine valve actuation systems involve complex designs and numerous components, which can increase manufacturing costs and pose challenges for mass production. Successfully addressing these gaps will result in the advancement of camless engine valve actuation systems. In this thesis work, an attempt has been made to integrate the concepts of mechanics, mechatronics, and electronics for designing an economical, low-emission, high-performance single-cylinder Cam-less engine. The concept is that by using sensors, an electric signal will be sent to the ECU. The ECU analyzes the signal and determines what to do on the actuator depending on the pre-sated programming, and then it automatically directs the actuator what to do on the valve. The methodology that is used in this thesis work is analytical analysis as well as a model and simulation of a work using ANSYS workbench/space claim and solid works 2022 for modeling mechanical system components and ANSYS workbench for simulation, MATLAB/Simulink for actuator model, and PROTEUS SUIT DESIGN 8.6 with Arduino IDE for simulating electrical systems functionality testing. The study reveals that the total weight of the analyzed system is 2.729 kilograms, compared to the 3.4 kilograms of the conventional valve actuation components of the selected model. These results in a 20% weight reduction, mainly due to the reduction of valve train components and camshaft itself. This results in improved engine efficiency and reduced fuel consumption. Also as seen from cost analysis the design is cost effective which means the design system has less expensive as compared to conventional camshaft engine with current market Value. Additionally these research findings indicate that the system achieves a maximum valve lift of approximately 6mm, which is comparable to conventional valve lift mechanisms. Through the PROTUES simulation, it is observed that the valve timing can infinitely vary based on control programming, enabling the decoupling of valve lift, timing, and actuation speed from the crankshaft position. Thus based on design results system can be implemented with technical adjustments, offering weight reduction, improved engine efficiency, and reduced fuel consumption.

Keywords: - Cam less Engine, Electromagnetic Actuators (EMA), Valve train, Valve Actuation.

CHAPTER ONE

1. INTRODUCTION

1.1 Background and Justification

The ICE engine has undergone significant evolution since the invention of the automobile and the camshaft hasn't changed since its invention. The cam regulates the "breathing channels" of the internal combustion engines (IC engines). These are the valves that supply and drive exhaust out of the fuel-air mixture (in SI engines) or air (in CI engines) (Kesav, 2013). The cam also regulates the timing and actuation of the valves, which impacts the vehicle's overall performance (Shewale et al., 2017).

Internal combustion engines have conventionally employed a mechanically operated camshaft to activate both the intake and exhaust valves, look the figure 1.1 as shown below. The engine's valves interact with the camshaft's attached cam lobes as the camshaft rotates. This interaction can occur through a mechanical connection, however, the result remains the same-as the came rotates, it applies force on the valve, leading to its opening. When cam stops providing opening force, spring return closes the valve. Their lift's profiles cannot be changed to maximize engine performance under various operating circumstances because they are a direct result of the engine crank angle (came shape) (Shewale et al., 2017). Because of this, a compromise design is created that affects the maximum torque and power, achievable engine efficiency, and pollutant emissions (Shewale et al., 2017).

The engine will either be more fuel efficient or have powerful performance, but it is challenging to have both at the same time with current technology (Deokar, 2016). Furthermore, the high work required to spin the camshaft and the train of valves through the pulley, as well as the friction forces acting on mechanical parts, increases energy loses when mechanically driven camshafts are used (Velasco, 2011). Automobile manufacturers have been working to offer vehicles with variable camshaft timing, cylinder deactivation, or VVT since they realized this compromise (Giglio et al., 2001).

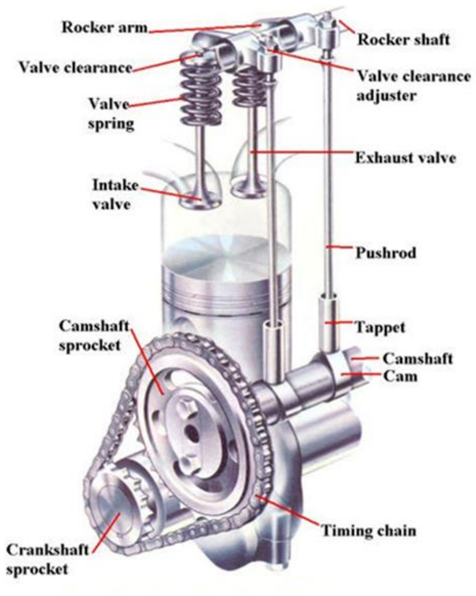

Figure 1.1: Components of conventional cam engines

The increasing demand for enhanced fuel efficiency and decreased exhaust emissions motivates the development of alternative valve operating techniques. To address these demands, some manufacturers have introduced mechanical devices with variable valve timing in order to partially or entirely overcome the constraints imposed by fixed valve timing. In essence, Honda variable timing electronics control (VTEC) engines shown below in the figure 1.2 are multiple cam lobe camshafts or multiple camshaft engines (Giglio et al., 2001).

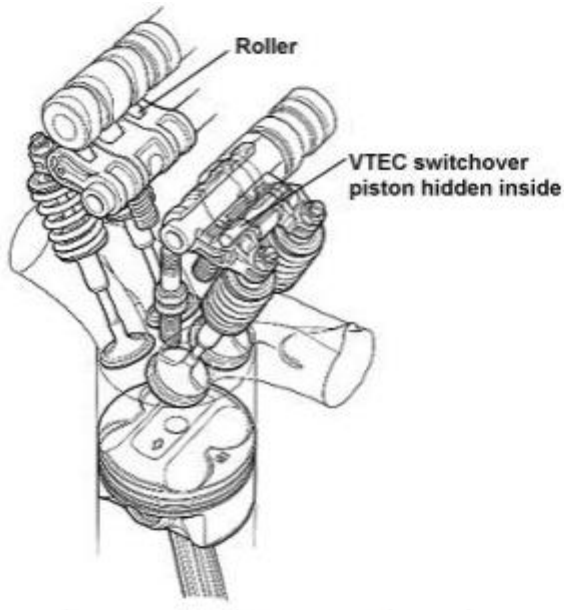

Figure 1.2: Honda variable timing electronic control (VTEC) schematic

From the figure 1.2 above the majority of these designs are mechanical in nature. While they do offer a higher degree of sophistication, the majority are still restricted to small range discrete valve timing adjustments (ANAN*, 2015). Regardless of the VVT technology differences among the above newly designed mechanical devices, the prime similarity of a camshaft remains. Therefore, limitations continue since timing is still a function of engine speed (Kesav, 2013).

On the other hand the new feature added on this research is, variable valve actuation (VVA) operations could be implemented using an active control approach, enabling real-time changes to all of the valve's distinguishing characteristics. Due to the decoupling of valve timing from piston motion and the decrease in energy losses brought on by the pumping action, they also help to improve fuel consumption, torque production, engine efficiency, and emissions reduction (Brader, 2001)**.**

In order to fully realize the capabilities of a system with fully variable valve timing (VVT), a great deal of research is currently being done on valve trains of camless engines. In these systems, the valve's movement is totally independent of the engine's speed or the pistons motion (Chukwuneke et al., 2013). Numerous manufacturers and academic institutions are involved in this research. This paper is concerned with an electromechanical valve actuator designed for engines without cams (Zibani et al., 2020).

1.2 Statement of the Problem

The intake and exhaust valves of IC engines are opened and closed by a mechanically driven camshaft in the current engine technology. As such, there is strong correlation between the crankshaft position and the profile of such valves. The cam provides reliable and accurate valve operation, but the degrees of freedom of the valve namely, valve timing, valve lift and event duration are inherently fixed to the cam profile. Because of this, the valve train is not a flexible device, and once the cam-follower mechanism is designed during engine development, it is not feasible to modify the valve features in real time to better optimize engine efficiency and lower pollution emissions across the whole speed range in accordance with the engine's operating conditions. And also, the conventional mechanical valve train has a greater weight (more engine size) since the valve train consists of many mechanical parts. Additionally, the crankshaft powers the camshaft via a timing belt, and this consumes much energy from the engine, especially when the cams are doubled, as most of the current double overhead camshaft engines do, which means increased fuel consumption and higher emissions. Replacing the valve train component and camshaft-controlled valves with electronic-controlled valves will definitely have many advantages, like reducing overall engine weight, improving engine efficiency just because of the simplified weight, and also due to the real-time valve actuation system and cylinder deactivation. And this, in turn, means improved emissions (Giglio et al., 2001) (Zibani et al., 2020).

1.3 Objectives of the Study

1.3.1 General Objective

The General objective of this thesis work is to design and simulation of a cam-less engine electromechanical valve actuation system for a four-stroke single-cylinder engine.

1.3.2 Specific Objectives

The specific objectives of this thesis work are as follows;

- To design and analysis of valve and valve springs
- To design an electromechanical actuation system
- To programme an electronic control system
- To simulate the system's functionality

1.4 Significance of the Study

The significance these studies are:

- **Enhanced fuel economy:** Reduction in wear and tear, friction and thermal losses in the camshaft mechanism are the only reason why there should be a 10-15% improvement in pumping loss and cylinder deactivation (Soares Machado et al., 2019).
- **Greater torque output:** The valve actuating mechanisms frictional losses are decreased. As such, it improves output power and mechanical efficiency. A camless valve train requires no operating torque, so power consumption is minimized. There should be a 20% increase in performance and a ramming effect at high engine speeds (Soares Machado et al., 2019) (Peterson & Stefanopoulou, 2004).
- **Lower emissions:** Correct combustion of the air-fuel mixture occurs when the valves operate in line with the engine‘s practical valve timing diagram. As a result, the gases burn through entirely. (Giglio et al., 2001) (Soares Machado et al., 2019).

- **Reduced weight of an engine:** since there is no cam shaft component or rocker arm, there is a weight reduction.
- **The small seating velocity of the valve** (less than 3 cm/s at 600 rpm engine speed and less than 30 cm/s at 6000 rpm engine speed): Enables the so-called soft landing of any system that activates variable valves should enable the valve to land softly to avoid excessive wear on engine valves (Peterson & Stefanopoulou, 2004)**.**

1.5 Scope of the Study

The scope of this research is to design and simulation of camless engine electromechanical valve actuation system for four stroke single cylinder engine. This research comprises; Designing system components for valve actuation, drawing of system components with assembly for a single cylinder, developing mathematical model for actuator simulation, Manual analysis and software simulation of mechanical and electrical system components.

1.6 Organization of the Thesis

This thesis work is organized into six chapters, including chapter one. Chapter one which covers introduction**,** background and justification, statement of the problem, objectives of the study, significance of the study and research scope are also explained in this chapter. Chapter two covers relevant literature on the design of electromechanical valve actuation systems is reviewed, and also reviews pervious work regarding the design of controller for valve actuation system. Chapter three covers theoretical framework, material selection and methods used in this research to obtain results. Chapter four covers design and analysis of system and mathematical modeling for electromechanical valve actuators, the Simulink model using MATLAB software are explained in this chapter. Chapter five includes comprehensive discussion for the result analysis which is obtained from computer simulation using ANSYS and MAT LAB/Simulink software. Finally chapter six covers conclusion and recommendation parts of the research.

CHAPTER TWO

2. LITERATURE REVIEW

2.1 Introduction

Initially, camless engines were developed for use as a design aid for automakers. The engineer had the opportunity to play around with valve timing in order to use a camless engine to create cam profiles. There were no dimensional or power consumption restrictions on these early units. Rather, they were created exclusively as a design tool in the laboratory (Shewale et al., 2017).

History reveals that the concept of a camless internal combustion engine dates back to 1899, when designs for variable valve timing first appeared, aside from laboratory use. A suggestion was made that more engine power could be obtained by independently controlling the actuation of the valves. However, in more recent times, the emphasis on more power has expanded to encompass reliability, energy efficiency, and pollution control (Brader, 2001)**.**

Researchers have been developing, testing, and prototyping new systems for internal combustion engine valve actuation over the past ten years in order to deliver the advantages mentioned above. They have created designs that range from electro-hydraulic to electro-pneumatic. Electric solenoids are the foundation of these designs; they are used to open and close hydraulic or pneumatic valves. Next, the engine valves are activated by the controlled fluid.

Gould et al. completed a thorough study in 1991 using solenoid control of pneumatic actuators. The project included testing typical Ford 1.9-liter engines with side-by-side four-cylinder engines with spark ignition, port fuel injection, and the same engine with camless actuation modified. It also involved the creation of actuators and a controllable 16-bit microprocessor. Researchers found that hydraulic systems reacted slowly, especially at cold temperatures. In order to reduce all flow path lengths and increase the actuator's response time, they employed electromagnetically operated valves to regulate the pressurized air. When compared to the 140 watts of power used by comparable production engines, this is extremely high. As Gould et al. note, the high power needs of the actuator prevent their work from being regarded as implementable. Researchers found that a camless engine produced 11% more torque at low engine speeds and lower emission gases, especially brake-specific emissions of nitrous oxide (Gould et al., 1991).

In 1996, Michael Schechter and Michael Levin at Ford's R&D Laboratory developed the next generation of camless engines. The multitude of parameters related to the uniformity and reliability of engine operation were assessed in detail by Ford. In addition to the basics, they introduce a new concept of hydrodynamic pendulums, which decreases a system's energy consumption because it reduces the kinetic power generated by closing valves, which could be used to store future energy in pressurized fluid. This also reduces the amount of energy needed to inject hydraulic fluid and permits a slower valve velocity to be achieved by the solenoid-based system. This softens the valve's seating, which is a benefit of the new system. They succeeded in creating a four-cylinder internal combustion engine using a hydraulic pendulum, but the system calls for a number of different parts and is complicated. Two solenoids, two check valves, a high-pressure and low-pressure hydraulic fluid supply, and the use of a hydraulic pendulum are required for each engine valve. Schechter et al. state that two solenoids, if synchronized, can operate a pair of valves. But this diminishes the benefit of independent valve control (Schechter & Levin, 1996).

Wolfgang Stefanopoulou (2001) reported that the equation of the two electromagnets and the magnetic force connect the mechanical and electrical subsystems. Internal combustion engine advances made possible by variable valve opening and shutting necessitate careful camless valve train actuator control. This research examines electromechanical camless valve trains (EMCV) valve position tracking. An iterative learning controller (ILC) combined with linear feedback in a tracking controller reduces noise and wear during valve closure and opening. A controller that combines linear feedback and a learning feed-forward controller were created to achieve low contact velocity at low engine speeds (idle operation). The presented controller achieves low contact velocity, hence the necessity for “soft landing.” Using the ILC methodology, the feed-forward signal of the feedback controller was modified every cycle depends on the error between the desired and actual valve positions (Hoffmann et al., 2001).

In 2009, Gillella & Sun introduced the modeling and design of a novel, adaptable engine valve actuation system that is compatible with camless engines. They use an internal hydro-mechanical feedback mechanism for precise valve motion control, enabling real-time control with straightforward two-state valves, which can be used to turn on or off this feedback mechanism in real time, lowering system costs and facilitating mass production. The internal feedback parameters determine the system's trajectory, and to evaluate each parameter's impact, a mathematical model is developed. One key design component that affects the system's trajectory is the "area schedule." A nonlinear optimal control problem is derived from the design problem and solved through numerical dynamic programming. Simulations validate the area schedules' efficacy, but implementing this design would be challenging due to the complex geometry in constrained areas (Gillella & Sun, 2009).

In 2016, SAE International published an essay by Venkatesh, D., and Selvakumar, A., from the University of Michigan, focusing on the design of pneumatic actuator-equipped camless engines. The goal of the study was to build a prototype and assess how well it performed at different engine speeds. The researchers also studied sensors for determining crankshaft position. They simulated pneumatic actuators using the Festo FliuidSIM program. The engine's weight and head size were reduced when traditional camshafts were replaced with the electro-pneumatic system. The 8-mm fixed valve lift was created as a test setup for pneumatic actuators. Control logic was created and tested based on valve timing analysis. The study explores the benefits of these engines over traditional ones and emphasizes the camless system's capabilities in low-rpm engines (Venkatesh & Selvakumar, 2016).

Independent actuators that use a minimal portion of the engine's output power to provide precise control and adequate force are necessary for camless engines. In 2016, Jr. et al. designed, modeled, and simulated an actuator system for valves that complies with this requirement with an engine speed of up to 6000 rpm. Control valves are used in series in the suggested system under a range of operating circumstances and design parameter vaules.The findings indicate that the suggested system can use 1% to 2% of the engine's available power to achieve the required engine speed of 6000 rpm. Without the need for a separate position sensor on each engine valve, the system can be used for either closed-loop or open-loop control, potentially reducing costs and improving reliability. But the study ran into a number of obstacles, consisting of the requirement for independent actuators, the power consumption of the engine, constant-pressure hydraulic systems, sensitivity to temperature changes in the characteristics of the hydraulic fluid, and the possible requirement for position transducers installed on each gas exchange valve (GEV), which raised concerns for some systems because it added an extra cost in addition to the extra component already present (Jr et al., 2016).

Nam et al. conducted research in 2017 with an emphasis on the analysis and design of an electro-hydraulic camless engine valve actuator (EH-CEVA) for use in automobiles. The purpose of the study is to verify whether EH-CEVA could take the place of the present cam-based valve trains. Various operating conditions are used to conduct dynamic simulations and experiments to fulfill performance standards. The dynamic properties of the EH-CEVA are affected by vibration, nose, and oil temperature when the valve is closed. The system was developed with AMESim, a powerful hydraulic analysis tool. Experiments from the prototype test bench were used to validate the EH-CEVA. It has been demonstrated that camless engine technologies improve power output, fuel efficiency, and emissions from internal combustion engines. Electro-mechanical and electro-hydraulic actuators can be used for camless engines to achieve variable valve actuation. The researchers offer motion control strategies and experimental results from a prototype system for actuating camless engine valves (Nam et al., 2017)**.**

In 2019, Lanusse et al. demonstrate the creative application of an electromagnetic actuator for a camless engine valve train utilizing tiny gasoline-powered engines. In order to produce a control-oriented model and enable efficient control, the design method is inverted. To establish a correlation between the control model and experimental measures, a test bench is built. The CRONE system design methodology is used for a robust controller approach. The investigation results show excellent dynamic performance of the innovative actuator (Lanusse et al., 2019).

For camless engines, Muhammad Arsalan et al. propose a novel shutter valve design in 2019 that replaces conventional camshaft-operated valves and enables precise control of fuel intake and exhaust flow. The Electronic Control Unit (ECU) directly operates the valves, while pulse width modulation provides total control over the driver's preferred performance. By doing away with the need for a camshaft, the suggested shutter valve design seeks to lower engine costs, enhance fuel efficiency, and raise overall engine economy. By regulating the quantity of fuel to be burned, the design also provides the possibility of lowering NOx emissions and improving environmental friendliness by lowering the production of exhaust gases. In addition to recommending additional research to assess performance, efficiency, and environmental impact, the paper highlights the future research potential of the modeled design of shutter valves for camless engines. It also explores potential applications in the automotive industry, particularly in the development of economical hybrid sports cars (Jalees Abro et al., 2019).

The mathematical modeling of an Electro-Hydraulic Valve Actuator (EHVA) prototype and its application to the design of cycle-by-cycle Valve Lift Control (VLC) are presented by Alessandro di Gaeta et al. in 2021. The EHVA is rated according to how well it can regulate camless engine valve lift parameters. In a camless four-stroke engine, they present a novel physical model of a shutter valve that takes the place of the conventional camshaft-operated valve. It suggests an internal combustion engine camless valve control system that selectively opens and closes intake and exhaust valves using a hydraulic pump and actuator. They also go over how to simulate and apply gas force to the exhaust valve of camless valve trains in semi-physical settings using an electric load simulator. By providing accurate control over valve lift, the EHVA seeks to maximize engine efficiency and performance. The effectiveness of the EHVA in controlling valve lift can be simulated and examined using the mathematical model created in the paper. Engine performance and efficiency can be improved with the help of the EHVA in the design of the cycle-by-cycle valve lift control (VLC). The modeling and control of electro-hydraulic valve actuators are discussed in the paper, which is helpful for the advancement of camless engine technologies (Di Gaeta et al., 2021).

2.2 Materials

Among the most challenging issues a designer faces is choosing the right material for an engineering application. The material that achieves the desired result with the least amount of expense is the best material. A primary goal of the camless engine's design is to use as many off-the-shelf, commercially available parts as possible and to steer clear of custom parts whenever feasible. With this goal in mind, many parts that are potentially available from more manufacturers or shops are incorporated into the final design. In this thesis for a camless engine, there are some components to be designed, like valves, valve springs, cylinder heads, and electrical system components. But overall material selection depends on the Honda CG 125 model engine.

2.2.1 Cylinder-head materials

The cylinder head material and its dimensions are taken from the standards of the Honda engine manufacturing materials, which are aluminum alloys and their properties are indicated in table 2.1.

In an internal combustion engine, the cylinder head sits above the cylinders on the top of the cylinder block. It closes at the top of the cylinder, forming the combustion chamber. A head gasket seals this joint. The passages that supply fuel and air to the cylinder and permit exhaust to exit are typically found in the head of an engine. The head can also be a place to mount the valves, spark plugs, and fuel injectors.

Table 2.1 Properties of aluminum alloy (Ashby, 2005)

Properties	**Value**	**Unit**
Density	2770	kg m^-3
Coefficient of thermal expansion	2.3E-05	C^-1
Young’s Modulus	7.1E+10	Pa
Poisson’s Ratio	0.33	-
Bulk Modulus	6.9608E+10	Pa
Tensile Yield strength	2.8E+08	Pa
Compressive Yield strength	2.8E+08	Pa
Tensile ultimate strength	3.1E+08	Pa

2.2.2 Engine valve materials

An engine can rev higher, pump more air, and generate more horsepower when it has a lighter valve, which usually weighs 8 to 10 percent less than a valve with a standard-sized stem. Less strain on the valve springs, retainers, rocker arms, pushrods, lifters, and cam lobes is another benefit of a lighter valve. Because intake valves with a larger head diameter tend to be heavier than exhaust valves, the weight of the intake valves has a greater effect on the engine's rpm potential than the exhaust valves.

Generally, both the inlet and exhaust valves are subjected to high temperatures of 1930°C to 2200°C during the power stroke; therefore, it is necessary that the material of the valves withstand these temperatures. Thus, the material of the valves must have good heat conduction, heat resistance, corrosion resistance, wear resistance, and shock resistance. It may be noted that the temperature at the inlet valve is lower as compared to the exhaust valve. As a result, the exhaust valve, which is exposed to extremely high temperatures for exhaust gases, is made of silchrome steel, a unique alloy of silicon and chromium, while the inlet valve is typically made of nickel-chromium alloy steel. These two materials have different physical and mechanical properties which are shown in table 2.2 and 2.3.

Table 2.2 Properties of nickel chromium alloy steel (Ashby, 2005)

Property	**Value**	**Unit**
Density	7.85	g/cm^3
Melting point	1432	^0C
Tensile strength, ultimate	560	MPa
Yield strength	460	Mpa
Modulus of elasticity	190-210	Gpa
Bulk modulus (Typical for steel)	140	Gpa
Shear modulus (Typical for steel)	80	Gpa
Permissible bending stress	100 to 120	Mpa

Table 2.3 Property of silchrome steel (Ashby, 2005)

Property	**Value**	**Unit**
Density	7.20	g/cm^3
Melting point	1800	^0C
Tensile strength, ultimate	520	MPa
Yield strength	460	MPa
Modulus of elasticity	190-210	Gpa
Bulk modulus	135	Gpa
Shear modulus	80	Gpa

2.2.3 Valve spring materials

The selected engine model uses an oil-tempered steel helical coil spring with round wire for the valve spring and a helical coil spring with round wire. Oil tempered steel wire has the good property to be a valve spring. Oil tempered steel wire have the following material properties, taken from the selected engine model material in table 2.4.

Table 2.4 Property of oil tempered steel wire (Izumida et al., 2023)

Parameter	**Value**	**Unit**
Elastic (young‘s ,tensile) modulus (E)	196.5	Gpa
Modulus of rigidity G	80	Gpa
Tensile strength: ultimate	1720 to 2220	MPa
Maximum melting point	1450	^{0}C
Density	7.8	g/cm^3
Poison ratio	0.29	-
Allowable shear stress	420	Mpa

2.2.4 Solenoid valve components and materials

The solenoid usually consists of a stationary current-carrying coil or winding, a steel housing core,and a movable iron core called the plunger and armature (Norman, 2019).

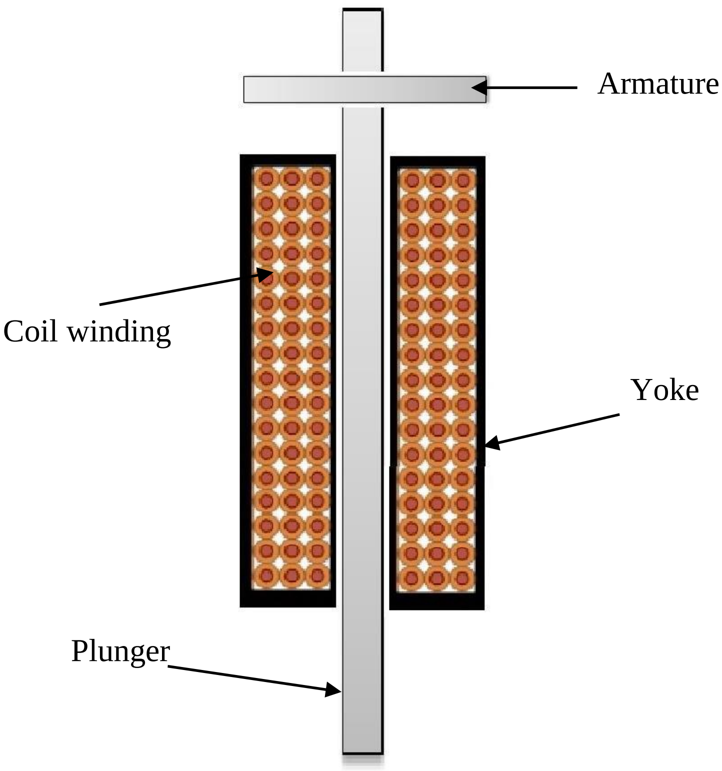

Figure 2.1 Solenoid valve components and materials

- **Coil winding**

As current is run across the terminals, an electromagnetic field is produced. The most economical and effective conductor of electricity, copper, is usually used to make them. The type of wire insulation and its thickness are chosen so as to determine the desired thermal rating of the coil. The coil insulation should be able to dissipate most of the heat that the coil will generate in a worst-case scenario without breaking down. The insulation chosen is a Class-C polyurethane nylon with a heavy build, rated for 200^0C.

- **Yoke**

The magnetic field is concentrated by the yoke, also called the shell or frame. It is usually composed of low-carbon steel and encircles the outside of the solenoid coil. This ferromagnetic material allows the flux produced by the solenoid to pass through it with ease. The magnetic field can also be strengthened by a ferromagnetic substance. The actuator would be ineffective if the yoke didn't exist because the magnetic field and flux lines would be haphazardly distributed. Most electromagnetic actuators are constructed from low-carbon steel. It is inexpensive and has a high permeability, making it a good magnetic conductor. Although there are superior magnetic materials, the cost increase is not justified by the increase in efficiency. The components of the actuator, which are made from iron, are the yoke and the armature.

- **Guide Tube**

The armature is guided by the guide tube. Usually, a nonmagnetic material like stainless steel is used to make it. To prevent the armature from being drawn to it, the material must be nonmagnetic.

- **Armature with a Plunger or Push Pin**

The armature is the piece of iron that the electromagnet coil attracts. This part is allowed to move freely. If nothing opposes the movement of the armature, it will be attracted to and move towards the electromagnetic coil when it is energized. But if something does resist the armature's motion, it will apply force to that object. The component that transmits the magnetic force to the component outside the actuator is the push pin. Furthermore, the push pin will transfer any forces opposing the magnetic force to the armature. The push pin is typically made of a nonmagnetic material, such as stainless steel, so that it is not attracted to the electromagnet. The physical and mechanical properties of cast iron, stainless steel and low carbon steel are shown in table 2.5.

Table 2.5 Property of cast iron, stainless steel and low carbon steel (Ashby, 2005)

	Materials		
Properties	**Cast iron**	**Stain less steel**	**Low carbon steel**
Elastic modulus	6.62×10^{10} N/m^2	8.5×10^{11} N/m^2	2x$\times 10^{11}$ N/m^2
Shear modulus	5×10^{10} N/m^2	10.1×10^{10} N/m^2	7.6×10^{10} N/m^2
Mass density	7200 kg/m^3	7700 kg/m^3	7800 kg/m^3
Tensile strength	1.517×10^8 N/m^2	1.517×10^8 N/m^2	4.825×10^8 N/m^2
Compressive strength	5.772×10^8 N/m^2	5.772×10^8 N/m^2	5.772×10^8 N/m^2
Coefficient of thermal exp.	1.2×10^{-5}	1.2×10^{-5}	1.2×10^{-5}
Yield stress	3.1×10^8 N/m^2	2.72×10^8N/m^2	2.482×10^8 N/m^2
Thermal conductivity	45 W/mK	28 W/mK	30 W/Mk
Shear strength	1.5×10^7N/mm^2	3.86×10^6 N/mm^2	200-300 MPa
Bending yield strength, flexural and compressive	248 - 655 MPa, 220 - 2520 MPa	(581-667) N/mm^2	250 MPa

2.2.5 Solenoid Valve Stand Material

The solenoid valve stand is a component that holds the solenoid valve in a desired position and supports it on the cylinder head. The solenoid valve stand can be made from cast iron and aluminum alloy. A stand made of cast iron is more durable and less expensive. Cast iron, on the other hand, dissipates heat less effectively and is heavy. For this reason, we prefer using a stand made of aluminum. These stands are much lighter than cast-iron stands, and the aluminum alloy material has a higher heat dissipation rate than cast iron. See the properties of cast iron in Table 2.5 and aluminum alloys in Table 2.1.

2.2.6 Coupling Member Material

A coupling member is a member that helps as an intermediate member to transmit a linear motion of the solenoid valve to the valve tip. In order to reduce the loss of magnetic force and to have good strength, the coupling is typically made of a nonmagnetic material such as stainless steel of grade 304 due to its excellent corrosion resistance and formability, so that it is not attracted to the electromagnet. The material is the same as the material of the plunger. See the properties of stainless steel in Table 2.5.

2.2.7 Controlling Devices and Program Selection

A controlling device is a device that is used to manage the electromechanical system of a machine. In this paper, the Arduino UNO is used as an ECU. The Arduino UNO is a widely used open-source microcontroller board based on the ATmega328P microcontroller (Deshmukh et al., 2018). Sets of digital and analog input/output (I/O) pins on the board allow it to be interfaced with different expansion boards (shields) and other circuits. There are six analog and fourteen digital pins on the board. It can be programmed using a type B USB cable and the Arduino IDE (Integrated Development Environment). It takes voltages between 7 and 20 volts, but it can be powered by an external 9-volt battery or a USB cable. It resembles the Leonardo and Arduino Nano as well. "Uno" was chosen to commemorate the release of the Arduino Software (IDE) because it means "one" in Italian. 1.0 (Shrushti B Walvekar, 2021).

The reference versions of Arduino, which have since evolved to newer releases, were the Uno board and version 1.0 of the Arduino Software (IDE). The Uno board serves as the platform's reference model and is the first in a line of USB Arduino boards. The ATmega328 on the Arduino Uno comes preprogrammed with a boot loader that allows uploading new code to it without the use of an external hardware programmer (Numayer, 2021). The physical demonstration of Arduino Uno is shown in figure 2.2.

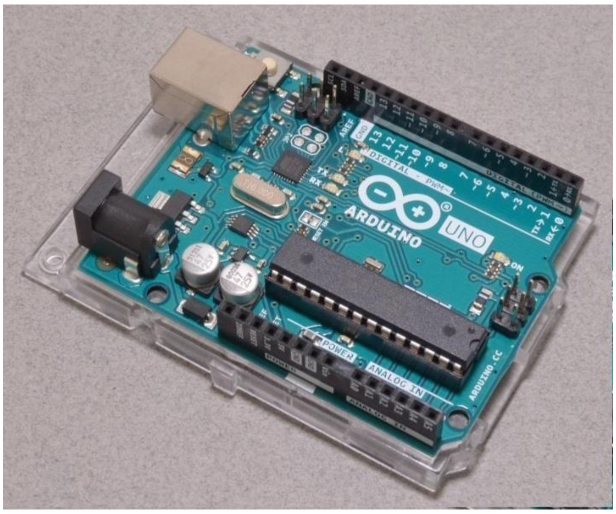

Figure 2.2 Arduino Uno or controller (Elprocus, 2013)

Technical specifications about the controlling device:

- Microcontroller: ATmega328P
- Operating Voltage: 5V
- Input Voltage: 7-20V
- Digital I/O Pins: 14 (of which 6 provide PWM output)
- Analog Input Pins: 6
- DC Current per I/O Pin: 20 mA
- DC Current for 3.3V Pin: 50 mA
- Flash Memory: 32 KB, of which 0.5 KB is used by the boot loader

- SRAM: 2 KB
- EEPROM: 1 KB
- Clock Speed: 16 MHz
- Length: 68.6 mm
- Width: 53.4 mm
- Weight: 25g

Since the actuation system of the solenoid uses a car battery, which has a 12 volt supply capacity, it needs to convert the power to 5 volts and last a long time. This can be done using a resistor in order to get the desired voltage. The ATmega328P acts as an Electronic Control Unit (ECU), which is any embedded system in automotive electronics that controls one or more of the electrical systems or subsystems in a vehicle. In this thesis, ATmega328P/Arduino Uno is used to control the electromechanical valve actuation system.

2.2.8 Voltage Control and Converter

It is a device used to suit the amount of voltage supplied to the ECU (in this case, the ATmega328P/Arduino/ in order to have proper operation and damage elimination. This may be done using different possible methods. The purpose of voltage control is to keep the system's voltage level within allowable bounds. Voltages must stay within a certain range in order for equipment to function properly (S.A.Annestrand, 2003). Some of these are:

- Using relay
- Using proper resister
- Transistor circuit system.

- **Relay:**

A relay is a switch that operates electrically and is also a simple electromechanical switch (Leela Prasad, 2022). Relays are mechanically operated switches that are powered by an electromagnet. Relays are used when multiple circuits need to be controlled by a single low-power signal or when a separate low-power signal is required to control a circuit. Most coils, like solenoid valve coils, require more current than Arduino pins or ECUs; therefore, it is preferable to use transistors.

- **Resistor:** It is an electrical component with two terminals that is passive and uses electrical resistance as a circuit element. The main purpose of a resistor is to reduce the current flow and lower the voltage in any particular portion of the circuit (JU'S, 2024). It is a good option to reduce the power supplied to the ECU or the system circuit.

- **Transistor**

It is a three-terminal semiconductor device that regulates current or voltage flow and acts as a switch or gate for signals (Point Team @ Tutorials, 2024). And they are used to switch on high current or high voltages in digital circuits. In an analog circuit, it serves as an amplifier of signals. A small current passing through the base results in a larger current flowing through the collector and emitter. From the above, it is preferable to use transistors for the exact EMVA for the engine valve train.

2.2.9 Electrical Power Source Selection:

A battery is an electrochemical cell that transfers chemical energy into electrical energy. For this research, a rechargeable lead-acid battery is used as a power or voltage source, but its capacity and detailed specification are determined in the design part of the system components.

2.2.10 Electrical System Components Damage Controller

This is a system component that prevents the circuit from being damaged by the back electromotive force. There are a number of ways to do this, but there are two most common methods used in access control.

I. Flywheel Diode

An electromagnets current flows similarly to that of a free-spinning bicycle wheel. The wheel continues to turn even after the pedal is depressed (the supply voltage is cut off). The fly wheel diode allows the fly wheel to be braked. The diode is reverse biased and functionally out of circuit when the supply voltage is applied (BSB.Progeny, 2024). Fly wheel current creates a back EMF with the opposite polarity when the switch is opened, which causes the diode to conduct. The diode clamps the voltage to about one volt and suppresses the back EMF very effectively. For small solenoids, such as those found in strikes, this is quite appropriate. However, these are not suitable for electromagnets (Ibex UK, 2024).

Figure 2.3: Flywheel diode

Diodes are not suitable for electromagnets. The power dissipated by the diode is low because the forward volt drop is less than a volt (Ibex UK, 2024). As a result, there is little energy being removed from the electromagnet. Therefore, the time it takes for the energy to dissipate will increase with a lower power loss through the diode. As a result, the magnet remains attached to the armature for a longer period of time, and the current continues to flow. This can be for as much as one to two seconds, leading to frustrating delayed door release (BSB.Progeny, 2024).

II. Metal Oxide Varistor (MOV)

The MOV (VDR) has a rated voltage; a varistor is an electronic component with an electrical resistance that varies with the applied voltage. Also known as a voltage-dependent resistor, it has a non-linear, non-ohmic, current-voltage characteristic that is similar to that of a diode. The response times for the MOV are in the 40–60 ns range. Its resistance is extremely high below this voltage. Therefore, a MOV with a rated voltage that is marginally higher than the standard supply voltage can be connected across the magnet's coil without risk, just as a diode has no effect when the supply is connected (BSB.Progeny, 2024). The back EMF will increase to the MOV's rated voltage when the supply is cut off. The MOV begin to conduct and clamp the voltage to a value slightly above this one (BSB.Progeny, 2024).

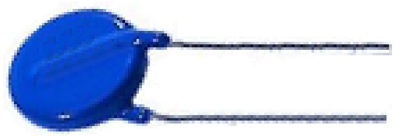

Figure 2.4 Metal Oxide Varistor (MOV) (Stock, 2024)

Figure 2.4 MOV have 30 times more power lost than the diode. The net result is that the energy is lost approximately 30 times quicker, and the magnet releases the armature in much less time (BSB.Progeny, 2024). Due to the above discussion of the two damage control systems, it is preferable to choose a metal oxide varistor (MOV).

2.2.11 Sensors

- **Crank Angle Sensor**

The crankshaft angle sensor also uses a trans-missive optoschmitt sensor to detect the current crankshaft angle with respect to the zero TDC position. When the zero TDC sensors come into contact with the zero TDC position, the crankshaft angle sensor begins to count. The output of this sensor is used by the ECU to count the current crankshaft angle position (Prof. Ir. Dr. Azhar Bin Abdul Aziz, 2006). Based on this information, the ECU can determine when to activate the solenoid valve.

An electronic device called a crank sensor is used in internal combustion engines, both gasoline and diesel, to track the crankshaft's position and rotational speed. This information is used by engine management systems to control the fuel injection or the ignition system timing and other engine parameters (Goss, 2018). For gasoline engines, the distributor would need to be manually adjusted to a timing mark prior to the development of electronic crank sensors (Wikimedia Foundation, 2023). The relationship between the engine's pistons and valves can be monitored by combining the crank sensor with a comparable camshaft position sensor. This is crucial for engines that have variable valve timing (Khayal, 2020). This method is also used to "synchronize" a four-stroke engine upon starting, allowing the management system to know when to inject the fuel (Wikimedia Foundation, 2023). Additionally, it is frequently utilized as the main resource for determining engine speed in revolutions per minute.

Common mounting locations include the main crank pulley, the flywheel, the camshaft, or the crankshaft itself (Khayal, 2020). This sensor is the second most important sensor in modern-day engines after the camshaft position sensor. The engine may not start at all or may cut out while operating if it fails.

2.2.12 Procedures to Conduct Finite Element Analysis for Each Component:

Conducting finite element analysis (FEA) of system components in ANSYS typically involves the following procedures:

1. **Geometry modeling** is performed by using ANSYS space claim 2023R2 and then importing the model to the ANSYS workbench.
2. **Material Properties**: Define the material properties of the model (each component), such as density, Young's modulus, Poisson's ratio, thermal conductivity, etc. of the solenoid stand, plunger with armature, and coupling member materials.
3. **Mesh Generation**: Discretize the model into a mesh of smaller elements (e.g., hexahedral elements are well-suited for meshing beam-like structures, as they can accurately capture the bending and shear behavior).
    - Adjust the mesh parameters, such as the element size, to achieve a balance between accuracy and computational efficiency.

- Refine the mesh in areas of interest or where high stress gradients are expected.

4. **Boundary Conditions and Loads:** Define the appropriate boundary conditions, such as fixed supports and applied forces, and Specify the loading conditions, including static analysis requirements.
5. **Solution Setup:** Select the structural analysis type and choose the solver settings, including the solution method, convergence criteria, and output options.
6. **Solve the Problem:** initiate the solution process in the ANSYS Workbench. The software will perform the necessary computations to obtain the results, such as displacements, stresses, strains, or temperature distributions.
7. **Results Evaluation:** Examine the results carefully, focusing on the areas of interest or potential failure locations. ANSYS Workbench provides a wide range of post-processing tools to visualize the results, including contour plots, deformed shapes, and stress/strain distributions.

2.3 Research Gap

The research gaps that are identified in the literature on camless engine valve actuation can be: the existing camless engine valve actuation system involves complex designs and a multitude of components, which can result in increased manufacturing costs and pose challenges for mass production. These obstacles are linked to the temperature sensitivity and characteristics of hydraulic fluids utilized in camless engine valve actuation systems, as well as practical implementation challenges such as the integration of camless valve systems into existing engine architectures. By developing solutions to address complex design s and multitude of components, improving control strategies and algorithms to reduce noise and minimize contact velocity, and validating proposed solutions through computer simulations, it is possible to diminish the number of components required while simultaneously maintaining or enhancing performance and addressing practical implementation challenges. Successfully addressing these gaps will result in the advancement of camless engine valve actuation systems, thereby improving engine performance, fuel efficiency, and emissions in internal combustion engines.

This thesis overcomes problems like fuel economy problems, torque and power problems; exhaust emissions problems, etc. by taking the ideas of the researchers as evidence. So for design purposes, select the Honda CG 125, which is a 124-cc air-cooled single-cylinder four-stroke engine with a speed range of 1000 to 5500 RPM.

CHAPTER THREE

3. MATERIALS AND METHODS

3.1 Theoretical Framework

This thesis may have a different layout and design because its primary focus is on the electromechanical control system of the engine valves (exhaust and intake valves). The conceptual design of the system presented in this research comprises the following components: voltage sources; electrical system circuits; electrical control systems (ECUs); sensors; actuated valves and springs with mounting cylinder heads; solenoid valves; solenoid stands or solenoid valve mounting members; and a coupling member between the plunger and the valve tip. The solenoid valve designed with the proper parameters will be mounted on the top of the cylinder head, aligned to the tip of the valve, and have linear contact with the valve through the coupling member. The coupling member may be changed when it is damaged. The actuation systems are operated by two solenoids for one valve; the upper is for closing and the lower one for opening. The solenoid has terminals for power supply. When the terminals get voltage, at the command of the ECU, the solenoid activates and generates a magnetic force to apply the desired actuation, and the sensors like the crankshaft position sensor and speed sensor are integrated by some calculation and give some pulse results to the ECU. The ECU is a programmable controller controlled by the related software. The heat generated by the solenoid is controlled by the fin system of cooling. The proposed block diagram is represented in figure 3.1 as follows:

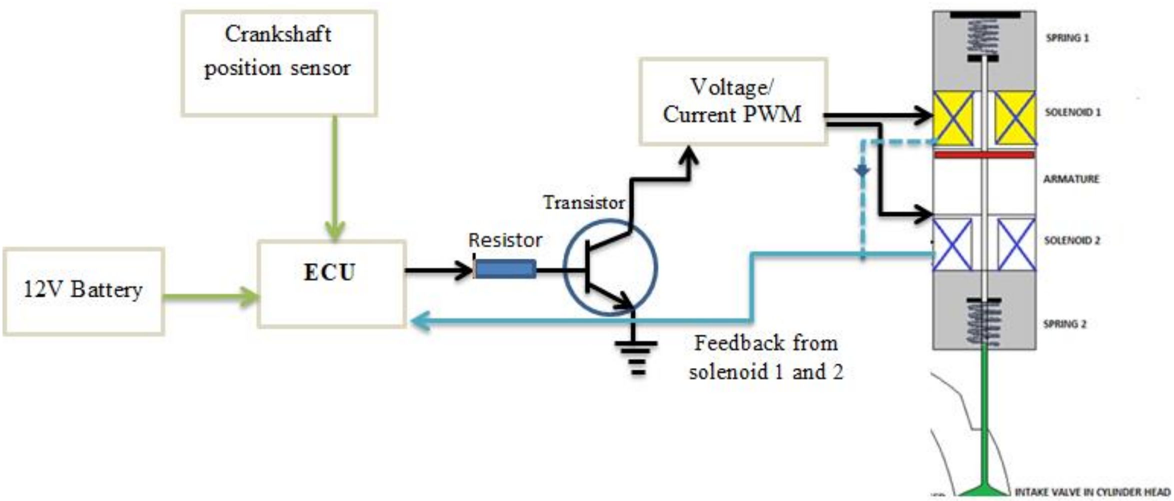

Figure 3.1: Electromechanical valve actuation system schematic diagram

3.2 Materials selection

The best material is one which serves the desired objective at a minimum cost and the material selection is depends on the Honda CG 125 model engine. Based on the definition in the literature and selection criteria, the material used in the research work is as follows in table 3.1.

Table 3.1 Material used in the research

Component Name	Material Made
Valves	Nickel chromium alloy steel and silchrome steel.
springs	Oil tempered steel
Armature	iron
Plunger	Stainless steel
Winding wire	Copper
Solenoid stand	Aluminum alloy
Coupling	Stainless steel

Table 3.2 Controlling devices and program selection

Function	Devices
Damage control/Back EMF/	Metal oxide varistor (MOV) /Diode and Resistor/
Switch	Transistor/Realy/
Sensors/Crank angle sensors/	Trans-missive Optoschmitt
Processing and Commanding	ECU/Arduino Uno/
Governing system programing software	Arduino IDE

3.3 Methods

Each of the specific tasks to be performed in the research work is described here. The whole research work is classified into four different divisions, namely numerical analysis, system modeling, program design, and simulation. Before and after title selection and problem identification, the previous research work was reviewed on the camless engine electromechanical valve actuation system. In the first part of this research manual, structural design analysis of system components can be carried out to determine the input parameters for modeling, stresses, and deformations to investigate whether the design is safe or not using different primary and secondary data sources. Next to the numerical analysis of the system, mathematical modeling of the solenoid valve actuator model and the full electromechanical valve actuator model was stated, including actuator dynamics. Thirdly, after the mathematical model is analyzed based on Newton's law of motion and Kirchhoff's law, the next task is the program design of the system by using input sources from numerical analysis in Arduino IDE software to show the operation of the system using electrical simulation software. The fourth division of this research work is computer simulation, and results are discussed.

3.4 Data Collection

The model is developed in MAT LAB/Simulink and estimated and validated using data collected from both primary and secondary sources.

The model is developed in ANSYS space claim and imported this model to ANSYS workbench for analysis using finite element analysis (FEA) method to estimate and validate the result using data collected from both primary and secondary sources.

Controlling system is modeled in PROTEUS DESIGN SUIT PROFESSIONAL 8.6 SP3 and Arduino IDE 2.3.2 version to recognize the functionality of the system using data collected from both primary and secondary sources.

3.4.1 Data Analysis

After reviewing the literature and selecting the best concepts, the electromechanical valve actuator model was numerically analyzed. Computer simulation was carried out using MATLAB/Simulink software for actuator dynamics, Arduino IDE for program design input to PROTEUS software, PROTEUS DESIGN SUIT PROFESSIONAL 8.6 SP3 for functionality testing, and ANSYS software for FEA analysis.

- **Mesh Convergence Study in the ANSYS Workbench:**

Mesh independence analysis, also known as grid independence study or mesh convergence analysis, is a technique used in computational modeling and simulations to determine the appropriate level of mesh or grid resolution required for the numerical solution to be independent of the mesh size (Bhattacharyya, 2023).

In numerical simulations, the computational domain is typically discretized into a mesh or grid of smaller elements or cells. The finer the mesh, the more accurately the geometry and physical processes can be represented. However, refining the mesh too much can significantly increase the computational cost without necessarily improving the accuracy of the solution.

Mesh independence analysis involves the following steps:

1. Perform the simulation using an initial, coarse mesh.
2. Refine the mesh, either uniformly or selectively in regions of interest.
3. Run the simulation again with the refined mesh.
4. Compare the results from the two simulations, such as key output variables or quantities of interest.
5. If the difference between the results is within an acceptable tolerance, the solution is considered mesh independent, and coarser mesh can be used.
6. If the difference is still significant, further refine the mesh and repeat the process until the solution becomes mesh-independent.

By following the above procedures, the mesh convergence analysis result of the solenoid stand in the ANSYS static structural workbench is shown in Table, and the corresponding mesh independence is located in chart as indicated in figure 3.2.

Equivalent (Von-miss) stress (MPa)	9.2241	9.288	10.0155	10.0161	10.0167
Number of Element	1925	7425	37925	219495	737878

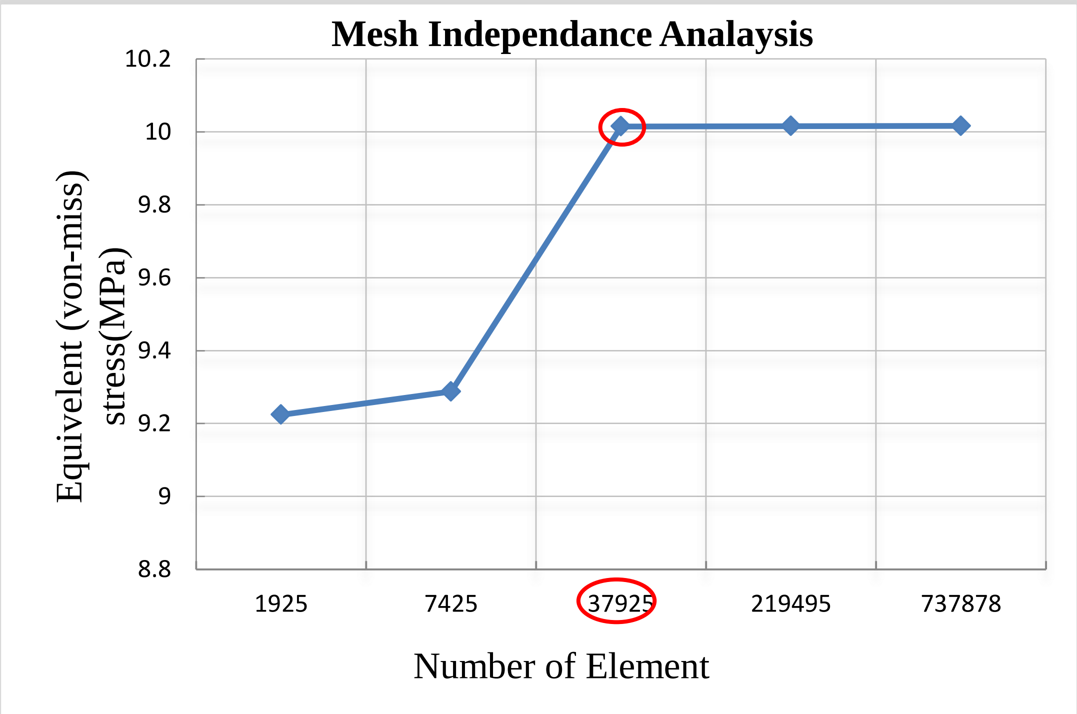

Figure 3.2 Mesh independence analysis of solenoid stand

As seen from the graph 3.2 shown a flat line indicates that there is minimal to no variation in the chosen parameter (commonly referred to as a convergence parameter) when the mesh is refined. The fluctuation of equivalent stress is noticeable in relation to the mesh. Variations in the results are negligible beyond the indicated cell zone; results no longer change significantly with further mesh refinement. However, refining the mesh too much (increasing number of elements beyond this point) can significantly increase the computational cost without necessarily improving the accuracy of the solution. The remaining components are done based on these procedures with fine mesh to get best result.

3.4.2 Research work flow

The overall research work flow for designing of electromechanical valve actuators is demonstrated in the flow chart in Figure 3.3. Initially, a literature survey is carried out on valve actuation mechanisms based on electromechanical valve actuator models.

Then, analytical design analysis of components in the system was carried out to study parameters for the mathematical model and simulation. Next the governing equation for the solenoid actuator of the armature and valve is established without considering the effect of actuator dynamics. The armature and valve actuator model for solenoid actuators is developed based on the armature actuator model for actuator dynamics. Finally, a two degree-of-freedom solenoid actuator model is developed based on the armature and valve actuator models of the solenoid actuator. The governing equation for the electrical system is established, and a full electrical and solenoid actuator model is developed.

The program is designed for controlling the valve actuation system and testing the functionality of the system. Computer simulation of the electromechanical valve actuator system is carried out separately for MATLAB/Simulink and PROTEUS SUIT DESIGN 8.6 for functionality testing. The result of the simulation should indicate the design is safe when comparing the analytical solution with secondary data sources/literatures/ and show the functionality of the system.

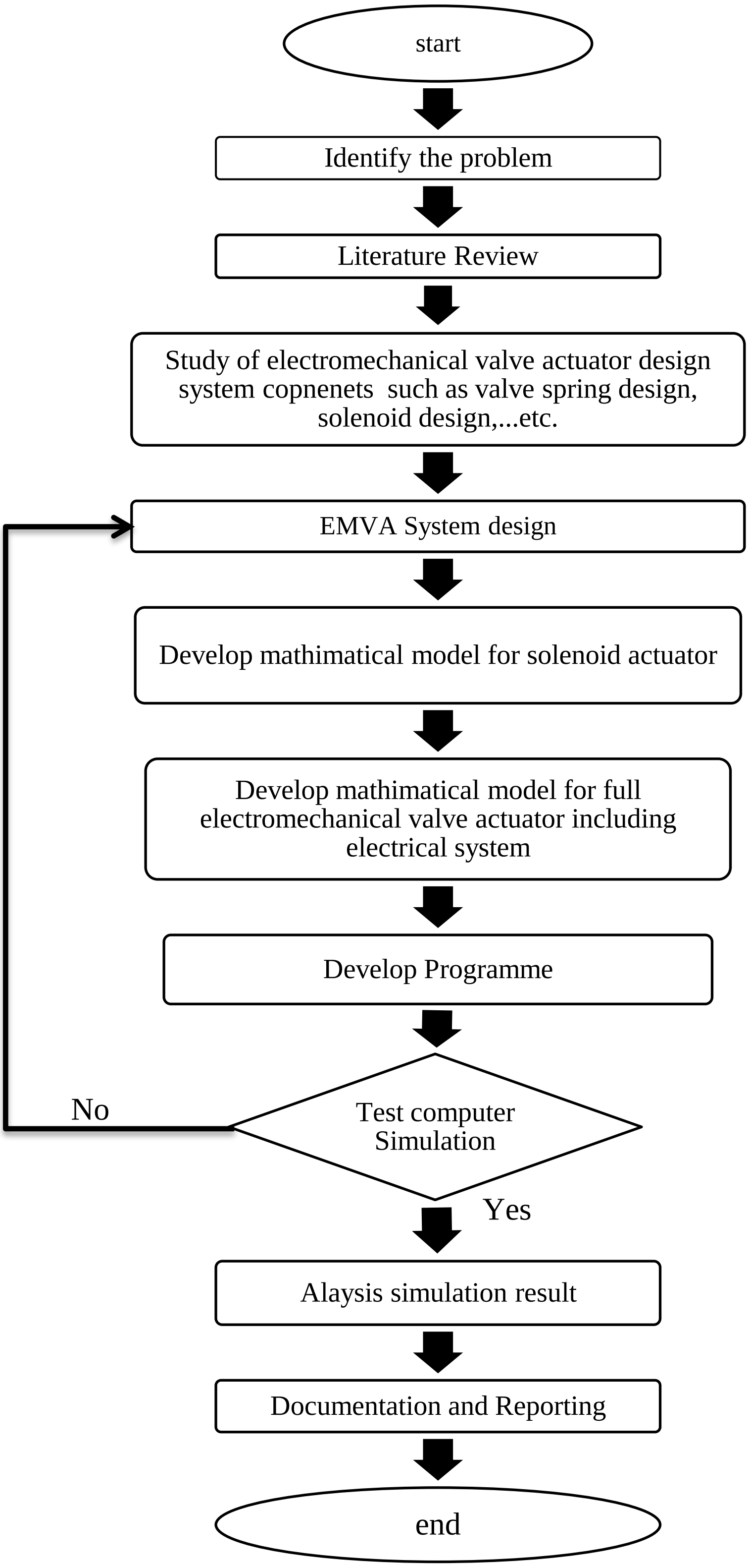

Figure 3.3: Flowchart of proposed research work

CHAPTER FOUR

4. DESIGN ANALYSIS, MATHEMATICAL MODELING AND PROGRAMMING OF THE SYSTEM

4.1 Introduction

The main objective of this chapter is to detail analytical design analysis of the system components, determining the force required for the actuating system, to develop mathematical model for mechanical solenoid actuator considering mass of armature and valve with 2 DOF systems, develop mathematical model including full electrical and mechanical solenoid actuator systems and programming of system for controller of EMVA system. Finally cost benefit analyzed after those activities to check that design is economical or not with comparison of selected model for replaced components.

4.2 Design of System Components

4.2.1 The engine specification and basic conditions for design

From the engine models Honda CG 125 is selected for this design and it‘s detail specification is expressed as follows.

Honda CG 125 (Shoemark & Churchill, 1994):

Parameters	Description
Engine Type	124cc air-cooled single-cylinder four-stroke
Bore and Stroke (mm)	56.50 x 49.50
Compression Ratio	9:1
Valve Train	SOHV(Single overhead camshaft); two-valve seat in vertically parallel
Engine speed (RPM) range	1000 to 5500
Rated Power (kW)	8.206
Max torque (Nm)	16.8
Valve Timing	**During low speed:** ❖ IVO- 10^0 BTDC ❖ IVC- 20^0 ABDC ❖ EVO- 25^0 BBDC ❖ EVC- 5^0 ATDC

Where: **BTDC** is before top dead center, **ATDC** is after top dead center, **BBDC** is before bottom dead center and **BBDC** is before bottom dead center.

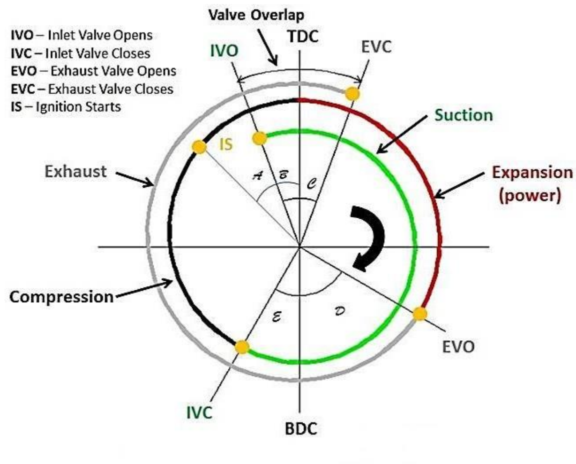

Figure 4.1: Valve timing diagram of four stroke petrol engine (in this design the actual one is used) (Ingenieria Y Mecanica Automotriz, 2019).

4.2.2 Design of the Cylinder Head

Most engines come with an additional cylinder head or cover as standard equipment. It is usually made of box-type section of considerable depth to accommodate ports for air and gas passages, an inlet valve, an exhaust valve, and a spark plug (in case of petrol engines) or an atomizer at the Center of the cover (in the case of diesel engines) (Khurmi & Gupta, 2005).

Calculating the following values is necessary when designing a cylinder head for an I.C. engine:

❖ **Thickness of the cylinder wall (t_w) and head**

The thickness of the cylinder wall usually varies from 4.5 mm to 25 mm or more, depending on the size of the cylinder (Khurmi & Gupta, 2005). But from the standards of the Honda engines, we take the thickness of the cylinder head at 16 millimeters, and from the given data, the thickness of the cylinder wall *(t)* may also be obtained from the following empirical relation (Khurmi & Gupta, 2005), i.e.

$$t = 0.045D + 1.6\,mm \qquad (4.1)$$

Where, D is the inside diameter of the cylinder in mm.

In these case D = 56.50 mm,

$$t = 0.045 \times 56.5\,mm + 1.6\,mm \approx 4.5\,mm.$$

❖ **Size of studs for the cylinder head**

From the selected engine, the number of studs is four, the nominal diameter of the stud is ten millimeters, and the core diameter of the stud is usually taken as $0.84d$ in mm (Co, Industrial Hartford., 1999) (Khurmi & Gupta, 2005).

4.2.3 Design of Valves and Valve Springs

Poppet-type valves are very frequently used since they are more efficient and simple than others. It consists of the head, face, and stem. The head and face of the valve are separated by a small margin to avoid a sharp edge of the valve and also to provide provision for the regrinding of the face. The face angle generally varies from 30° to 45°. The lower part of the stem is provided with a groove in which a spring retainer lock is installed (Khurmi & Gupta, 2005).

Valve timing is one of the most important engine design variable (factor), which may seriously affect the performance of IC engines unless and otherwise it is designed meticulously.

❖ **Exhaust Valve and Spring Design:** It is required to determine the following dimensions: Valve Port Diameter (d_1 or d_p), Valve Face Angle (α_v), Maximum Valve Lift (h), Margin Thickness (t), Valve Face Width (b), Valve Head Diameter (d_2), and Valve Stem Diameter (d_0)

A. Exhaust valve design: Valve Port Diameter (d_1)

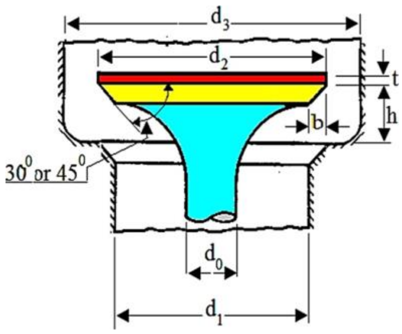

Figure 4.2: Geometry of a Poppet Valve (Patil et al., 2023)

Neglecting losses and assuming the fluid (gas) is incompressible, the volume flow rate of the fluid passing through the valve port is equal to the fluid (gas) passing through the cylinder bore. Hence, from the continuity equation (fluid mechanics),

$$a \times v_{mp} \times \rho_{g1} = a_p \times v_{mg} \times \rho_{gp} \quad (4.2)$$

Since the density of gas is the same through the cylinder bore and valve port which is $\rho_{g1} = \rho_{gp}$ and the equation simplifies to:

$$a_p = \frac{v_{mp} \times a}{v_{mg}}$$

Where:

a_p = Area of valve port,

v_{mg} = Mean velocity of gas flowing through the port.

a = Area of the piston.

v_{mp} = Mean piston velocity.

S = Stroke of the engine.

N = Engine speed.

Area of the piston is obtained as

$$a = \frac{\pi \times b^2}{4}$$

$$a = \frac{\pi \times (56.5mm)^2}{4}$$

$$a = 2507.18728mm^2 = 2.5072 \times 10^{-3}m^2$$

Table 4.1: Mean velocity of the gas ($\boldsymbol{V_p}$)

Type of engine	*Mean velocity of the gas* (v_p) m/s	
	Inlet valve	*Exhaust valve*
Low speed	33 – 40	40 – 50
High speed	80 – 90	90 – 100

And take mean velocity of exhaust gas (V_p) at high speed is 90 m/s (Khurmi & Gupta, 2005). The mean velocity of the piston can be obtained as follows:

$$v_{mp} = 2 \times S \times N \tag{4.3}$$

$$v_{mp} = 2 \times 49.5\, mm \times 5500\, rpm$$

$$v_{mp} = 9.075\, m/s$$

Then the area of the exhaust port is:

$$a_p = \frac{v_{mp} \times a}{v_1} = \frac{9.075m/s \times 2.5072 \times 10^{-3}m^2}{90\, m/s}$$

$$a_p = 0.00025281m^2$$

Thus, the diameter of the valve port is:

$$a_p = \frac{\pi \times {d_p}^2}{4} \rightarrow d_p = \sqrt{\frac{a_p \times 4}{\pi}} = \sqrt{\frac{0.00025281m^2 \times 4}{\pi}} = 0.017941m$$

$$d_p = 0.017941\, m = 17.941mm$$

Thickness of the valve disc ($\mathbf{t}_d$):

The thickness of the valve disc (t), as shown in figure 4.2 above, may be determined empirically from the following relation:

$$t_d = kd_p\sqrt{\frac{p}{\sigma_b}} \tag{4.4}$$

Where; k = Constant = 0.42 for steel and 0.54 for cast iron (Khurmi & Gupta, 2005),

d_p= Diameter of the port in mm,

p = Maximum gas pressure in N/mm2, for engines at light loads which ranges 300 psi to 1000psi, for this case select 600 psi is taken which is the same as 4 N/mm2 (Performance, 1986).

σ_b = Permissible bending stress in MPa or N/mm^2.

= Near 28 MPa for cast iron; 50 to 60 MPa for alloy steel and, 100 to 120 MPa for high grade alloy steel. And from this taken as 50 MPa = 50 $\mathrm{N/mm^2}$.

$$t_d = kd_p\sqrt{\frac{p}{\sigma_b}} = 0.42 \times 17.941mm \times \sqrt{\frac{4\ N/mm^2}{50\ N/mm^2}}$$

$$t_d = 2.13\ mm$$

Valve Face Angle ($\boldsymbol{\alpha_v}$):

The valve face angle refers to the angle at which the valve face is machined or ground. It is an important characteristic of engine valves, particularly in internal combustion engines. The valve face angle can be taken as 30^0 or 45^0. In this design, it is taken as 30^0.

Maximum Valve Lift($\mathbf{h_{max}}$):

The mean velocity of the gas flow through the valve for continuous flow is the same as the flow through the valve's opening when it is raised to its maximum. As a result, the area across the valve seat and the port area are equalized to determine the valve's maximum lift. The maximum valve lift for a conical head is given by:

$$aera\ of\ valve\ set(a_{vs}) = area\ of\ port(a_p)$$

$$\boldsymbol{\pi \times d_p \times h_{max} cos(\alpha) = \frac{\pi}{4} \times (d_p)^2\ or\ h_{max} = \frac{d_p}{4 \times \cos(\alpha)}}$$

$$where;\ \alpha = \ Angle\ at\ which\ the\ valve\ seat\ is\ tapered\ = \ 30°.$$

$$h_{max} = \frac{17.941mm}{4\times\cos(30)} \tag{4.5}$$

$$h_{max} \approx 6\ mm$$

Margin Thickness ($\boldsymbol{t}$):

The margin thickness of the valve t will be 1.50 mm to 2.00 mm, for this design 1.50 mm of the margin thickness is selected.

Valve Head Diameter($\boldsymbol{d_2}$ $\boldsymbol{or}$ $\boldsymbol{d_v}$):

The projected width w of the valve seat is shown in Fig. 3.8. For a seat angle of 45° or 30^0, the projected width of the valve seat is given by the following empirical relationship:

$$w = (0.05\ to\ 0.07)d_p\ or\ w = 0.06d_p$$

$$w = 0.06d_p = 0.06 \times 17.941mm = 1.0764\ mm$$

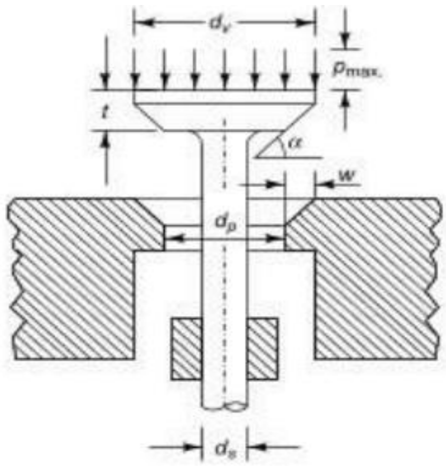

Figure 4.3: Forces on valves.

The diameter of the valve head ($\boldsymbol{d_v}$) is given by,

$$d_v = d_p + 2w = 17.941mm + 2 \times 1.0764mm$$

$$d_v = 20.0938mm \approx 20.1mm$$

Valve Stem Diameter ($\boldsymbol{d_s}$) (Patil et al., 2023)**:** The valve stem diameter is given by,

$$d_s = \frac{d_p}{8} + 4\ mm\ to\ d_s = \frac{d_p}{8} + 11mm \tag{4.6}$$

$$d_s = \frac{d_p}{8} + 4\ mm = \frac{17.941mm}{8} + 4\ mm$$

$$d_s = 6\ mm$$

Diameter of the valve head opening area$(\mathbf{d_3})$ see on figure 4.2 above:

$$d_3 = \sqrt{{d_p}^2 + {d_v}^2} = \sqrt{(17.942\, mm)^2 + (20.0938\, mm)^2}$$

$$d_3 = 26.93837713\text{mm}$$

The mass of the valve is taken as about 0.1 to 0.3 kg (Khurmi & Gupta, 2005), so in this design of engine valve the mass is assumed to be 0.2 kg.

Check the diameter and size of the valve port to know whether the design is safe or not (Patil et al., 2023):

Diameter check:

$$({d_3}^2 - {d_v}^2) \geq {d_p}^2 \qquad (4.7)$$

$$0.7854\,((26.93837713\text{mm})^2 - (20.0938mm)^2) \geq 0.7854\,(17.941mm)^2$$

$321.915364 \geq 321.879481$, this is true so design is safe.

Size of valve ports Check:

$$\mathrm{v_g} \times a_p = a \times v_{mp} \qquad (4.8)$$

Where; $\mathrm{v_g}$ = mean velocity of exhaust gas $= 90\,\frac{\text{m}}{\text{s}}$.

a = Area of the piston $= 2.5072 \times 10^{-3} m^2$

a_p = area of the exhaust port $= 0.00025281 m^2$

v_{mp} = mean velocity of the piston $= 9.075\, m/s$

$$90\text{ m/s} \times 0.00025281\, m^2 = 2.5072 \times 10^{-3} m^2 \times 9.075\, m/s$$

$0.022753 = 0.022753$, Hence the design is safe.

B. Exhaust valve spring design and selection:

In this case, only the forces and the deflection are considered design valve actuation system for this particular engine. The spring maximum deflection (compressed length) should be to the minimum of the value of the maximum lift. So, in this case, it is taken as a 6 mm deflection.

Let's assume the greatest back pressure when the exhaust valve opens is 0.4 N/mm2 and the greatest suction pressure is 0.02 N/mm2 below atmosphere.

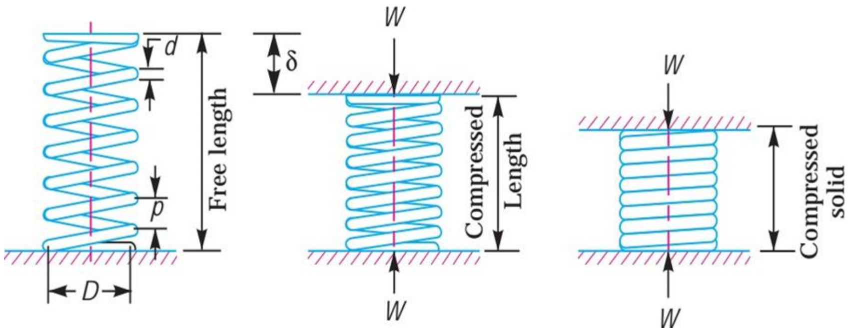

Figure 4.4: Compression spring nomenclature (Khurmi & Gupta, 2005).

Let's first determine the overall load on the valve spring. It is well known that the initial spring force takes the valve's weight into account.

- The initial spring force, considering weight of the valve, is given by the force on the valve tending to draw it into the cylinder on the suction stroke (Khurmi & Gupta, 2005).

$$F_s = \frac{\pi}{4}(d_v)^2 \times P_s - W \qquad (4.9)$$

Where: d_v= is diameter of the valve head.

P_s = Is the greatest suction pressure

F_S = intial spring force of spring

W = Is the weight of the valve$(m \times g)$,

m - is the mass of the valve

g = Is gravity

$$F_s = \frac{\pi}{4}(d_v)^2 \times P_s - W$$

$$F_s = \frac{\pi}{4}(20.0928\text{mm})^2 \times 0.02 \frac{\text{N}}{mm^2} - (0.2 \text{ kg} \times 9.81 \frac{\text{m}}{s^2})$$

$$F_s = 4.38 \text{ N}$$

- It‘s known that gas load on the exhaust valve is given by (Khurmi & Gupta, 2005);

$$F_{gv} = \frac{\pi}{4}(d_v)^2 \times P_c \qquad (4.10)$$

Where: F_{gv} is gas load on the valve,

P_c is the greatest back pressure.

$$F_{gv} = \frac{\pi}{4}(20.0928\text{mm})^2 \times 0.4 \frac{\text{N}}{mm^2}$$

$$F_{gv} = 126.833 \text{ N}$$

- Weight of the valve's related components,,

$$W = m \times g = 0.2 \text{ kg} \times 9.81 \frac{\text{m}}{s^2} = 1.962\ N$$

- Total load on the valve (F_v) is;

$$F_v = F_{gv} + W$$

$$F_v = 126.833 \text{ N} + 1.962 \text{ N}$$

$$F_v = 128.795 \text{ N}$$

- The force due to valve acceleration (F_a) may be obtained as discussed below (Khurmi & Gupta, 2005);

$$F_a = m \times a_v + W = \Delta x \times K + W \tag{4.11}$$

$Where;\, a_v$ is valve acceleration;

K is stiffness of the spring;

Δx is change in length of the spring(deflection δ).

Since the change in deflection can be greater than or equal to the maximum lift of the valve, let us assume that change in length of the spring during maximum load is equal to the lift is taken as approximate value of 6mm and stiffness of the spring is 10.557 N/mm.

$$F_a = \Delta x \times K + W$$

$$F_a = 6\text{mm} \times 10.557 \frac{\text{N}}{mm} + 1.962 \text{ N}$$

$$F_a = 65.304 \text{ N}$$

- Maximum load on the valve actuating component to operate the exhaust valve is obtained as;

$$F_e = F_v + F_a + F_s \tag{4.12}$$

Maximum load on the valve actuating component to operate the intake valve is obtained as;

$$F_{sp} = F_a + F_s \tag{4.13}$$

Since the maximum load on the valve actuating component to operate the exhaust valve is more than that of inlet valve, therefore, the valve actuating component (valve pushing component) must be designed on the basis of maximum load to the valve actuating component for exhaust valve.

Thus, the equivalent load should be applied to operate the exhaust valve is Fe;

$$F_e = F_v + F_a + F_s$$

$$F_e = 128.795 \text{ N} + 65.304 \text{ N} + 4.38 \text{ N}$$

$$F_e = 198.479 \text{ N}$$

The selected engine model uses the oil tempered steel wire for the valve spring, helical coil spring with round wire (See table 3 in the material selection section).

- The total load on the spring (F_{sp}) for the designing of the valve spring is;

Total load on the spring (F_{sp}) = Initial spring force (F_s) + load at full lift (F_a)

$$F_{sp} = F_a + F_s$$

$$F_{sp} = 65.304\ N + 4.38\ N$$

$$F_{sp} = 69.684\ N$$

Maximum shear stress induced in the wire (τ)(Khurmi & Gupta, 2005) given by;

$$\tau = k \times \frac{8 \times F_{sp} \times D}{\pi \times d^3} = k \times \frac{8 \times F_{sp} \times C}{\pi \times d^2} \qquad (4.14)$$

Where; F_{sp} is total load on the spring,

K is Wahl's stress factor

C is spring index, $\frac{D}{d} = C$

D is mean diameter of spring coil,

d is diameter of spring wire

It's know that Wahl's stress factor given by;

$$K = \frac{4C-1}{4C-4} + \frac{0.615}{C} \qquad (4.15)$$

The values of K for a given spring index (C) (Khurmi & Gupta, 2005) may be obtained from the graph as shown in Fig. 3.10.

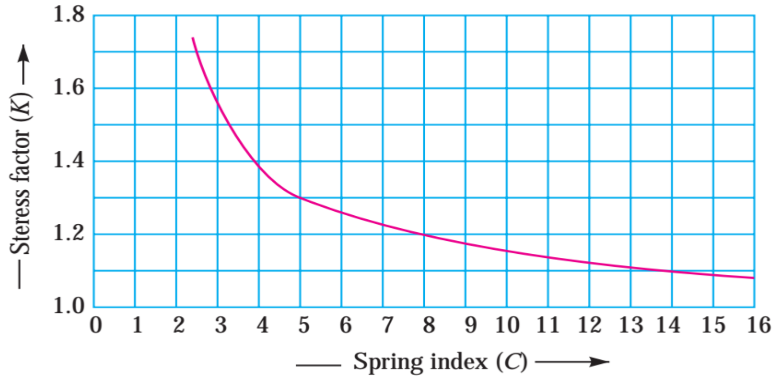

Figure 4.5 Graph of spring index related to stress factor.

From Fig. 4.5 as shown above, Wahl's stress factor increases very rapidly as the spring index decreases. The majority of springs used in machinery have a spring index greater than 3. So let's take $C = 6$, i.e $D = 6d$. then find whale's stress factor.

$$K = \frac{4C-1}{4C-4} + \frac{0.615}{C} = \frac{4 \times 6 - 1}{4 \times 6 - 4} + \frac{0.615}{6}$$

$$K = 1.2525$$

Now calculate the diameter of spring wire using maximum shear stress ($\boldsymbol{\tau}$) formula;

$$\tau = k \times \frac{8 \times F_{sp} \times C}{\pi \times d^2}, \quad \text{since } \tau = \tau_{allowable} = 420\ N/mm^2$$

$$420\ N/mm^2 = 1.2525 \times \frac{8 \times 69.684\ \text{N} \times 6}{\pi \times d^2}$$

$$d = \sqrt{\frac{(1.2525 \times 8 \times 69.684\ N \times 6) \times mm^2}{420\ N \times \pi}}$$

$$d = 1.7819\ mm$$

So by using this dimension, the standard size of the wire is SWG 15 having diameter $(\ d\ )\ =\ 1.829\ mm.$ (See table A-2 in the appendix).

Therefore, the mean diameter of the spring coil is D = 6 × 1.829mm = 10.974mm. And outer diameter of the spring coil is;

$$Do\ =\ D\ +\ d \tag{4.16}$$

$$Do\ =\ 10.974\text{mm} + 1.829\text{mm}$$

$$Do\ =\ 12.803\text{mm}\ =\ 13\text{mm}$$

- **Number of turns of the coil in exahust valve spring;**

Let n = the coil's number of active turns.

Maximum compression of the spring determined by using the following equation;

$$\delta = \frac{8 \times F_{sp} \times C^3 \times n}{G \times d} \tag{4.17}$$

Where; n is number of active turns of the coil, G is modulus of rigidity (= 80 GPa), $\delta = maximum\ compression\ of\ spring (= 6mm),$ thus;

$$6mm = \frac{8 \times 69.684\ \text{N}\ \times 6^3 \times n}{(80kN/mm^2) \times (1.829\text{mm})}$$

$n =\ 7.29 \approx 8.$ Therefore, the number of active turns of coil is 8.

The spring is square and ground ends, so for square and ground ends the total number of turns is;

$$n' = n + 2 \tag{4.18}$$

$$n' = 8 + 2 = 10$$

Since the compression produced under the load of 65.304 N is 6mm (i.e. equal to full valve lift), therefore, maximum compression produced (δ_{max}) under the maximum load of spring,Fsp = 69.684 N is;

$$\delta_{max} =\ \frac{\delta}{\text{F}_\text{a}} \times \text{F}_\text{sp} = \frac{6mm}{65.304\ N} \times 69.684\ N$$

$$\delta_{max} = 6.4 \text{ mm}$$

Then, the free length of the spring (L_f) from the selected model is 33.5mm, and then the pitch of the coil(p_c) is;

$$p_c = \frac{\text{Free length of coil}}{\text{Total number of turns+1}} = \frac{L_f}{n'-1} \quad (4.19)$$

$$p_c = \frac{33.5\ mm}{10-1} = 3.72\ mm$$

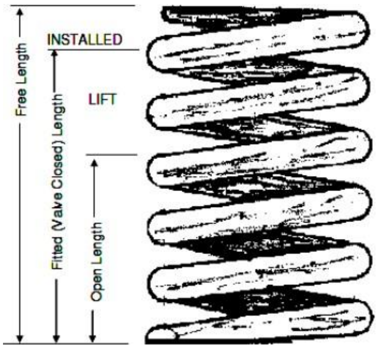

Figure 4.6: Nomenclature of the spring installed and open/compressed length.

The installed length of the spring is taken as 33.5 mm by considering the free length of the spring. This means that it has 0.4mm deflection.

I. Intake valve and spring design

The diameters of intake valves are generally 10 to 20% greater than diameter of exhaust valves. Assume the intake valve is 15% greater than the diameter of the exhaust valve. So, the basic parameters of the intake valves are given in table 4.2 as follows:

Table 4.2: Intake valve dimensions

Parameters	**Value**
Valve Port Diameter(d_1 or d_p)	20.7mm
Valve Face Angle (a_v)	30^0
Maximum Valve Lift (h_{max})	5.9mm ≈ $6mm$
Margin Thickness (t)	1.5mm
Valve Face Width (b)	≈ 1.242 mm
Valve Head Diameter (d_2 or d_v)	23.12mm
Valve Stem Diameter (d_0)	6 mm
Valve guide bore diameter	6.03 mm
Mass of the valve (m)	0.23kg

- **Intake valve spring design;**

A valve spring is wrapped around the valve stem and secured in position with a retainer. Its main function is to control the entire valve-train, ensuring that the proper amount of spring pressure is applied consistently to prevent valve bounce. Let's determine the valve spring's total load. The initial spring force consideringweight of the valve by using equation (4.9).

$$F_s = \text{Initial spring force}$$

$$F_s = \frac{\pi}{4}(d_v)^2 \times P_s - W$$

Where; d_v is diameter of the valve head

P_s is the greatest suction pressure

W is the weight of the valve(m. g) m is mass of the valve

g is gravity.

$$F_s = \frac{\pi}{4}(23.12\ \text{mm})^2 \times 0.02\ \text{N}/_{mm^2} - (0.23\text{kg} \times 9.81\ \text{m}/_{s^2})$$

$$F_s = 6.14\ \text{N}$$

- The force due to valve acceleration (F_a) may be obtained by using formula in $eq(4.11)$ as discussed below:

$$F_a = m \times a_v + W = \Delta x \times K + W$$

Where; a_v is valve acceleration.

K is stiffness of the spring.

Δx is change in length of the spring (deflection δ).

Since the change in deflection can be greater than or equal to the maximum lift of the valve, let us assume that the change in length of the spring during the maximum load is equal to the lift. This is taken as an approximate value of 6 mm. As previously mentioned, K = 10.55 N/mm.

$$F_a = \Delta x \times K + W = 6\,mm \times 10.55\frac{N}{mm} + 2.2563\,N$$

$$F_a = 65.56\ \text{N}$$

Total load on the spring (F_{sp}) for the designing of the valve spring is calculated by using $eq(4.13)$;

$$F_{sp} = F_a + F_s$$

$$F_{sp} = 65.56\ \text{N} + 6.14\ \text{N}$$

$$F_{sp} = 71.7\ \text{N}$$

To find the diameter of spring wire first find Wahl‘s stress factor, by using known formula:

$$\mathrm{K} = \frac{4C-1}{4C-4} + \frac{0.615}{C}$$

$$\text{Where: K is Wahl‘s stress factor}$$

$$\text{C is the spring index} = \mathrm{D/d}$$

$$\text{D is Mean diameter of the spring coil, and}$$

$$\text{d is Diameter of the spring wire.}$$

Taking C=6, i.e. D=6d;

$$\mathrm{K} = \frac{4\times 6-1}{4\times 6-4} + \frac{0.615}{6} = 1.2525$$

Now, maximum shear stress(τ)is given by;

$$\tau = K\frac{8\times F_{sp}\times C}{\pi d^2}$$

$$420\ N/mm^2 = 1.2525\ \times\frac{8\times 71.7\ \mathrm{N}\times 6}{\pi d^2}$$

$$d = \sqrt{\frac{1.2525\times 8\times 71.7\ \mathrm{N}\times 6}{420N/mm^2\times\pi}} = 1.807\ mm$$

$$d = 1.807\ mm$$

The standard size of the wire is SWG 15 having diameter (d) = 1.829 mm. (See Table 4.2 above) Therefore, the mean diameter of the spring coil is $\mathrm{D} = \mathrm{Cd} = 6\times 1.829\mathrm{mm}\approx 11\mathrm{mm}$ and outer diameter of the spring coil is;

$$\mathrm{D_o} = \mathrm{D} + \mathrm{d} = 11\mathrm{mm} + 1.829\mathrm{mm}$$

$$\mathrm{D_o} = 12.829\ \mathrm{mm}\approx 13\ \mathrm{mm}$$

- **Number of turns of the coil in the intake valve spring;**

Let n = the coil's number of active turns. And the maximum compression of the spring is given by eq(4.17);

$$\delta = \frac{8\times F_{sp}\times C^3\times n}{G\times d}$$

Where; G is modulus of rigidity = 80GPa.

$$6\ mm = \frac{8\times 71.7\ \mathrm{N}\times (6)^3\times n}{80k\dfrac{N}{mm^2}\times 1.829\mathrm{mm}}$$

$$n = 7.086\approx 8$$

The spring is square and ground ends, so for this case, the total number of turns using

$eq(4.18)$ is;

$$n' = n + 2$$

$$n' = 8 + 2 = 10$$

Since the compression produced under the load of 65.56 N is 6mm (i.e. equal to full valve lift), therefore, maximum compression produced (δ_{max}) under the maximum load of $F_{sp} = 71.7\ N$ is;

$$\delta_{max} = \frac{\delta}{\mathrm{F_a}} \times \mathrm{F_{sp}} = \frac{6\mathrm{mm}}{65.56\ \mathrm{N}} \times 71.7\ N$$

$$\delta_{max} = 6.56\ \mathrm{mm}$$

Then, the free length of the intake valve spring (L_f) for the selected model is 33.5 mm, and the pitch of the coil is determined by using the equation $eq(4.19)$;

$$\mathrm{p_c} = \frac{L_f}{n' - 1} = \frac{33.5\ mm}{10 - 1} = 3.72\ mm$$

The installed length of the spring is taken as 33.5 mm by considering the free length of the spring. This means that it has 0.5 mm of deflection. Since the exhaust and intake valves need different amounts of force to operate in proper condition, the required actuating system solenoid of the two valves have in different capacity; but in this research design, the solenoids and springs are taken as they have the same capacity depending on the exhaust valve requirements.

- **Valve spring fatigue analysis:**

Valve spring fatigue analysis is an important aspect of engine design and performance evaluation. Valve springs are crucial components in internal combustion engine that control the opening and closing of the engine's valves. They are subjected to high loads and cyclic stress which can lead to fatigue failure over time.

To perform fatigue analysis on a valve spring that is made of oil tampered steel, we consider various factors such as applied force, spring dimensions and material properties.

The spring analysis is based on the maximum load applied to the exhaust valve, so analysis is done on the exhaust valve spring and uses its dimensions for analysis.

Oil tempered steel is a common choice for valve springs due to its good combination of strength, ductility, and fatigue resistance. Typical ranges for oil tempered steel used in valve springs:

- Ultimate tensile strength (S_{ut}): $1650 - 2930\ MPa$ ($depending\ on\ specific\ grade$)

- Fatigue strength at 10^7 cycles (S_f): $1200 - 1500\ MPa\ at\ 10^7\ cycles$. This information can be estimated from N-S curves for specific oil tempered steel grades or obtained from manufacturer's data sheets (Izumida et al., 2023).

Material properties and other requirements for fatigue analysis are:

- Spring material: oil tempered steel
- $s_{ut} = 1800MPa\ (asumed\ valve\ from\ the\ above\ range)$
- $s_f = 1300MPa\ (assumed\ value\ from\ above\ reference\ ranges\ for\ 10^7 cycles)$
- Applied force =393.82N.
- $Outer\ diameter\ (D_O)$: $13\ mm,\ and$ Wire diameter (d): 1.829 mm
- Mean diameter (D_m): 11 mm and $Number\ of\ active\ coils\ (N_a)$: 8.

Now first determine the spring constant (k): modulus of rigidity for oil tempered steel is 80GPa. This is determined by rearranging using equation (4.14).

$$k = \frac{(\tau \times \pi \times d^4)}{8 \times N_a \times (D_m)^3} = \frac{80000MPa \times \pi \times (1.829mm)^4}{8 \times 8 \times (11mm)^3}$$

$$k = \frac{80000MPa \times \pi \times (1.829mm)^4}{8 \times 8 \times (11mm)^3} = 33.02$$

Secondly, shear stress produced due to the applied load is given by;

$$\tau = \frac{F}{A} = \frac{4F}{\pi \times ({D_o}^2 - d^2)} = \frac{393.82N \times 4}{\pi \times ((13mm)^2 - (1.829mm)^2)}$$

$$\tau = 3.027MPa$$

Thirdly, equivalent stress(σ_{eq}); assuming equivalent stress is equal to shear stress for this case.

$$\sigma_{eq} = \tau = 3.027MPa$$

Fourthly, determine the safety factor (SF) to know whether the design is safe or not; it is determined by Using the Goodman Equation;

$$SF = \frac{s_{ut} - \sigma_{eq}}{s_{ut} - s_f} \tag{4.20}$$

$$SF = \frac{1800MPa - 3.027MPa}{1800MPa - 1300MPa} = 3.594$$

The safety factor (SF) is 3.594, which indicates a significant margin of safety under the applied load based on the Goodman Equation. This suggests the design is robust against fatigue failure.

Based on the calculations and the assumed material properties, the valve spring design appears safe under the given applied force and with the updated number of active coils.

However, for a definitive assessment and optimal design, considering the factors mentioned above and potentially utilizing advanced analysis techniques is crucial.

4.2.4 Valve Timing Calculations

The engine has different speed of operation, i.e. from 1000 rpm to 5500 rpm speed range. And for this ranges it has different speed and time of opening and closing of valves. These valves are intake and exhaust valves.

A. During low engine speed

The engine has four strokes, so for one complete cycle of combustion, the crank shaft rotates two revolutions or 720^0. Thus, at low engine speed (1000 RPM) the crank shaft rotates 1000 revolutions per 60seconds. Therefore, the time taken to complete cycle will be:

$$\mathrm{T} = \frac{2\mathrm{rev}*60}{N} \tag{4.21}$$

$$T = \frac{2\mathrm{rev} \times 60\mathrm{sec}}{1000rev} = 0.12 \text{ sec.}$$

- **For exhaust valve:**

To calculate the duration of any exhaust valve timing event, add 180° to the exhaust opening and closing times (Rick Kertes, 2016).

- EVO = 25^0 BBDC and EVC = 5^0 ATDC.

The total duration of valve opening (θ_{dvo});

$$\theta_{dvo} = 180^{\,0} + \theta_B + \theta_A \tag{4.22}$$

Where: $\Theta_B -$ opening angle before.

$\Theta_B -$ opening angle after.

$$\theta_{dvo} = 180^{\,0} + 25^0 + 5^0$$

$$\theta_{dvo} = 210^0$$

During low speed engine operation, the total time taken to exhaust valve stays open (t_{evo});

$$t_{evo} = \frac{60\times\ \theta_{dvo}}{N\times 360^0} \tag{4.23}$$

Where; N – is the engine speed

$$t_{evo} = \frac{60\times\ 210^0}{1000\times 360^0} = 0.035\ sec$$

For maximum lift of exhaust valves the time taken (t_{ehmax}) is half of the total time (t_{evo}).

$$t_{ehmax} = \frac{t_{evo}}{2} = \frac{0.035\,sec}{2}$$

$$t_{ehmax} = 0.0175\,sec$$

- **For intake valve**:

To calculate the duration of any intake valve timing event, add 180° to the intake opening and closing times (Rick Kertes, 2016).

- IVO = 10^0 BTDC and IVC = 20^0 ABDC.

The total duration of valve opening (θ_{dvo}) by using eq(3.22);

$$\theta_{dvo} \;=\; 180\,^0 + \;\theta_B \;+\; \theta_A$$

$$\theta_{dvo} \;=\; 180\,^0 + 10^0 \;+ 20^0 = 210^0$$

During low speed engine operation, the total time taken to intake valve stays open;

$$t_{ivo} = \frac{60 \times \quad \theta_{dvo}}{N \times 360^0} = \frac{60\text{ sec} \times \quad 210^0}{1000 \times 360^0} = 0.035\text{ sec}$$

The time taken for maximum lift of the intake valve (t_{ihmx});

$$t_{ihmax} = \frac{t_{ivo}}{2} = \frac{0.035\,sec}{2} = 0.0175\,sec$$

- **Duration of the Compression and Expansion Process;**

In compression and expansion strokes, the crankshaft rotates for 300° out of the full 720°; it rotates in 0.12 sec. Therefore, the time spent during the compression and expansion stroke;

$$T_{cE} = \frac{\theta_{CE} \times T}{720^0}$$

$$\text{Where; } \mathrm{T_{cE}} - \text{is time spent during comprssion and expansion.}$$

$$\theta_{\mathrm{CE}} - \text{duration of copression and expansion.}$$

$$\mathrm{T} - \text{time taken to one complete cycle}$$

$$T_{cE} = \frac{\theta_{CE} \times T}{720^0} = \frac{300^0 \times 0.12sec}{720^0} = \; 0.05\,sec$$

Time of valve overlap (T_{vo}) between initialization of the intake stroke and completion of the exhaust stroke:

First find valve overlap duration (θ_{dvo});

$$\theta_{dvo} = 10^0\,BTDC + 5^0 ATDC = 15^0$$

Time of overlap (T_{vo}) during low engine speed is given by;

$$T_{vo} = \frac{\theta_{dvo} \times T}{720^0} = \frac{15^0 \times 0.12\,sec}{720^0} = \; 0.0025\,sec$$

- **Formula Generation to Govern the Valve Timing:**

As RPM varies, IVC, EVO, and EVC will vary in some factors to increase the opening degree of duration before and after TDC and BDC. So, it is possible to generate some formula that governs the opening and closing of valves by considering the given optimum valve timing specification of the selected engine model. Intake valve opening angle before TDC at all engine speeds is always equal to ten degrees for better engine operation and efficiency, but all others (IVC,IVO, and EVC) vary by some factors. This is done by using some superposition analysis method.

IVC angle after BDC is;

$$2.2 \times \alpha x = by \qquad (i)$$

EVO angle before BDC;

$$3.1 \times \alpha x = by \qquad (ii)$$

EVC angle after TDC;

$$1.375 \times \alpha x = by \qquad (ii)$$

Where; α- minimum speed (rpm), b- new speed (rpm), x- required degree of valve opening /closing/ and y- given degree of valve opening/closing/.

B. During high engine speed

The engine has four strokes, so for one complete cycle of combustion the crank shaft rotates two revolutions, or 720^0. Thus, at high engine speed (5500 RPM), the crank shaft rotates 5500 revs or revolutions per 60 seconds. Therefore, the time taken to complete one cycle will be:

$$T = \frac{2rev \times 60}{N} = \frac{2rev \times 60}{5500rev}$$

$$T = 0.02182\ sec$$

- **Exhaust valve:**

To calculate the duration of any exhaust valve timing event, add 180° to the exhaust opening and closing time.

- EVO = 45^0 BBDC and EVC = 20^0 ATDC (This are calculated based on the above formula)

The total duration of valve opening (θ_{dvo});

$$\theta_{dvo} = 180^{\,0} + \theta_B + \theta_A$$

$$\theta_{dvo} = 180^{\,0} + 45^0 + 20^0 = 245^0$$

$$\theta_{dvo} = 245^0$$

During low speed engine operation, the total time taken to exhaust valve stays open (t_{evo}) by using $eq(3.22)$;

$$t_{evo} = \frac{60 \times \quad \theta_{dvo}}{N \times 360^0} = \frac{60 \times 245^0}{5500 \times 360^0}$$

$$t_{evo} = 0.0074242\ sec$$

The time taken for the maximum lift of the exhaust valves (t_{ehmax}) is half of the total time (t_{evo});

$$t_{ehmax} = \frac{t_{evo}}{2} = \frac{0.0074242}{2} = 0.0037121\ sec$$

- **Intake valve:**

To calculate the duration of any intake valve timing event, add 180° to the intake opening and closing time.

- IVO = 10^0 BTDC and IVC = 50^0 ADC (This are calculated based on the above formula)

The total duration of intake valve opening (Θ_{dvo}) at high engine speed by using eq(4.22);

$$\theta_{dvo} = 180^{\ 0} + \theta_B + \theta_A$$

$$\theta_{dvo} = 180^{\ 0} + 10^0 + 50^0 = 240^0$$

During high speed engine operation, the total time taken to intake valve stays open;

$$t_{ivo} = \frac{60 \times \quad \theta_{dvo}}{N \times 360^0} = \frac{60\ \text{sec} \times \quad 240^0}{5500 \times 360^0} = 0.007273\ \text{sec}$$

The time taken for maximum lift of the intake valve (t_{ihmx}) at high engine speed is half of the total time (t_{ivo});

$$t_{ihmax} = \frac{t_{ivo}}{2} = \frac{0.007273\ \text{sec}}{2} = 0.0036364\ sec$$

Sample calculations of variable valve timing at different possible engine speeds are done. See thefollowing table.

Table 4.3: Sample opening duration of valves in different possible engine speeds.

Conditions	Engine Speed(RPM)					
	1000	2000	3500	4200	4800	5500
Intake valve stay open (in second)	0.035	0.01735	0.0106	0.00906	0.00811	0.00727
Exhaust valve stay open (in second)	0.035	0.01695	0.01052	0.00910	0.0082	0.00742

4.2.5 Required Power and Current Calculations for the Valve Actuation System Operation

From the above design, the equivalent load applied to operate the exhaust valve is greater than equivalent load applied to intake valves. So design and battery power selection depends on it.

Case 1: During low speed

The work done by the exhaust valve (since the exhaust valve needs more power supply, the battery selection will depend on it) is W (Kumar, 2020).

$$W = F \times d \tag{3.24}$$

$Where;\ W$ is work done during maximum lift of valve

$F\ is\ applied\ load\ to\ operate\ valve = 198.479$ N

$d\ is$ distance is equal to maximum lift, $d = 6mm$

$$W = F \times d = 198.379\ N \times 6mm$$

$$W = 1190.274\ Nmm = 1.190274\ \text{J}$$

Power (P) required operating the valve at low speed (Kumar, 2020):

$$P = \frac{w}{t} \tag{3.25}$$

Where; P is power required to operate the valve

W is work done during maximum lift of the valve

$t = t_{ehmax} \rightarrow$ Time taken of maximum lift of the valve $= 0.0175\ sec$

$$P = \frac{w}{t} = \frac{1.190274\ \text{J}}{0.0175\ sec} = 68.01565714\ watt$$

$$P = 68.016\ watt$$

Then the current (I) required can be obtained from the following relation (Howe, 2022);

$$P = V * I \tag{4.26}$$

Where, P is power required during maximum lift at low rpm.

V is battery voltage, 12v,

I is current required to actuate solenoid

$$\text{P} = \text{V} * \text{I} \rightarrow 68.01565714 = 12.5\text{v} \times \text{I}$$

$$\text{I} = 5.667971428\ \text{A} \approx 6\ \text{A}$$

Case 2: During highest speed

- Work done by the exhaust valve is the same as pervious calculated value using $eq(3.21)$. Which is: W =1.190274J, and time at high speed is:

$$t_{ehmax} = 0.0037121\, sec$$

The power required to operate the valve is given by using $eq(4.25)$:

$$P = \frac{w}{t} = \frac{1.190274\ \mathrm{J}}{0.0037121\, sec} = 320.6470731\, watt$$

$$P = 321\, watt$$

Then, the current (I) required can be obtained the above eq(4.26);

$$\mathrm{P = V * I} \rightarrow 320.6470731\, watt = 12.5\mathrm{v} \times \mathrm{I}$$

$$\mathrm{I} = 25.7 \text{ ampere}$$

So, for better operation and design, the exhaust valve solenoid should have P = 321 watts and I = 25.7 amperes with a voltage supply of 12.5 volts. The power required to operate the intake valve is much less than the power required operating the exhaust valve. So, the battery required for system operation depends on the maximum power required (the required power of the exhaust valve). Since the electromechanical valve actuation system uses a solenoid valve, there are many factors (like wire coil resistance) that reduce this supply of the battery, so it needs further design using a solenoid design to select the proper power source.

4.2.6 Solenoid Valve Design

A solenoid valve is an electromechanically operated valve. The features of solenoid valves vary in terms of the electric current they use, the intensity of the magnetic field they produce, the method by which they control the fluid, and the kind and properties of the fluid they regulate.

- **Air Gap**

The air gap is the distance between the electromagnet and the armature. The product to which the electromagnetic actuator is coupled determines the air gap's size. If the actuator was not connected to anything, the air gap would not exist because the parts would remain attracted to each other once the current was applied (McGraw, 2018).

- **Calculating force due to the coil and its design:**

The force due to the coil (the magnetic force acting on the armature or plunger) is obtained from the Lorentz force equation. Since the design of the solenoid is done based on the maximum load that applies to the valve, the maximum load (force) is on the exhaust valve, which is 198.479 N. The force due to the coil from the Lorentz force equation (Electrical Engineering Stack Exchange, 2024);

$$F = \frac{(NI)^2 \mu A}{2g^2} \tag{4.27}$$

Where: F - is maximum magnetic force in newton.

N - Number of turns of coil.

A - Cross sectional area of the electromagnet.

g - Least distance between the solenoid and the armature.

(The minimum is ≈ 0.02mm up to maximum lift). Since 0.02mm is the clearance between the armature and the top of electromagnetic coil.

μ - Permeability of free space = $4\pi \times 10^{-7}$

I - Current pass through the coil.

Equation 4.27 shows that the solenoid force depends on various design parameters such as the area of the coil (inner and outer diameters) of the solenoid, the number of coil turns, the air gap between the armature and the solenoid coil, and the input current.

The minimum gap between the armature and electromagnetic coil should be maintained to have no direct contact with them in order to control the impact load on each other. Since the exhaust valve steam has a 6 mm diameter, the inside diameter of the solenoid (coil) will be almost equal to it or greater, i.e., 8 mm, since one millimeter thick insulator guide liner is used to round the inner diameter. To determine the diameter of the copper wire of the solenoid that can handle the required current in order to produce the required magnetic force, the optimum dimension of the American wire gauge is used. The selected optimum AWG is 18; see the table in appendix A.

The table shows various data, including both the diameter of the various wire gauges and the allowable resistance based on a copper conductor with plastic insulation. The diameter of an A.W.G. wire is determined according to the following formula (Wikimedia Foundation, 2024):

$$d_n = 0.127\, mm \times 92^{\left(\frac{36-n}{39}\right)} \tag{4.28}$$

For gauges ranging from 36 to 0, the AWG size is represented by n, which is equal to −1 for No. 00, −2 for No. 000, and −3 for No. 0000. For this design, $n = 18$

$$d_n = 0.127\, mm \times 92^{\left(\frac{36-18}{39}\right)} = 1.02\, mm \approx 1\, mm.$$

Now, space is another limiting factor that needs to fix the value of the outer diameter of solenoid coil, which is 38 mm diameter(which is determined from the engine layout design) and inner diameter (hole diameter) of coil is plunger diameter plus 1mm insulation thick and diameter of wire (8mm +1mm = 9mm). The cross sectional area of electromagnet is given by;

$$A = \frac{\pi}{4}(D^2 - d^2) \tag{4.29}$$

Where: A - Cross sectional area.

D - Outer diameter of solenoid/ the armature diameter/.

d - Inner diameter (ole diameter).

$$A = \frac{\pi}{4}(D^2 - d^2) = \frac{\pi}{4}(38^2 - 9^2)$$

$$A = 1070.5mm^2 = 0.0010705m^2$$

The distance (air gap) between the solenoid and movable armature will vary from the minimum (allowable gap (distance)) or 0.02mm to the maximum lift of the value.

i.e., the range is 0.02mm ≤ g ≤ 6.02mm.

The current is approximately 25.7 ampere (obtained in the previous).Then from electromagneticforce equation 3.26; it is possible to get the number of turns,

$$\mathrm{F} = \frac{(\mathrm{NI})^2 \mu \mathrm{A}}{2\mathrm{g}^2}$$

At maximum distance or air gap (g = 0.00602 m);

$$198.479\mathrm{N} = \frac{(\mathrm{N} \times 25.7)^2 \times 4\pi \times 10^{-7} \times 1070.5\, mm^2}{2 \times (6.02\mathrm{mm})^2}$$

$$\mathrm{N} = \sqrt{\frac{2 \times (6.02\mathrm{mm})^2 \times 198.479}{(25.7)^2 \times 4\pi \times 10^{-7} \times 1070.5\, mm^2}} = 127.2440195 \approx 128 \text{ turns}$$

But to reduce the required amount of current required generating about 198.479 N force and increase the battery life, it is possible to use more number of turns of coil and reduce the supplied current amount (Magnetic Sensor, 1998). Thus, take 250 numbers of turns and the diameter of the wire approximately to one millimeter form previously calculated. In this case the equivalent current will be obtained from Lenz's law relation as (Blech, 1976);

$\Phi = \mu_0 n I$, but $\mathrm{n} = \frac{\mathrm{N}}{\mathrm{l}} \rightarrow \frac{\Phi \mathrm{l}}{\mu_0} = \mathrm{NI}$.

$$N_1 I_1 = NI \rightarrow I = {N_1 I_1}/{N} = \frac{128\ turns \times 25.65A}{250\ turns} \approx 13.2\ A$$

$$I = 13.2\ A$$

The length of the winding coil is l_c ; where d_w is wire diameter, D and d are outer and inner diametersof the solenoid coil (Had2Know, 2010) (Hedges, 2013).

$$\mathrm{N} = \frac{l_c}{d_w}\left(\frac{\mathrm{D}-\mathrm{d}}{2d_w}\right) \qquad (4.30)$$

$$250 = \frac{l_c}{1mm}\left(\frac{38\mathrm{mm} - 9\mathrm{mm}}{2 \times 1mm}\right) \rightarrow l_c = 17.24137931\ mm \approx 18\ mm$$

Now, the length of the wire in the coil is given by;

$$l_w = \pi\left(\frac{\mathrm{D}+\mathrm{d}}{2}\right) \times \mathrm{N} \qquad (4.31)$$

$$l_w = \pi\left(\frac{38\mathrm{mm}+9\mathrm{m}}{2}\right) \times 250 = 18456.85684\ \mathrm{mm}$$

$$l_w = 18.5\ \mathrm{m}$$

Area of the wire section is;

$$a_w = \frac{\pi(d_w)^2}{4} = \frac{\pi(1mm)^2}{4} = 0.7854\mathrm{mm2}$$

$$a_w = 7.854 \times 10^{-7} m^2$$

And then the resistance (R) of wire in the coil (Scott, 2024);

$$R = \frac{\rho_w l_w}{a_w} \qquad (4.32)$$

Where, ρ_w= Resistivity copper wire which is $1.724 \times 10^{-8} ohm - m$,

l_w = Wire length=18.5 m, a_w = Cross-sectional area.

$$R = \frac{(1.724 \times 10^{-8}\mathrm{ohm} - \mathrm{m}) \times 18.5\ \mathrm{m}}{7.854 \times 10^{-7} m^2} = 0.405\ ohm$$

Since we have a 12.5 V battery current will be,

$$I = \frac{V}{R} = \frac{12.5\ volt}{0.405\ ohm} = 30.8 \approx 30.8\ A$$

Inductance of the coil of wire (L) is given by (EETech Media, 2024) (Guelph, 2000):

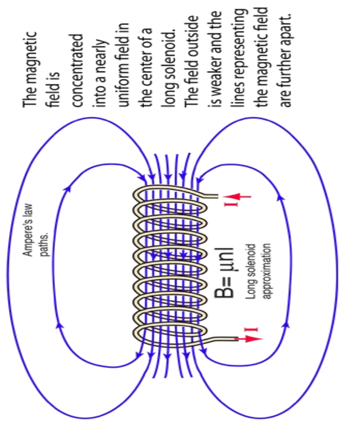

Figure 4.7 Inductance of solenoid

$$L = \frac{\mu N^2 A}{l} \tag{4.33}$$

Where L is inductance of coil of wire, l_w is length of the wire solenoid coil and μ is permeability of free space and A is cross-sectional area of wire.

$$L = \frac{(4\,\pi \times 10^{-7} H/m) \times 250^2 \times (7.854\ \times\ 10^{-7} m^2)}{18.5\,m}$$

$$L = 1.024 \times 10^{-4}\ H$$

Magnetic flux (Φ) is a measurement of the total magnetic field which passes through a given area (Kahan Acadamy, 2024). It is obtained by;

$\Phi = \mathrm{BA}, \mathrm{Since}\ B\ = \frac{(\mu \times NIA)}{g} = \frac{IL}{N}$, where, B is magnetic flux density in weber, A cross sectional area in m^2, g is max. Lift distance of valve is 0.006m, N is number of turns is 250, I is current supplied, A is cross-sectional area of solenoid.

$$\phi = \frac{(\mu \times NIA)}{g} \tag{4.34}$$

$$\phi = \frac{4\pi \times \frac{10^{-7} H}{m} \times 250 \times 13.2\ A \times 0.0010705\ m^2}{0.006 m}$$

$$\phi = 0.000739876486\ weber$$

Magnetic flux density (B) is;

It is determined by the flux per unit area that travels at a right angle to the flux through a plane. It is usually designed by the capital letter B and is measured in weber/meter square (BL Theraja, 1959).

$$\mathrm{B} = \frac{\Phi}{A} = \frac{0.000739876486\ weber}{0.0010705\ m^2} = \ 0.6911503839\ weber/m^2$$

$$\mathrm{B} = 0.69\ Tesla,$$

- **Forces on current carrying wire in the magnetic fields** (BL Theraja, 1959)**;**

When a current carrying coiled wire is placed at right angle in a magnetic field, the force experienced on a plunger is given by (Gross, 2006):

$$F = B \times I \times l_w \tag{4.35}$$

$$F = 0.691151\ Tesla \times 30.8A \times 18.5\ m$$

$$F = 393.82\ N$$

From this there is some magnetic force lost by the resistance of the coil. But from these the valve train needs only about 198.479 N, so the calculated design force is too satisfactory.

The power developed by the solenoid is P from equation 4.25 and 4.26;

$$P = V \times I = \frac{W}{t}$$

Where P is power, W is work done, I stands for current, V voltage and t is time taken.

$$P = V \times I = 12.5v \times 30.8A = 385\ watt$$

Power due to work done from equation 4.26;

$$P = \frac{W}{t} = \frac{F \times d}{t}$$

Then the time taken can be calculated as follows; at initial equilibrium condition the valve is installed at half lift of the valve or there is three millimeter deflection of valve spring. Thus,

$$385\ watt = \frac{393.82\ N \times 0.003m}{t} \rightarrow t = \frac{393.82\ N \times 0.003m}{385\ watt}$$

$$t = 0.00306873\ second$$

This calculated time is a response time of the solenoid valve, which is designed in this section (in the above). Since the design of the solenoid valve is designed on the basis of the maximum load requirements, it can use for both the intake and exhaust valves, i.e. the same capacity and specification solenoid valve is used.

- **Induced electromotive force can be calculated from the flux linkage is λ;**

If the current I created the magnetic flux density B, then the flux linkage is given by $\lambda =$ LI. Here, $emf\ =\ L\ di/dt$, where L is the coil's self-inductance. In a coil with N turns, the induced emf is equal to N times the rate at which the magnetic flux changes on a single coil loop. But electromotive force can be:

$$e.m.f = \frac{Ld(I)}{dt} = \frac{L\Delta I}{\Delta t} \tag{4.36}$$

$$e.m.f = \frac{1.024 \times 10^{-4}H\ (30.8A - 13.2\ A)}{0.00306873\ second}$$

$$e.m.f = 0.59V$$

The electromagnetic correlation can be established with Kirchhoff’s law and it is given as follows.

$$e(t) = RI(t) + \frac{Ld(I)}{dt} \tag{4.37}$$

$$e(t) = 0.405\ ohms \times 30.8A + 0.59V$$

$$e(t) \approx 13.3V$$

Here, e is the input voltage (V), R is the coil resistance (ohm), L is the inductance (Henry) and I is the current (ampere) and t is response time (sec).

Magneto motive Force$(\boldsymbol{m.m.f})$: The current flowing in an electric circuit is due to the existence of electromotive force similarly magneto motive force $(m.m.f)$ is required to drive the magnetic flux in the magnetic circuit. Magneto motive force is the magnetic pressure that creates the magnetic flux in a magnetic circuit. The SI unit of $m.m.f$ is Ampere-turn (AT) (Iii, 2020). Magneto motive force $(m.m.f.)$ can be calculated as follows:

$$m.m.f = \left[\frac{g}{\mu A}\right] \times \phi \tag{4.38}$$

$$m.m.f = \left[\frac{0.006m}{4\pi \times \frac{10^{-7}H}{m} \times 0.0010705m^2}\right] \times 0.000739876486\ HA$$

$$m.m.f = 3300\ AT$$

Thus the new source is about 14 volt and the power will be 385 watt.

4.2.7 Battery capacity

The battery that is selected to the best operation of the system is on the basis of the above calculation and there is 14 volt and 30.8 ampere current with the required power development of 385 watt, so the ampere hour is calculated by considering 20 hour of operation.

$$Ampere - Hour = \frac{\text{required power} \times \text{operating time}}{\text{requred battery volt}} \tag{4.39}$$

$$Ampere - Hour = \frac{385\ watt \times 20\ hour}{14\ volt}$$

$$Ampere - Hour = 550\ AH$$

For good operation of the system rechargeable 14volt and 30.8ampere power source /battery/ should be used.

4.2.8 Design of Armature with Plunger

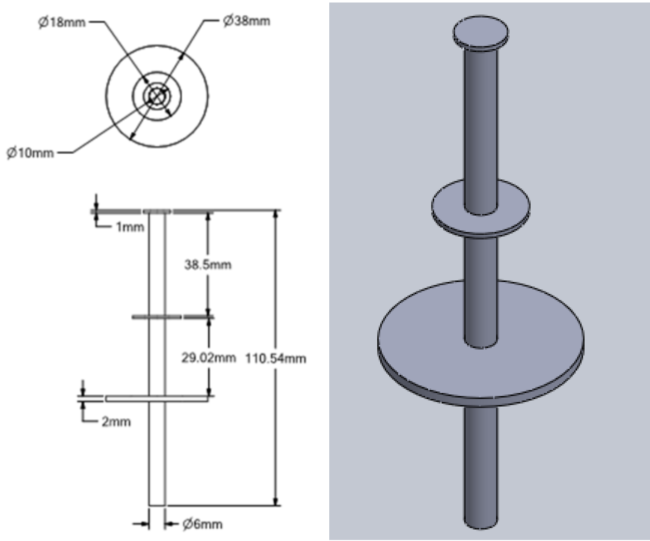

Figure 4.8: Basic dimensions of the armature with plunger. All in mm

Checking the compressive stress (σ_c) on the plunger; F_1 is the maximum force applied on the plunger, and let us consider as one end is fixed and the other is exposed to maximum load F_1.

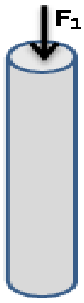

Figure 4.9 Compressive loads on the plunger.

Then the compressive stress (Bansal, 2009) is given by:

$$\sigma_c = \frac{F}{A}, since\ the\ member\ is\ short\ column \tag{4.40}$$

where, F is axial load on the member, A is Cross sectional area of body/plunger.

$$A = \frac{\pi}{4}d^2 = \frac{\pi}{4} \times (6mm)^2 = 28.274mm^2\ and\ \mathrm{F} = \mathrm{F}_1 = 393.82\ N$$

$$\sigma_c = \frac{F}{A} = \frac{393.82\ N}{28.274mm^2}$$

$$\sigma_c = 13.93N/mm^2$$

Since the calculated compressive stress is much less than the allowable compressive stress 129 MPa) of the stainless steel. So the design is safe.

Mass of armature with plunger is m;

$$m = \rho \times V \tag{4.41}$$

Where V is volume, ρ is density, and m is mass.

$$m_1 = density\ of\ stainless\ steel \times\ volume\ of\ plunger$$

$$m_2 = density\ of\ iron \times\ volume\ of\ armature$$

$$Total\ mass\ (m) = m_1 + m_2\ ,$$

Calculating the volume;

$$Volume\ of\ plunger = \frac{\pi}{4} D^2 \times h = \frac{\pi}{4}(0.006m)^2 \times 0.10404m = 2.66 \times 10^{-6} m^3$$

$$Volume\ of\ armature = \frac{\pi}{4}(D^2 - d^2) \times h = \frac{\pi}{4}((0.038m)^2 - (0.006m)^2) \times 0.002m$$

$$= 2.212 \times 10^{-6} m^3$$

The given densities for stainless steel and iron are 7700 kg/m^3 and 7860 kg/m^3 respectively.

$$Total\ mass\ (m) = 7700 \frac{kg}{m^3} \times 2.66 \times 10^{-6} m^3 + \frac{7860kg}{m^3} \times 2.212 \times 10^{-6} m^3$$

$$= 0.204kg,$$

$$\text{Attractive force by mass of plunger and armature is equals to weight} = \text{mg}$$

$$= 0.204\text{kg} \times \frac{9.81\text{m}}{\text{s}^2} = 2.0012\text{N}$$

Relative to the generated magnetic force the loss of attractive force by the mass of the armature and plunger is very small, so it is assumed as it has no effect on the system.

4.2.9 Back Electromotive Force and Circuit Damage Control System

Operating some kind of electromagnetic locking mechanism is nearly always required for physical electronic access control. It could be a tiny solenoid inside a strike or bolt, or it could be a strong magnet. When the electromagnet is powered, it will store energy. When the supply is turned off, it will produce a "back EMF," also known as a counter EMF (CEMF). Current passes through the electromagnet coil's windings when the supply is connected. The final resting current is determined by the direct current resistance of the coil winding and connecting wires. This current produces a magnetizing field which aligns the magnetic domains in the metal core of the electromagnet. This alignment re-enforces the field making magnetic force greater but also storing a lot more energy in the process (BSB, 2024).

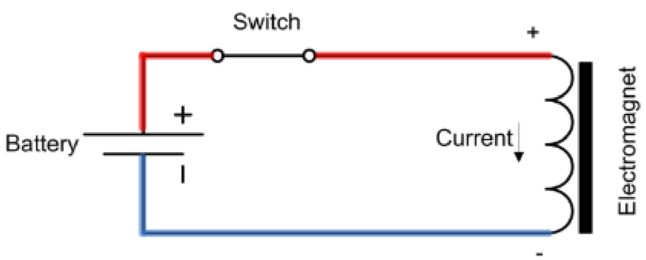

Figure 4.10 simple circuit of electromagnet (BSB, 2024)

If this back EMF is not suppressed or controlled, it will produce extremely high voltages, which can then:

- Reduce switch life by causing arcing at contacts
- Generate interference
- Damage electronics and Cause loss of data

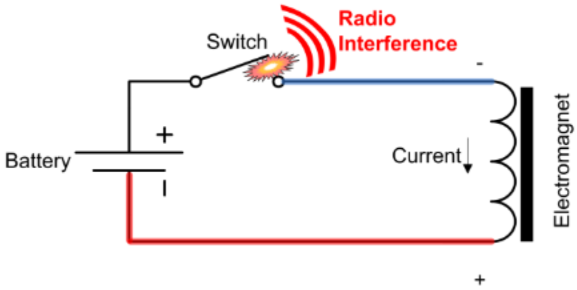

Figure 4.11: Back EMF generates interference/arcing (BSB, 2024).

Back EMF can be managed but cannot be avoided. The goal of back EMF suppression is to avoid extremely high voltages and release the stored energy in a regulated manner.

- **Metal Oxide Varistor (MOV)**

The MOV is already selected in the previous section by different satisfactory reasons. The installation circuit seam as follows.

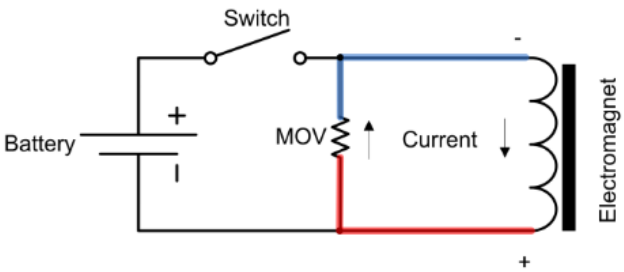

Figure 4.12 Electrical circuit with installed MOV (BSB, 2024)

As a result, the magnet releases the armature much faster and the energy is lost about thirty times faster. To find the voltage rating of the MOV, allow for 20% headroom to account for voltage swell and power-supply tolerances: $14Vdc \times 1.2 = 16.8V\ dc$. Given that no varistors have a voltage rating of exactly 16.8V, check the datasheets for specifications for 28-V dc MOV‘s.

Table 4.4: Standard data‘s of different MOVs (Patel, 2015)

TYPES OF MOVs														
Part number (base part)	Branding	Part number (base part)	Branding	Size (mm)	V_{RMS} (V)	V_{DC} (V)	Min (V)	Nom (V)	Max (V)	V_C (V)	I_{PK} (A)	(A)	(J)	(pF)
V14E23P	P14E23	V14P23P	P14P23	14	23	28	32.4	36	39.6	71	10	4000	23	7000
V05E25P	P5E25	V05P25P	P5P25	5	25	31	35.1	39	42.9	77	1	500	2.5	750
V07E25P	P7E25	V07P25P	P7P25	7	25	31	35.1	39	42.9	77	2.5	1000	5.5	1500
V10E25P	P10E25	V10P25P	P10P25	10	25	31	35.1	39	42.9	77	5	2000	13	2900
V14E25P	P14E25	V14P25P	P14P25	14	25	31	35.1	39	42.9	77	10	4000	25	6200
V20E25P	P20E25	V20P25P	P20P25	20	25	31	35.1	39	42.9	77	20	8000	77	13500
V10E30P	P10E30	V10P30P	P10P30	10	30	38	42.3	47	51.7	93	5	2000	15.5	2550
V14E30P	P14E30	V14P30P	P14P30	14	30	38	42.3	47	51.7	93	10	4000	32	5550
V20E30P	P20E30	V20P30P	P20P30	20	30	38	42.3	47	51.7	93	20	8000	90	12000

4.2.10 Size of Stud on the solenoid cover

A stud is a round bar threaded at both ends. The components to be fastened have one end of the stud screwed into a tapped hole, and the other end is fitted with a nut. It’s must have nominal diameter and core diameter. Where: d = Nominal diameter of the stud in mm,

$d_c =$ Core diameter of the stud in mm. It is usually taken as 0.84 d.

$\sigma_t =$ Tensile stress for the stud′s material, typically nickel steel.

$n_s = Number\ of\ studs$

It is known that the force acting on the studs (the stud that holds the solenoid with the solenoid stand).

Maximum force that produced by solenoid obtained on the above analysis is 393.82 N and let us take $n_s = 2$, the resisting force offered by all studs (Khurmi & Gupta, 2005) is;

$$F = n_s \times \frac{\pi}{4}(d_c)^2 \times \sigma_t \qquad (4.42)$$

$$393.82\ N = 2 \times \frac{\pi}{4} 0.84d)^2 \times 65\ MPa$$

($Taking\ tensile\ stress\ of$ nickel steel $\sigma t = 65\ MPa = 65\ ^{N}/_{mm}2$).

$$d = \sqrt{\frac{393.82\ N \times 4}{2 \times \pi \times (0.84)^2 \times 65\ ^{N}/_{mm^2}}} \approx 3\ mm$$

From standard design dimensions of screw threads, bolts and nuts M3xP0.5 is selected (Khurmi & Gupta, 2005)

4.2.11 Design of solenoid stand

The solenoid stand is component that holds in place the solenoid by supporting it over the valve spring. The material of this member is the same as the cylinder head material (aluminum alloy). Geometrical dimensions (mm) and 3D model are shown in figure 4.13.

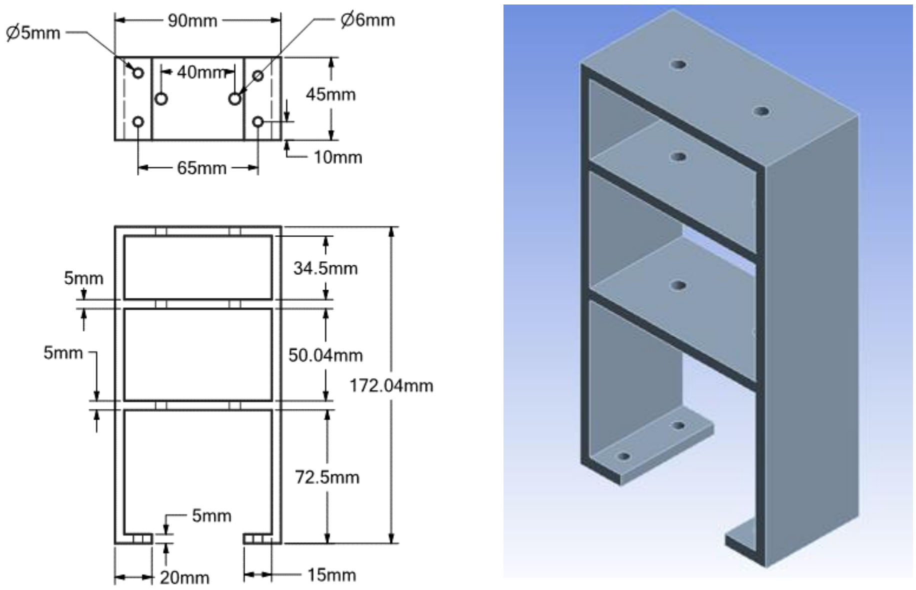

Figure 4.13: (A) Geometrical representation of solenoid stands B) 3D of solenoid stand

- **Force analysis of solenoid stand;**

This member should be designed by considering the forces applied on it. During the normal operation of the valves have overlapping period, so it is preferable to use both forces will appliedat the same time and the forces that are to be considered are forces due to magnetic field of the coil. These are F_1 and F_2 and consider member A is simply supported beam at its ends which carries these two forces. $F_1 = F_2 = 393.82$ N Illustrates as follows in figure 4.14: Consider member A;

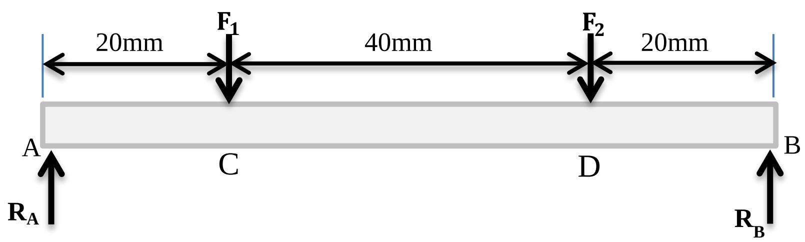

Figure 4.14 Representation of forces applied on member A.

Where, R_A = reaction force at A, R_B= Reaction force at B.

First determine the reactions R_A and R_B;

Taking moment about A, we get

$$\sum M_A = 0\,, Anticlockwise\ direction \tag{4.43}$$

$$R_B \times 80mm = 393.82\ \text{N} \times 20\text{mm} + 393.82\ \text{N} \times 60\text{mm}$$

$$R_B = \frac{31505.6\ \text{Nmm}}{80\ mm} = 393.82\ \text{N}$$

Then the force on the vertical direction (F_V) is given by:

$$\sum F_V = F_1 + F_2 - (R_A + R_B) = 0$$

$$393.82\ \text{N} + 393.82\ \text{N} - (R_A + 393.82\ \text{N}) = 0 \rightarrow R_A = 393.82\ \text{N}$$

To draw bending moment diagram first calculate bending moment at each point as follows. At any point along the path between A and C, at a distance x from A, the bending moment is given by:

$$M_x = R_A \times x \tag{4.44}$$

Bending moment at A $(BM_{@A})$ from the left side:

$$(BM_{@A}) = 0, because\ x_{@A} = 0$$

Bending moment at B $(BM_{@B})$ from right side:

$$(BM_{@B}) = 0, because\ of\ \ x_{@B} = 0\ and\ hinged\ point\ (BM = 0)$$

Bending moment C $(BM_{@C})$ $from\ lift\ side\ clockwise\ direction$:

$$BM_{@C} = 20mm \times F_1 = 20mm \times 393.82N = 7876.4\ Nmm$$

Bending moment D $(BM_{@D})$ $from\ right\ side\ clockwise\ direction$

$$BM_{@D} = 20mm \times F_1 = 20mm \times (-393.82)N$$

$$= 7876.4\ Nmm\ to\ counter\ clockwise\ direction.$$

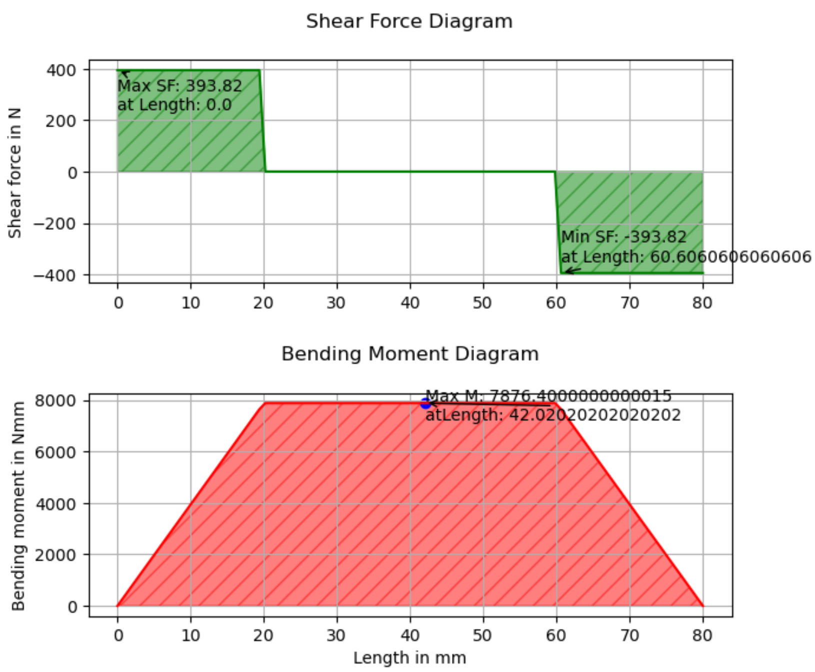

Figure 4.15: Shear force and bending moment diagram of member A

- **Shear stress for member A:**

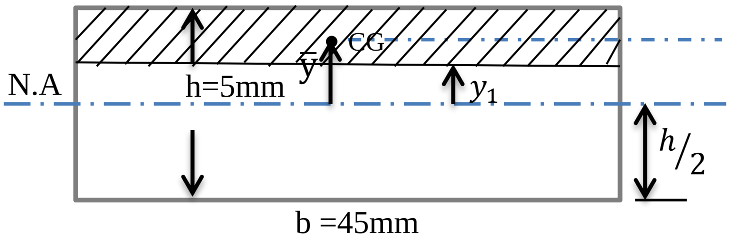

Figure 4.16: Location of the center of gravity for member A

Member A is rectangular cross section of a beam of width b and depth h. let F is shear force acting at the section. Consider a level EF at a distance of y_1 from the natural axis. The shear stress for this rectangular member A (Bansal, 2009) is given by:

$$\tau = F(\frac{A \times \bar{y}}{b \times I}) \quad (4.45)$$

Where: Fs – shear force that applied to the member.

A – Cross sectional area for the section; which is

$A = (\frac{h}{2} - y1)b$ but in this case y_1 is zero.

$\bar{y}$ – Distance from N.A to C.G of the section.

b – The width of the section, which is 45 mm.

I – Moment of inertia for the section, which is;

$$= \frac{bh^3}{12} = \frac{45mm \times (5mm)^3}{12} = 468.75mm^4$$

The Distance from N.A to C.G of the section is given by;

$$\bar{y} = y_1 + \frac{1}{2}\left(\frac{h}{2} - y_1\right) = y_1 + \frac{h}{4} - \frac{y_1}{2} = \frac{1}{2}(y_1 + \frac{h}{2})$$

Then shear stress of the member A section is given by:

$$\tau = F\frac{A \times \bar{y}}{b \times I} = F\frac{(\frac{h}{2} - y_1) \times b \times \frac{1}{2}(y_1 + \frac{h}{2})}{b \times I}$$

$$\tau = \frac{F}{2I}(\frac{h^2}{4} - (y_1)^2) \quad (4.46)$$

From equation 4.46 see that as τ increases as y_1 decreases. Also the variation of τ with respect to y_1 is a parabola.

At the top edge, $y_1 = \pm\frac{h}{2}$, shear stress from equation 3.44:

$$\tau = \frac{F}{2I}\left(\frac{h^2}{4} - \left(\pm\frac{h}{2}\right)^2\right) = \frac{F}{2I}\left(\frac{h^2}{4} - \frac{h^2}{4}\right) = 0$$

At the natural axis, $y_1 = 0$ and hence

$$\tau = \frac{F}{2I}\left(\frac{h^2}{4} - (y_1)^2\right) = \frac{F}{2I} \times \frac{h^2}{4} = \frac{Fh^2}{8I}$$

$$\tau = \frac{Fh^2}{8I} = \frac{393.82N \times (5mm)^2}{8 \times 468.75mm^4} = 2.63\ {}^{N}/_{mm^2} \text{ …… is the maximum shear stress}$$

The shear stress diagram is as shown below;

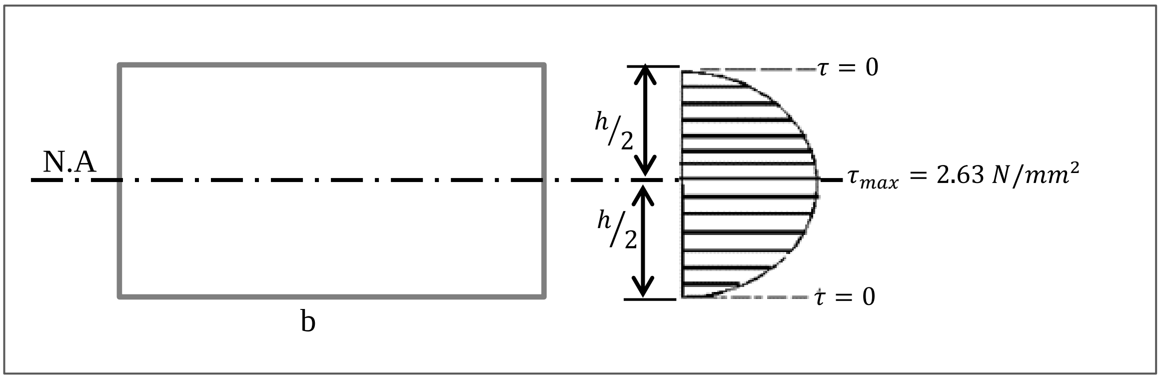

Figure 4.17: Shear stress diagram of member A

Figure 4.17 shows the variation of shear stress across the section. Since the calculated shear stress is very smaller than the allowable shear stress of the material, it is safe. In the same way the shear stress for the other members can be analyzed and from this other members are not out of the allowable one; so all members are safe.

Maximum bending stress (σ_{max}) of the member A (Bansal, 2009) is given by:

$$\sigma_{bmax} = \frac{M_{bmax}}{Z} \tag{4.47}$$

$where, \sigma_{bmax}\ is\ maximum\ bending\ stress\ of\ member\ A$

$M_{bmax}\ is\ maximum\ bending\ stress\ of\ member\ A$

$Z\ is\ section\ modulus\ of\ memeber\ A$

The member is taken as a simply supported member,

Figure 4.18: Side view geometry of member A

Member A is a rectangular section, so the section modulus (Z) for rectangular section (Bansal, 2009) is given by;

$$Z = \frac{bh^2}{6} \tag{4.48}$$

$$Z = \frac{45mm \times (5mm)^2}{6} = 187.5\ mm^3$$

Maximum bending stress is:

$$\sigma_{bmax} = \frac{M_{bmax}}{Z} = \frac{7876.4\ Nmm}{187.5\ mm^3} = 42.00746667\ ^{N}/_{mm^2}$$

So the allowable bending stress of the material ($310MPa$) greater than the calculated one, therefore it issafe.

- ✓ For the rest horizontal members the force analysis and value is the same as member A analysis, so it is safe design.

- **Deflections of solenoid stand for member A:**

A simply supported beam member AB of length 80 mm is simply supported at its ends and carries two a point loads of F_1 = 393.82 N and F_2 = 393.82 N at a distance of 20 mm and 60 mm respectively from the left support.

Let $E = 7 \times 10^4\ ^{N}/_{mm^2}$ and moment of inertia for rectangular section I is given by;

$$I = \frac{bh^3}{12} = \frac{5mm\times(45mm)^3}{12} = 37968.75\ mm^4$$

It is possible to compute the fixing moments and end reactions directly by applying Macaulay's method. This method is used where the area of B.M diagram cannot be determined conveniently.

The reaction R_A and R_B are calculated in the above, which is $R_A = R_B$ = 393.82 N.

Consider the section x in the last part of the beam (i.e., in the length DB) at a distance x from theleft support A.

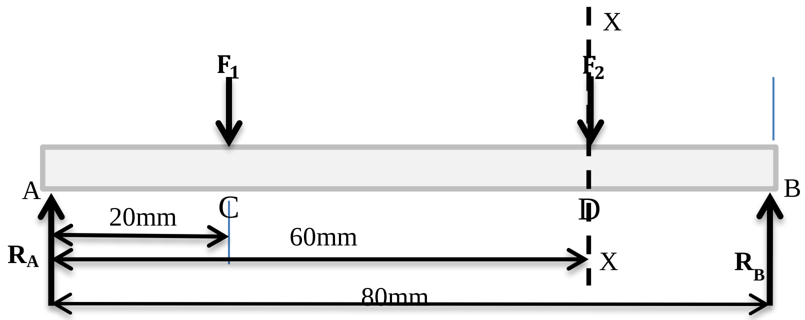

Figure 4.19: Section of beam

Here, from figure 4.19 the bending moment of section beam is provided by;

$$BM_{@X} = R_A \times x \vdots -F_1(x-20) \vdots -F2(x-60)$$

But generally bending moment (Bansal, 2009) is given by;

$$M_b = EI\frac{d^2y}{dx^2} \tag{4.49}$$

$$EI\frac{d^2y}{dx^2} = R_A \times x \vdots -F_1(x-20) \vdots -F_2(x-60)$$

$$= 393.82N \times x \vdots -393.82\ N(x-20) \vdots -393.82N(x-60)$$

Integrating the above equation, we get

$$EI\frac{dy}{dx} = 393.82N \times \frac{X^2}{2} + C_1 \vdots -393.82\,N\frac{(X-20)^2}{2} \vdots -393.82N\frac{(X-60)^2}{2} \qquad (i)$$

Integrating again the above equation (i), we get

$$EIy = 393.82N \times \frac{x^3}{6} + C_1 x + C_2 \vdots -393.82\,N\frac{(x-20)^3}{6} \vdots -393.82N\frac{(x-60)^3}{6} \qquad \text{(ii)}$$

To find the values of C_1 and C_2 use two boundary conditions. The boundary conditions are;

$(i) At\ x = 0, y = 0\ and \qquad (ii) At\ x = 80mm, y = 0$

1. Substituting the first boundary condition i.e., at x = 0 and y = 0 in equation (ii) and considering the equation up to first square bracket (as x = 0 lies in the first part of the beam), we get;

$$EI \times 0 = 393.82N \times \frac{(0)^3}{6} + C_1 \times 0 + C_2$$

$$0 = 0 + 0 + C_2 \rightarrow \therefore\ C_2 = 0$$

2. Substituting the second boundary condition i.e., at x = 80 mm, y = 0 in equation (ii) and considering the complete equation (as x = 80 lies in the final segment of the beam), we obtain;

$$EIy = 393.82N \times \frac{x^3}{6} + C_1 x + C_2 \vdots -393.82\,N\frac{(x-20)^3}{6} \vdots -393.82N\frac{(x-60)^3}{6}$$

$$EI \times 0 = 393.82 \times \frac{80^3}{6} + C_1 80 + C_2 \vdots -393.82\ \frac{(80-20)^3}{6} \vdots -393.82\frac{(80-60)^3}{6}$$

$$0 = 393.82 \times 85333.33333 + 80C_1 + 0 \vdots -393.82 \times 36000 \vdots -393.82 \times 1333.333333$$

$$0 = 18903360 + 80C_1 \rightarrow C_1 = \frac{-18903360}{80} = -236292, Therefore\ C_1 = -236292$$

Now substituting the values of c_1 and c_2 in equation (ii), we get;

$$EIy = 393.82N \times \frac{X^3}{6} - 236292X \vdots -393.82\,N\frac{(X-20)^3}{6} \vdots -393.82N\frac{(X-60)^3}{6} \qquad (iii)$$

a. The deflection under first load i.e. at point C. This is obtained by substituting x = 20 mmin equation (iii) up to the first open square bracket (as the point C lies in the first part of the beam). Hence , we get;

$$EIy = 393.82N \times \frac{x^3}{6} - 236292x$$

$$y_C = \frac{393.82N \times \frac{(20mm)^3}{6} - 236292N \times (20mm)}{EI}$$

$$y_C = \frac{(525093.3332 - 4725840)Nmm^3}{7 \times 10^4\, {}^{N}\!/_{mm^2} \times 37968.75\ \text{mm}^4}$$

$$y_C = \frac{-4200746.667\ Nmm^3}{2.6578125 \times 10^9 Nmm^2} = -0.001580527846\ mm$$

The negative sign shows that deflection is downwards. And this deflection value is very small;therefore it has no significant effect on the member, so the design is safe.

b. Deflection under the second load i.e. at point D. This is obtained by substituting x = 60 mm in equation (iii) up to the second square bracket (as the point D lies in the second part of the beam). Hence, we get;

$$EIy = 393.82N \times \frac{x^3}{6} - 236292X \vdots -393.82\ N\frac{(x-20)^3}{6}$$

$$EIy_D = 393.82N \times \frac{(60mm)^3}{6} - 236292Nmm^2 \times 60mm \vdots -393.82\ N\frac{(60mm-20)^3}{6}$$

$$y_D = \frac{-4200746.667Nmm^3}{2.6578125 \times 10^9 Nmm^2}$$

$$y_D = -0.001580527846\ mm$$

The negative sign shows that deflection is downwards. And the deflection is very small; therefore it has no significant effect on the member, so the design is safe.

c. Maximum deflection:

The deflection is likely to be Maximum at section between C and D. For maximum deflection, $\frac{dy}{dx}$ should be zero. Hence, equate equation (i) equal to zero up to the vertical dots.

$$EI\frac{dy}{dx} = 393.82N \times \frac{x^2}{2} + C_1 \vdots -393.82\ N\frac{(x-20)^2}{2} \vdots$$

$$EI \times 0 = 393.82N \times \frac{x^2}{2} - 236292 \vdots -393.82\ N\frac{(x-20)^2}{2} \vdots$$

$$0 = 393.82 \times \frac{x^2}{2} - 236292 \vdots -393.82 \times \frac{1}{2}x^2 + 393.82 \times 20x - 393.82 \times 200 \vdots$$

$$0 = -236292 \vdots +7876.4x - 78764 \vdots \rightarrow 7876.4x = 236292 + 78764$$

$$7876.4Nmmx = 315056Nmm^2 \rightarrow x = \frac{315056Nmm^2}{7876.4Nmm} = 40mm$$

At x= 40 mm between C and D maximum deflection occurs. Now substituting x = 40mm in equation (iii) up to vertical dots, we get maximum deflection (y_{max}) as:

$$EIy_{max} = 393.82N \times \frac{X^3}{6} - 236292X - 393.82\ N\frac{(X-20)^3}{6}$$

$$y_{max} = \frac{393.82 \times \frac{(40)^3}{6} - 236292 \times 40 - 393.82\frac{(40-20)^3}{6}}{E \times I}$$

$$y_{max} = \frac{393.82 \times \frac{(40)^3}{6} - 236292 \times 40 - 393.82 \frac{(40-20)^3}{6}}{7 \times 10^4 \, {}^{N}/_{mm^2} \times 37968.75 \text{ mm}^4}$$

$$y_{max} = \frac{-5776026.666Nmm^3}{2.6578125 \times 10^9 Nmm^2} = -0.002173225789mm$$

The negative sign shows that deflection is downwards. And the deflection is very small; therefore it has no significant effect on the member, so the design is safe. The deflection of the other horizontal members should be analyzed in the same way of member A and they have no more deflection value than the member A, so the design is safe.

- **Consider member B;**

Consider a column of rectangular cross section subjected by compressive load of F_1 acting along the axis of the column as shown in the figure 4.20 below. This load will cause a direct compressive stress whose intensity will be uniform across the cross section of the column.

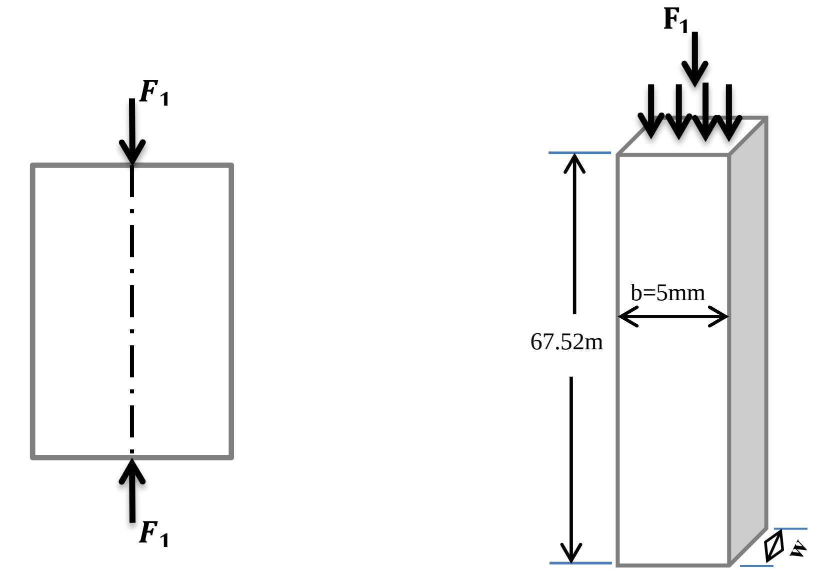

A. load acting along axis of column B. Geometries of member B

Figure 4.20: Geometry of vertical member B and load applied on it (A). Load acting along axis of column, (B). Geometries of column B

Compressive/tensile stress ($\sigma_c or \ \sigma_t$) (Bansal, 2009) is given by;

$$\sigma_c = \frac{F}{A} \tag{4.50}$$

Where, $\sigma_c or \ \sigma_t$ is compressive stress, F is load acting on the column and A is area of cross-section. Thus the area is given by;

$$A = b \times w = 45mm \times 5mm = 225mm^2$$

Then the compressive stress is:

$$\sigma_c = \frac{F}{A} = \frac{393.82N}{225mm^2} = 1.75\ N/mm^2$$

Since the tensile/compressive stress of member B is less than the allowable tensile stress of the material, so it is safe. Member C, E and F has equivalent design analysis with member A; it is also checked by the software and the design is safe.

4.2.12 Coupling member design

Coupling member is a member that helps as an intermediate member to transmit a linear motion of the solenoid valve to the valve tip. It is made of stainless steel. The figure 4.21 below shows geometry and basic dimensions of the coupling member.

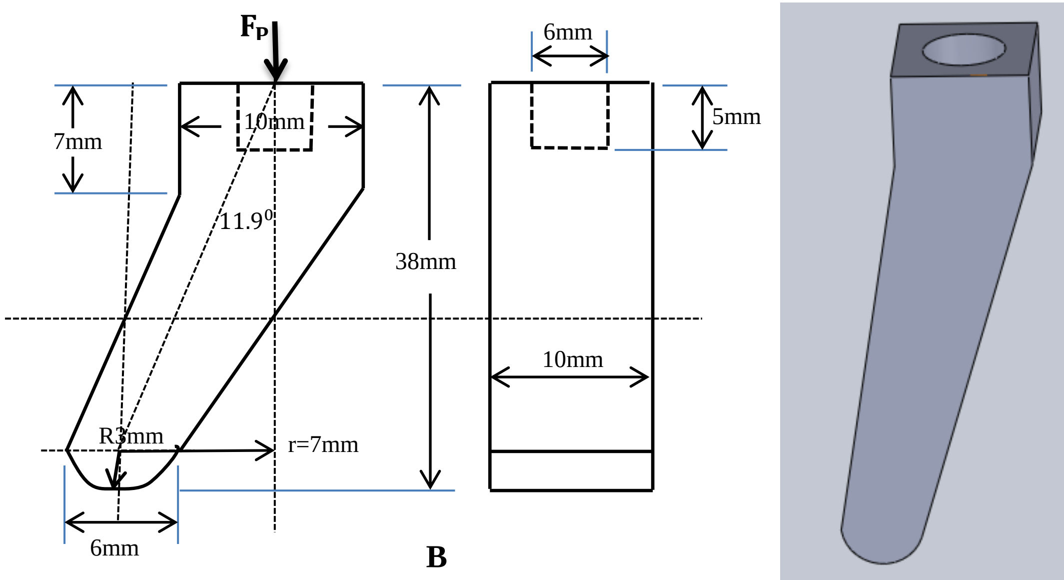

Figure 4.21: Geometry and basic dimensions of the coupling member.

Since the center distance between the coupling and plunger is 7 millimeter and it is a short member it is better to check the compressive stress by considering one side fixed. This stress is given by using equation 4.40:

$$\sigma_c = \frac{F_P}{A}, but\ A = \frac{\pi D^2}{4} = \frac{\pi \times (6mm)^2}{4} = 28.27mm^2,$$

Then the compressive/tensile stress will be:

$$\sigma_c = \frac{F_P}{A} = \frac{393.82N}{28.27mm^2} = 13.66N/mm^2$$

Since the allowable compressive stress $(577.2\ MPa)$ is greater than the calculated compressive stress value, therefore, the member can safely handle the load, and it is safe.

And also, it is possible to check for bending stress by taking the center distance between the plunger and the valve stem and by considering one side of the coupling member as fixed. This member should be designed by considering the forces applied to it, $F_P = 393.82N$

Consider the geometries of coupling member to check the bending stress as shown figure 4.22 below.

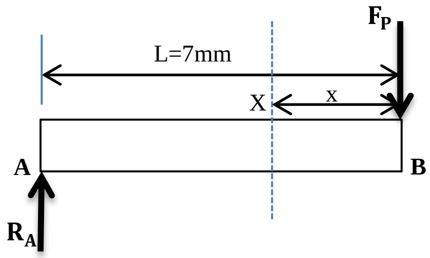

Figure 4.22: The shortest length of the coupling member as a horizontal member.

Then the force in the vertical direction is getting by summing all and equal to zero to find the reaction force.

$$+\uparrow \sum F_V = (R_A - F_B) = 0$$

$$(R_A - F_B) = R_A - 393.82N = 0 \rightarrow R_A = 393.82N$$

In order to calculate bending stress, first calculate the bending moment of each point, draw a bending moment diagram, and take the maximum one (Bansal, 2009). So the bending moment at each point is as follows;

Take a section X at a distance of x from the free end. Consider the right portion of the section. The bending moment at section X is given by; $M_x = -F_p \times x$ (4.51)

The bending moment will be negative, as for the right portion of the section, the moment F_P at X is clockwise. So from equation 4.51, it is clear that BM at any section is proportional to the distance of the section from the free end.

Bending moment at B ($\mathrm{BM_{@B}}$):

$$\mathrm{BM_{@B}} = 0 \;\; \mathit{because\ at\ B}, x = 0$$

Bending moment at A ($\mathrm{BM_{@A}}$), $at\ x = L$,

$$\mathrm{BM_{@B}} = R_A \times L = 393.82N \times 7mm$$

$$= 2756.74Nmm, \mathit{in\ the\ downward\ direction}$$

Hence BM follows the straight line laws. At point A from BM diagram as shown the figure 4.23 below, take $AC = F_P \times L$ in the downward direction.

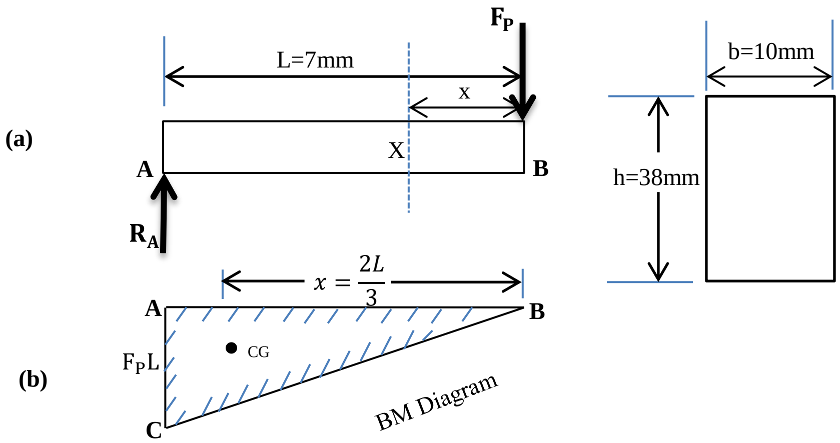

Figure 4.23: Applied force on the member (a), bending moment diagram of coupling member (b).

The bending moment will be zero at B and will be maximum (F_P.L) at A. The variation of B.M between A and B is linear as shown above in figure 4.23. Now maximum bending stress is given by equation 4.47;

$$\sigma_{bmax} = \frac{M_{bmax}}{Z}$$

Section modulus for rectangular section is, $Z = \frac{bh^2}{6} = \frac{10mm\times(38mm)^2}{6} = 2406.67mm^3$

and $M_{bmax} = 2756.74\ Nmm$, then maximum bending stress is:

$$\sigma_{bmax} = \frac{M_{bmax}}{Z} = \frac{2756.74\ Nmm}{2406.67mm^3} = 1.145\ N/mm^2$$

So the allowable bending stress (581N/mm^2) of the material greater than the calculated one, therefore it issafe.

- **Shear stress for couple member**

Consider a narrow cantilever beam of a rectangular cross section of width b and depth h subjected to a load F at its free end shown figure 4.24 (A) below. Since, the shear F_s in the beam isconstant and equal in magnitude to load F.

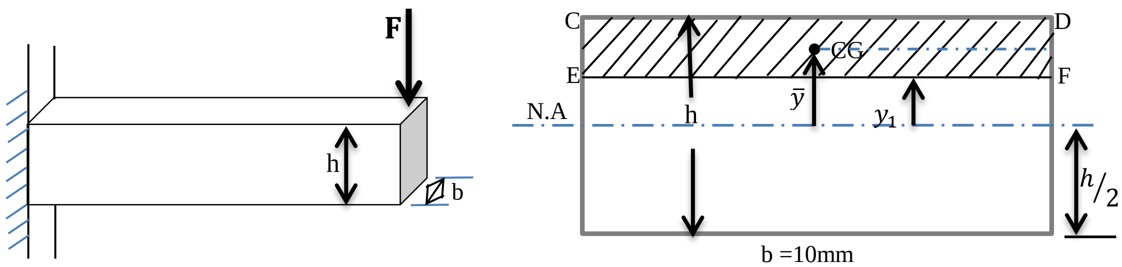

(A) (B)

Figure 4.24: Cantilever beam of a rectangular cross section, (A) shear force acting at free end of coupling member, (B) Location of the center of gravity for coupling.

Consider a level EF at a distance of y_1 from the natural axis as shown figure 4.24 (B) above. The shear stress for this rectangular member is given by equation 4.45;

$$\tau = F(\frac{A \times \bar{y}}{b \times I})$$

Where, F is shear force which is 393.82N, $\bar{y}$ is distance from N.A to CG of the section, b is width of the section which is 10mm, I is moment of inertia for the section which is given by; $I = \frac{bh^3}{12} = \frac{(10mm)(38mm)^3}{12} = 45726.67mm^4$. and A = area of section above figure 4.24 (B) (i.e. shaded area CDFE) $= \left(\frac{h}{2} - y_1\right) \times b$.

The Distance from N.A to C.G of the section is given by;

$$\bar{y} = y_1 + \frac{1}{2}\left(\frac{h}{2} - y_1\right) = y_1 + \frac{h}{4} - \frac{y_1}{2} = \frac{1}{2}\left(y_1 + \frac{h}{2}\right)$$

Then shear stress of the couple member section is given by:

$$\tau = F\frac{A \times \bar{y}}{b \times I} = F\frac{(\frac{h}{2} - y_1) \times b \times \frac{1}{2}(y_1 + \frac{h}{2})}{b \times I}$$

$$\tau = \frac{F}{2I}(\frac{h^2}{4} - (y_1)^2) \qquad (4.52)$$

From equation 4.52 above see that as τ increases as y_1 decreases. Also the variation of τ with respect to y_1 is a parabola. At the top edge, $y_1 = \pm\frac{h}{2}$, shear stress from equation 4.52 above:

$$\tau = \frac{F}{2I}\left(\frac{h^2}{4} - \left(\pm\frac{h}{2}\right)^2\right) = \frac{F}{2I}\left(\frac{h^2}{4} - \frac{h^2}{4}\right) = 0, \therefore at\ \ y_1 = \pm\frac{h}{2}, \tau = 0$$

At the natural axis, $y_1 = 0$ and hence

$$\tau = \frac{F}{2I}\left(\frac{h^2}{4} - (y_1)^2\right) = \frac{F}{2I} \times \frac{h^2}{4} = \frac{Fh^2}{8I}$$

$$\tau = \frac{Fh^2}{8I} = \frac{393.82N \times (38mm)^2}{8 \times 45726.67mm^4} = 1.55\, {}^{N}\!/_{mm^2} \text{ ... ... is the maximum shear stress}$$

And the shear stress diagram of the coupling member is as shown figure 4.25 below;

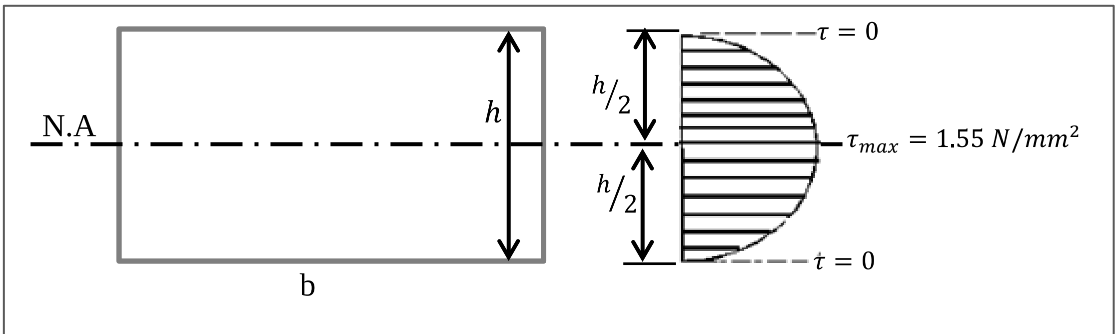

Figure 4.25: Shear stress diagram of coupling member.

The calculated maximum shear stress of the coupling member is less than the permissible shear stress of the material (386 N/mm^2), so it is safe.

- **Deflection on coupling member:**

The deflection of the coupling member is determined by considering the cantilever beam carrying a point load at the free end and by considering the length of the beam as equal to the center distance between the plunger and the valve stem, as shown in figure 4.26 above, with a cantilever of length L = 7mm fixed at end A and free at end B.

The bending moment will be zero at B and will be F_P.L at A. The variation of B.M. between Aand B is linear, as shown in figure 4.24 (b).

At the fixed end A, the slop and deflection are zero due to the distance being zero.

Let $\theta_B = slope\ of\ at\ B, i.e\ \left(\frac{dy}{dx}\right) at\ B$ and y_B = defelection at B,

Then by using the moment area method, slop at B is given by;

$$\theta_B = \frac{Area\ of\ B.M\ diagram\ between\ A\ and\ B}{E \times I}$$

$$\theta_B = \frac{\frac{1}{2} \times AB \times AC}{E \times I} = \frac{\frac{1}{2} \times L \times F_P \times L}{E \times I}$$

$$\theta_B = \frac{\frac{1}{2} \times AB \times AC}{E \times I} = \frac{\frac{1}{2} \times L \times F_P \times L}{E \times I}$$

The given parameters are: L = 7mm, $F_P = 393.82N$, moment of inertia (I) which is given by from the figure 3.26; $I = \frac{bh^4}{12} = \frac{10mm \times (38mm)^3}{12} = 45726.67mm^4$ and young's modulus (E) of coupling material is E = 1.9×10^5MPa. Then deflection at B is given by:

$$\theta_B = \frac{\frac{1}{2} \times 7mm \times 393.82N \times 7mm}{1.9 \times 10^5 N/mm^2 \times 45726.67mm^4}$$

$$\theta_B = 0.0000011056$$

Deflection (y_B) is given by:

$$y_B = \frac{A \times \bar{x}}{E \times I} \qquad (4.53)$$

Where A is area of B.M diagram between A and B, $A = \frac{1}{2} \times F_P \times L \times L = \frac{F_P \times L^2}{2}$ and

$$\bar{x}\ =\ distance\ of\ CG\ of\ the\ area\ of\ B.M\ diagram = \frac{2x}{3}.$$

Then;

$$y_B = \frac{\frac{F_P \times L^2}{2} \times \frac{2x}{3}}{E \times I} = \frac{F_P \times L^3}{3 \times E \times I}$$

$$y_B = \frac{393.82N \times (7mm)^3}{3 \times 1.9 \times 10^5 \times 45726.67mm^4}$$

$$y_B = 0.000005183\ mm$$

It shows that the deflection is very small; therefore it has no significant effect on the member, sothe design is safe.

- **Checking the impact of the valve landing:**

Impact occurs when one of the moving bodies in the system (the valve, armature, or plunger) hits the mechanical constraints. From the application view point, impacts with a velocity greater than 0.3 m/sec are undesirable since they are responsible mechanical wear and high intensity of noise, and mainly they can cause a loss of controllability at the holding phase (loss of valve). Possible impacts occur when the valve heats the valve seat during closing and the armature attracted from the lower magnet impacts the lower coil core during opening (Peterson & Stefanopoulou, 2004).

To calculate the landing velocity, it‘s preferable to take into account that at maximum compression, the valve spring has maximum velocity of motion, but gradually reduced when it becomes near the free length/load free length of the spring. During this time, the upper coil spring or the closing spring also tries to absorb the force near the valve seat, so the landing velocity can be obtained as follows: by taking the mass of the valve, the plunger with the armature, and the spring. Total mass is about 0.564 kilograms. And during this time the force is less than one-third of the total load because the lift becomes too close to the valve seat. Thus;

$$\text{ma} = \frac{1}{3} k \times x \qquad (4.54)$$

$$0.564\text{kg} \times \text{a} = \frac{1}{3} \times 10.55\ N/mm \times 6mm$$

$$\text{a} = \frac{10.55\ N/mm \times 6mm}{3 \times 0.564\text{kg}} = 37.411 m/s^2$$

The time taken to get maximum lift is about 0.00306873 second. And for linear motion the speed of equation is given by;

$$\text{V} = \text{V}_0 + \text{at} \qquad (4.54)$$

Initially speed is zero (i.e. $V_0 = 0$), then

$$V = V_0 + \mathrm{at}$$

$$V = 0 + 37.411\, m/s^2 \times 0.00306873 \text{ sec}$$

$$V = 0.1148 \text{ m/sec},$$

From hear the landing velocity (V= 0.1148 m/s) less than 0.3m/s at 6000RPM (Peterson & Stefanopoulou, 2004), and found within the desired range and this shows the system is stable and durable in this velocity operation, but to reduce the landing velocity further use optimization control tool to ensure stability and durability more.

4.2.13 Size determinations of the stud on the cylinder head to the solenoid stand

On the lift member (member A) there is about 393.82 N**.**

$$F = 393.82\text{N} \qquad (i)$$

The force on the top of cylinder head is 393.82N (left one) and the same amount to the right side.Let number of stud is 2; so $n_s = 2$.

Resisting force offered by all the studs (F_{RS}) by using equation 4.42 is**:**

$$F_{RS} = n_s \times \frac{\pi}{4} \times (d_c)^2 \times \sigma_t$$

Where: n_s = number of studs, d_c = core diameter of the stud in mm = 0.84d.,

d = is the stud's nominal diameter in millimeters.

A = the area that the force is applied in mm^2 and σ_t = tensile stress for the material of the stud which is usually nickel steel = $65 N/mm^2$.

$$F_{RS} = n_s \times \frac{\pi}{4} \times (d_c)^2 \times \sigma_t$$

$$F_{RS} = 2 \times \frac{\pi}{4} \times (0.84d)^2 \times 65N/mm^2 \qquad (ii)$$

By equating equation (i) and (ii) nominal diameter is obtained

$$F_{RS} = 2 \times \frac{\pi}{4} \times (0.84d)^2 \times \frac{65N}{mm^2} = F$$

$$2 \times \frac{\pi}{4} \times (0.84d)^2 \times \frac{65N}{mm^2} = 393.82N \rightarrow d = \sqrt{\frac{393.82N \times 4}{2 \times \pi \times 0.84^2 \times 65N/mm^2}}$$

$$d = 2.34\, mm$$

Thus from the standard design dimensions of screw threads, bolts and nuts M3xP0.5 is selected. i.e. nominal diameter is 3 mm and pitch is 0.5 mm (Khurmi & Gupta, 2005).

Right side stud (for member B fitting) has the same resisting force as the stud calculated previously. So the stud size is M3xP0.5. So, the data for the nut design will be by the standard that is taken from table, i.e. M3xP0.5.

4.2.14 Design of Cooling System for Solenoid Valve

i. Determination of temperature of conductor during operation

The temperature generated by the solenoid has its own effect on the operation of the electrical system and it should be controlled from overheating. So this temperature is obtained by using Resistance values for conductors at any temperature is given by (Kuphaldt, 2002):

$$R = R_{ref}[1 + a(T - T_{ref})] \tag{4.55}$$

Where, R = is the conductor resistance at temperature "T" in this case.

R_{ref} = Conductor resistance at reference temperature, T_{ref} usually 35^0c, at reference cylinder head surface temperature (35^0c or 95^0F) (Suresh et al., 2014) for 1 mm diameter of copper wire, R_{ref}= 0.3706 ohm per degree Celsius.

α = is the conductor material′s temperature coefficient of resistance.

= has a temperature coefficient of 0.00393 degrees Celsius, See on appendix A

T = Conductor temperature in degrees Celsius.

T_{ref} = Reference temperature that α is specified at for the conductor material

$T_{ref} = 35^0C\ or\ 95^0$F

The resistance (R) of the wire at temperature "T" in the coil is 0.405 which is determined from equation 3.31. From the above equation 3.52, the temperature 'T" determined as follows;

$$T = \frac{\frac{R}{R_{ref}} - 1}{a} + T_{ref}$$

$$T = \frac{\frac{0.405}{0.3706} - 1}{0.00393} + 35^0C = 58.6189^0C \approx 60^0C$$

ii. Design of cooling fins for solenoid valve

Fins are used to reduce the thermal resistance at a surface and thereby increase the heat transfer rate from the surface to the adjacent fluid. The heat transfer system is done by convection system.

Aluminum alloys are selected for fin material as the thermal conductivity of aluminum alloys is higher. Because of unique properties, Aluminum is the best material to manufacture many automobile components. It has excellent corrosion resistance and good machinability and it possess good strength and ductility. Detail design is discussed as follows.

Let T_b= the base temperature inside the solenoid T, 333 k

T_f = the surrounding temperature, 308 k,

x = the thickness of wall.

t = over all covering the thickness of fin

H = Width of fin, 0.090 m.

A = Cross-sectional area of fin

h = Heat transfer coefficient, 6000 W/m^{2}k,

L = Length of fin,

K = Thermal conductivity, 167 W/mk.

q= heat flux

t_f = 3mm and number of fins = 2coil length with space/3mm*2= 7

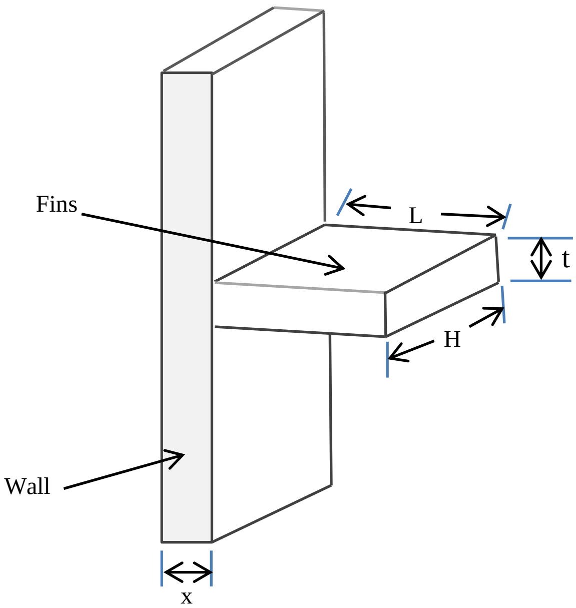

Figure 4.26: Cooling fin dimensions

The convection heat transfer from the surface of the fin to atmospheric air is given as (equation (3.55)):

$$q = h(T_b - T_{ref}) \tag{4.56}$$

$$q = 6000W/m^2k(333k - 308k)$$

$$q = 150{,}000\ W/m^2$$

Then the thickness of the wall, **x** can be calculated by considering the Heat transfer (conduction) from the wall surface (inner) to fin tip surface is given as:

$$q = \frac{k}{x}(T_b - T_{ref}) \qquad (4.57)$$

$$x = \frac{167\ \mathrm{W/mk}}{150{,}000\ W/m^2}(333k - 313k)$$

$$x = 0.02783m = 27.83mm$$

Length of the fins given by;

$$L = \frac{k}{h} \qquad (4.58)$$

$$L = \frac{167\ \mathrm{W/mk}}{6000W/m^2k} = 25\ mm$$

The cross-sectional area; $A = (H \times t) = 0.045t$

The perimeter of the fins is given by; $P = 2(H + t) = 2(0.045 + t) = 0.09 + 2t$

The heat flux (q) is given by;

$$q = \Delta T\sqrt{PhkA} \rightarrow P \times A = \left(\frac{q}{\Delta T}\right)^2 \times \frac{1}{hk}$$

$$(0.09 + 2t) \times 0.045t = \left(\frac{150000}{333 - 308}\right)^2 \times \frac{1}{6000 \times 167}$$

$$0.00405t + 0.09t^2 = (6000)^2 \times \frac{1}{1002000}$$

$$0.09t^2 + 0.00405t - 35.92814371 = 0$$

Then by using quadratic equation formula it is possible to determine the value of t;

$$\mathrm{at}^2 + \mathrm{bt} + \mathrm{c} = 0$$

$$t = \frac{-b \pm \sqrt{b^2 - 4ac}}{2a}$$

$$t = \frac{-0.09 \pm \sqrt{0.09^2 - 4 \times 0.00405 \times (-35.92814371)}}{2 \times 0.09 \times 1000} = 0.01995m$$

$$t = 0.01995m = 19.95mm$$

Thus the value of t is 19.9 millimeter, i.e. the thickness of the fin is about19.9mm. Remember that the height of the solenoid is 21 millimeter containing the thickness of the housing and when we compare with the thickness of the fin it as almost the same as the solenoid height, this indicates that the solenoid does not need more fins. But for the greater safety of the solenoid it is preferable to use some fins on the round of the solenoid stand having direct contact with the solenoid cover.

- **Fins effectiveness**

Fin effectiveness($\mathcal{E}_f$) describes how well a fine can improve heat transfer. In order to enhance heat transfer, ($\mathcal{E}_f > 1$) checking the effectiveness of fins for heat transfer: $\mathcal{E}_f = \sqrt{\frac{kP}{A_C}}\tanh(ml)\,, where, m = \sqrt{\frac{hP}{kA_c}}$

$m = \sqrt{\frac{hP}{kA_c}} = \sqrt{\frac{6000\times2(0.045+0.01995)}{167(0.045\times0.01995)}} = 72.1014\ then\ ml = 72.1014\times0.025 = 2.006,$

which is,$mL > 2, then\ tanh(mL) \rightarrow 1$ it can be consider an infinite fin. Therefore, fin effectiveness is given by:

$$\mathcal{E}_f = \sqrt{\frac{k}{h}\frac{P}{A_C}} = \sqrt{\frac{167w/mk}{6000w/m^2k}\frac{2(0.045+0.01995)m}{(0.045m\times0.01995m)}} = 2.007$$

It is preferable to use thin and closely spaced fins to increase the total number of fins and heat transfer rate.

4.3 Mathematical modeling for EMVA system for simulation

Two electric magnets, an armature, two springs, and an engine valve make up the EMCV system. The armature moves between the two electromagnets coil. The two springs on either side of the armature hold it in place at the midpoint of the two magnets when neither magnet is energized. This system is then used to control the motion of the engine valve. The airflow into and out of a combustion engine cylinder is then managed by the engine valve. Using circuit analysis, one can express the magnetic current in an electromagnetic poppet valve. The magnetic field vector (H), magnetic flux density vector (B_f) and total magnetic flux (λ_m) are the most frequently used quantities in a magnetic circuit. Magnetic field vector and magnetic flux density (Gross, 2006) are expressed by equation 4.59.

$$B_f = \mu H = \mu_r\mu_0 H \qquad (4.59)$$

Where µ is the total permeability, μ_r is the relative permeability and μ_0 is the free-space permeability. Typically, energy systems employ unique magnetic materials with exceptionally high permeability. These materials (iron, steel, nickel, cobalt, etc.), called “ferromagnetic materials”, are highly efficient magnetic field conductors and their relative permeability can vary between a few to a hundred thousand. Moreover, the relative permeability of these materials is dependent on the magnetic field and is not constant due to their high non-linearity. Their dependence can be obtained from equation (4.60).

$$B_f = B_s \times \sinh(h_s H) \qquad (4.60)$$

Valve velocity and acceleration is defined using equation (4.61).

$$v = \frac{dx}{dt} \quad and \quad a = \frac{dv}{dt} \tag{4.61}$$

The electromagnetic poppet valve model is illustrated in figure (4.27).

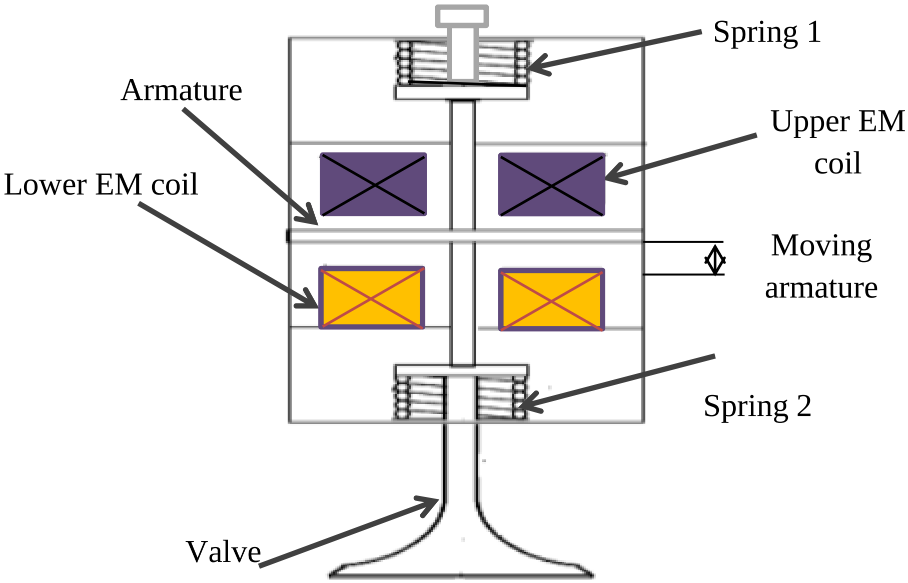

Figure 4.27: Electromagnetic poppet valve model diagram

Magnetic flux and current are related by equation (4.62) as shown below.

$$\begin{cases} V = Ri + \frac{d\lambda(x,i)}{dt} \\ \lambda = N\phi = N(\phi_L + \phi_m) \end{cases} \tag{4.62}$$

Where $\phi_L = Ni/R_l$ and $\phi_m = Ni/R_m$ are the settling flux and magnetic flux respectively. For dynamic controlling, we had to use a nonlinear model for the flux settling (equation 4.63).

$$\begin{cases} \lambda(x,i) = \lambda_s\left(1 - e^{-if(x)}\right) \qquad i \geq 0 \\ f(x) = \frac{2C_1}{(C_2 - x) + C_3} \end{cases} \tag{4.63}$$

Where λ_s the maximum flux saturation and C_1, C_2, C_3 are constant parameters. The electromagnetic force induction occurs in opposite direction of the generator's pole, therefore the generators has to exert work in order to charge the coil (the work is stored, in energy form, in the magnetic field). This energy can be calculated from equation (4.64).

$$E = \int_0^i \lambda(x,i)di = \frac{1}{2\mu_0} {B_f}^2 AL \tag{4.64}$$

And inductance is obtained by equation (4.65).

$$L = \frac{\lambda}{i} = \frac{N(\phi_L + \phi_m)}{i} \tag{4.65}$$

Armature control linear solenoid is illustrated in diagram below;

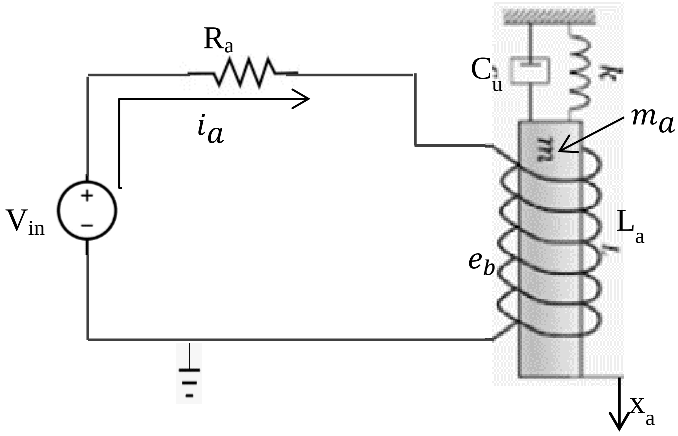

Figure 4.28: Electrical circuit diagram of EMV system for armature

From the above figure 4.28, the input is voltage V_{in} and the output is linear armature displacement(x_a). From Kirchhoff's voltage law, electrical sub system (loop method) the input voltage is equal to the sum of voltage drop across resistance, voltage drop on the inductor coil and back EMF voltage. Mathematically:

$$V_{in} = R_a i_a + L_a \frac{di_a}{dt} + e_b \tag{4.66}$$

Where; V_{in} is input voltage (source voltage), R_a is resistance of coil, i_a is current in the coil, L_a is inductance in the coil and e_b is back emf voltage.

Mechanical sub systems for equation of motion are described in next to this part. Power transmission is expressed as:

Force – current: $F_a = F_m = k_f i_a$ and Voltage – speed: $e_b = k_b v = k_b \frac{dx_a}{dt}$, where; k_f is magnetic force constant, k_b is velocity constant for an ideal linear solenoid actuator, that is: $k_f = k_b$

Rearrange of equation 4.66 with higher order to lower one;

$$L_a \frac{di_a}{dt} + R_a i_a + e_b = V_{in}$$

Taking the Laplace transform of the systems differential equations with zero initials conditions gives:

$$L_a S I_a(S) + R_a I_a(S) + k_b v_a(S) = V_{in}(S)$$

$$(L_a S + R_a) I_a(S) + k_b v_b(S) = V_{in}(S) \tag{i}$$

This is the equation of motion for electrical system with an input voltage and output velocity.

4.3.1 EMV system model analysis

The studied model of the valve actuator system is shown in Figure (4.29).

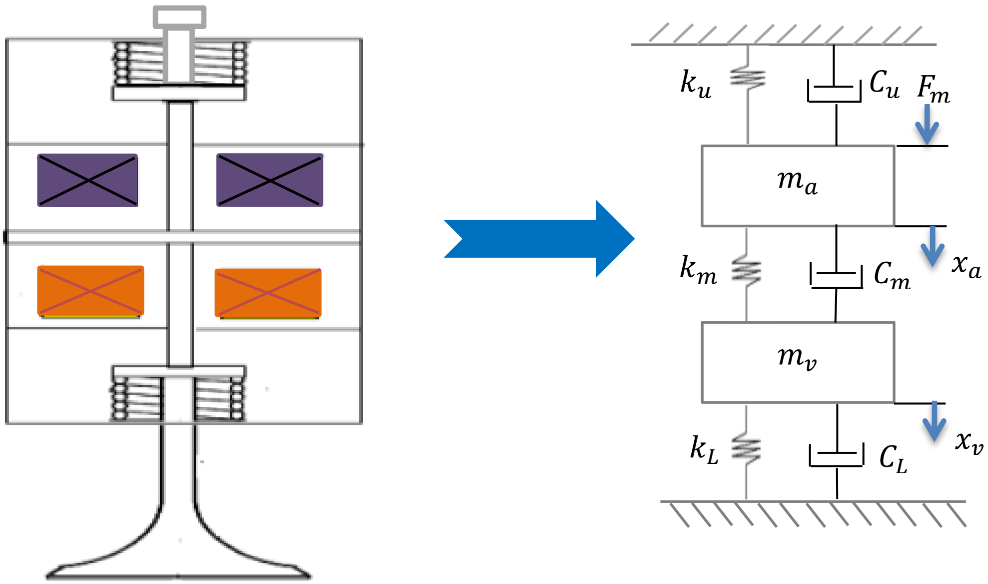

Figure 4.29: Modeling EMVA system as two degree of freedom

The system has two masses, m_a (armature) and m_v (valve), the first mass is equivalent to the armature and the second mass is equivalent to the valve and spring. The valve actuator system connects to mass m_a through spring stiffness K_u and damper coefficient C_u and valve stem stiffness K_m and damper coeff. C_m, between two masses and mass m_v is mounted by K_L, C_L By summing forces and applying Newton's 2nd law:

Now the system has two point masses as shown figure 4.29. And then the free body diagram of each mass are drawn as shown below in figure (4.30).

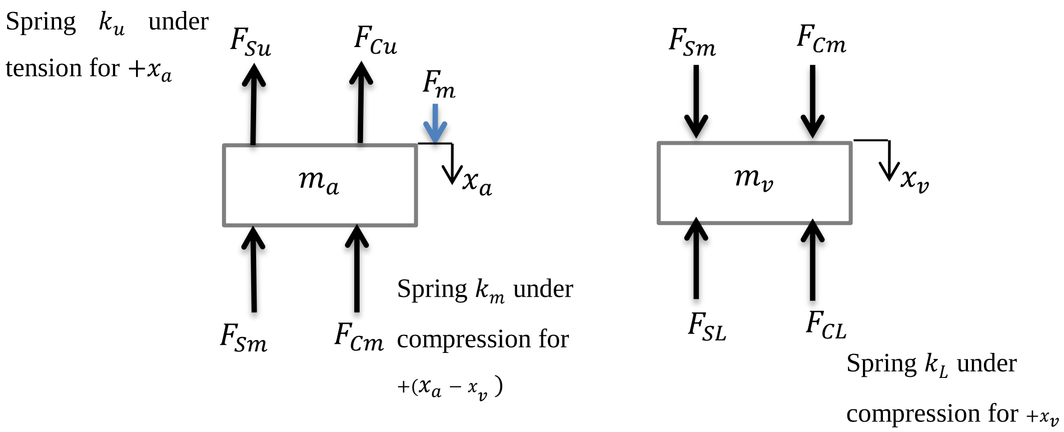

Figure 4.30: Free body diagrams of the masses

The expression of spring and damper forces by applying newton's second law it can be written in the following ways:

$$F_{Su} = k_u x_a \qquad F_{Sm} = k_m(x_a - x_v) \qquad F_{SL} = k_L x_v$$

$$F_{Cu} = C_u \dot{x_a} \qquad F_{Cm} = C_m(\dot{x_a} - \dot{x_v}) \qquad F_{SL} = C_L \dot{x_v}$$

Then apply newton's second law;

From free body diagram for the mass of armature:

$$+\downarrow \sum F_{x_a} = m_a a_a = m_a \ddot{x_a} = m_a \frac{d^2 x_a}{dt^2} \tag{4.67}$$

$$m_a \ddot{x_a} = -F_{Su} - F_{Sm} - F_{Cu} - F_{Cm} + F_m$$

$$m_a \ddot{x_a} = -k_u x_a - k_m(x_a - x_v) - C_u \dot{x_a} - C_m(\dot{x_a} - \dot{x_v}) + F_m$$

Collecting like terms rewrite as;

$$m_a \ddot{x_a} + (C_u + C_m)\dot{x_a} - C_m \dot{x_v} + (k_u + k_m)x_a - k_m x_v = F_m, \qquad \text{Since } F_m = k_f i_a$$

then $m_a \ddot{x_a} + (C_u + C_m)\dot{x_a} - C_m \dot{x_v} + (k_u + k_m)x_a - k_m x_v = k_f i_a \qquad (ii)$

Taking the Laplace transform of the equation of the system differential equations with zero initial conditions gives:

$$m_a S^2 X_a(S) + (C_u + C_m)SX_a(S) - C_m SX_v(S) + (k_u + k_m)X_a(S) - k_m X_v(S) = k_f I_a(S) \qquad \text{(iii)}$$

Rearranging equation (iii) in terms of $I_a(S)$

$$I_a(S) = \frac{m_a S^2 X_a(S) + (C_u + C_m)SX_a(S) - C_m SX_v(S) + (k_u + k_m)X_a(S) - k_m X_v(S)}{k_f}$$

And substitute in place $I_a(S)$ in equation (i) above: and $v_b(S) = \frac{dx_a}{dt} = sX_a(S)$ and $k_f = \frac{-NAB}{x_a}$

$$(L_a S + R_a)\left[\frac{m_a S^2 X_a(S) + (C_u + C_m)SX_a(S) - C_m SX_v(S) + (k_u + k_m)X_a(S) - k_m X_v(S)}{k_f}\right] + k_b s X_a(S) = V_{in}(S),$$

Now rearrange this equation output to input form which yields:

$$\frac{X_a(S)}{V_{in}(S)} = \frac{k_f + \frac{C_M L_a}{V_{in}(S)} S^2 X_v(S) + \left[\frac{k_m L_a + C_m R_a}{V_{in}(S)}\right] SX_v(S) + \frac{k_m R_a}{V_{in}(S)} X_v(S)}{m_a L_a S^3 + [(k_u + C_m)L_a + m_a R_a]S^2 + [(k_u + k_m)L_a + (k_u + k_m)R_a + k_b k_f]S + (k_u + k_m)R_a} \qquad (iv)$$

This is the output input equation of motion for electrical system and armature mass.

Applying newton's second law by using equation 4.67, summations of forces that acts on ***valve mass***;

$$+\downarrow \sum F_{x_v} = m_v a_v = m_v \ddot{x_v} = m_v \frac{d^2 x_v}{dt^2}$$

$$m_v \ddot{x_v} = F_{Sm} - F_{SL} + F_{Cm} - F_{CL}$$

$$m_v \ddot{x_v} = k_m(x_a - x_v) - k_L x_v + C_m(\dot{x_a} - \dot{x_v}) - C_L \dot{x_v}$$

Collecting like terms for mass of valves rewrite as;

$$m_v \ddot{x_v} - C_m \dot{x_a} + (C_m + C_L)\dot{x_v} - k_m x_a + (k_m + k_L)x_v = 0 \qquad (v)$$

Finally the equation of motion for EMVA system as shown on equation (iii);

$$\begin{cases} m_a\ddot{x_a} + (C_u + C_m)\dot{x_a} - C_m\dot{x_v} + (k_u + k_m)x_a - k_m x_v = F \\ m_v\ddot{x_v} - C_m\dot{x_a} + (C_m + C_L)\dot{x_v} - k_m x_a + (k_m + k_L)x_v = 0 \end{cases} \qquad (vi)$$

OR
$$\begin{cases} m_a\frac{d^2x_a}{dt^2} + (C_u + C_m)\frac{dx_a}{dt} - C_m\frac{dx_v}{dt} + (k_u + k_m)x_a - k_m x_v = F \\ m_v\frac{d^2x_v}{dt^2} - C_m\frac{dx_a}{dt} + (C_m + C_L)\frac{dx_v}{dt} - k_m x_a + (k_m + k_L)x_v = 0 \end{cases}$$

Laplace transform is a linear operator that converts a function, from time domain, to frequency domain. By applying the Laplace transform to equation (iii), which leads;

$$m_v s^2 X_v(s) - C_m s X_a(s) + (C_m + C_L)sX_v(s) - k_m X_a(s) + (k_m + k_L)X_v(s) = 0 \qquad (vii)$$

Expressing equation (vii) in terms of output to input (Gains) forms for easy math lab Simulink modeling purpose gives;

$$\frac{X_v(S)}{X_a(S)} = \frac{C_m S + k_m}{m_v S^2 + (C_m + C_L)S + (k_m + k_L)} \qquad (viii)$$

This is the equation of motion for valve mass.

Table 4.5: Technical data for EMV

Definition	**Symbol**	**Value**
The upper spring stiffness	k_u	10.557 KN/m
Upper viscous damping coefficient between armature and sleeve	C_u	60 N.s/m
Valve Stem Stiffness	k_m	250 KN/m
Viscous damping coefficient between armature and sleeve	C_m	60 N.s/m
The lower spring stiffness	k_L	10.557KN/m
Viscous damping coefficient between valve and guide.	C_L	60N.s/m
The maximum valve displacement (lift)	h_{max}	$6 \times 10^{-3} m$
Mass of armature	m_a	0.10012kg
Mass of valve and spring	m_v	0.204kg
Input voltage	V_{in}	14v
Inductance of coil	L_a	0.0001024 H
Resistance of coil	R_a	0.405Ω

4.3.2 Building the Actuator Model in Simulink

This system is modeled by summing the force acting on the solenoid plunger and integrating the acceleration to give velocity. Also, newton's law is applied to the solenoid actuator mass spring system. First, we model the integrals of the linear acceleration and of the rate of change of the armature and valve displacement.

$$\int \frac{d^2x_a}{dt^2}dt = \frac{dx_a}{dt} \ \& \int \frac{d^2x_v}{dt^2}dt = \frac{dx_v}{dt} \ \text{ And } \int \frac{dx_a}{dt}dt = \boldsymbol{x_a} \ \& \int \frac{dx_v}{dt}dt = \boldsymbol{x_v}$$

Then the equations of motion for actuator model are obtained on the above analysis, which is:

For the mass of armature: $\ddot{x_a} = \frac{1}{m_a}\left[F_p - (C_u + C_m)\dot{x_a} + C_m\dot{x_v} - (k_u + k_m)x_a + k_m x_v\right]$

For the mass of valve: $\ddot{x_v} = \frac{1}{m_v}\left[C_m\dot{x_a} - (C_m + C_L)\dot{x_v} + k_m x_a - (k_m + k_L)x_v\right]$

To build the simulation model, open MATLAB Simulink and click Simulink to open a new model window. Then following these listed steps below.

- Draw lines to and from the input and output terminals of an integrator block that you've inserted from the Simulink/continuous library.
- Label the input line “d2/dt2 (xv)” and the output line “d/dt(xv)” for acceleration of valve mass and label the input line “d/dt(xv)” and the output line xv for velocity valve integrator.
- Draw lines to and from the input and output terminals of the additional integrator block that is positioned above the preceding one.
- Label the input line “d2/dt2 (xa)” and the output line “d/dt(xa)” for acceleration of armature mass and label the input line “d/dt(xa)” and the output line xa for velocity integrator.

The linear acceleration of an armature is equal to 1/ma multiplied by the sum of seven terms (three positive, four negative). Similarly, the linear acceleration of valve mass is equal to 1/mv multiplied by the sum of six terms (two positive, four negative). And continue this equation in Simulink, by following the steps given below.

- Insert two gain blocks from the Simulink/Math operations library, one attached to each of the integrators.
- Double-clicking the gain block that corresponds to linear acceleration will allow you to edit its value to "1/ma and 1/mv.”
- Change the label of this Gain block to "armature and valve" by clicking on the word "Gain" underneath the block respectively.
- Put one Add block connected by a line to each of the gain blocks and two Add blocks from the Simulink/Math operations library.

- Edit the signs of the Add block corresponding to rotation to "+-" since three terms is positive and four is negative, two terms positive and four terms negative respectively.
- Continuing adding gain blocks of the coefficient of integrator/derivatives and connecting the corresponding integrator by considering signs from added blocks to all blocks in input/output forms.

The final design look likes as follows:

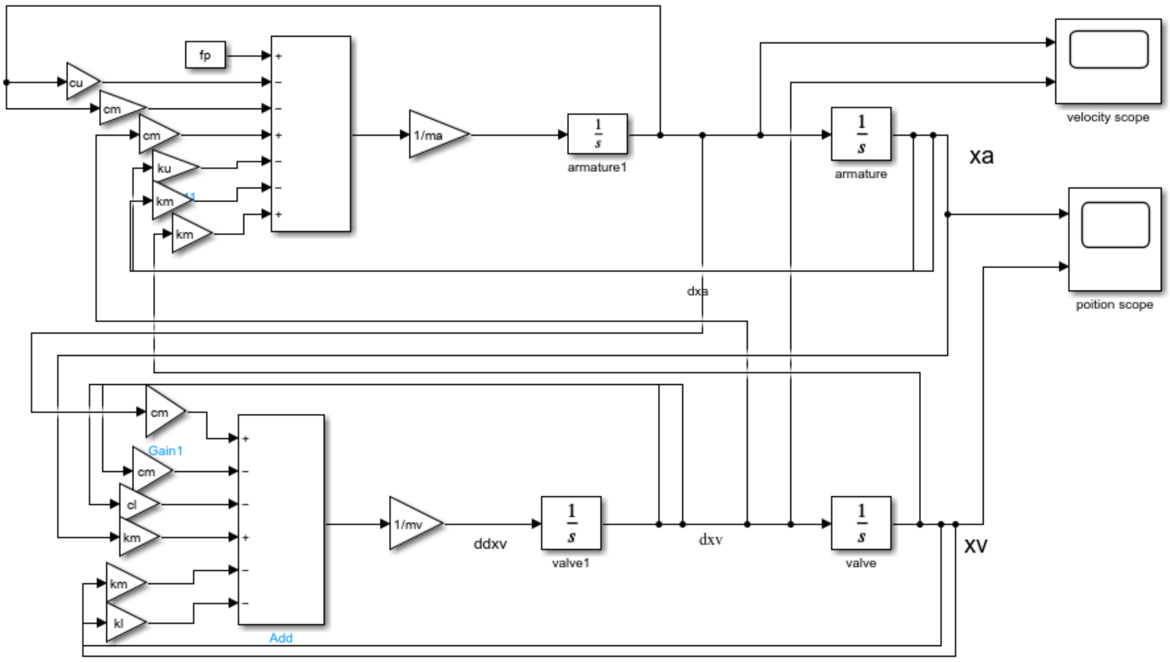

Figure 4.31: Solenoid actuator Simulink model

4.3.3 Building Whole Electromechanical System in Simulink:

The system comprises electrical and mechanical systems that are model in MATLAB Simulink. This system is modeled by summing the force acting on the plunger/armature and integrating the acceleration to give displacement, and Also applied the Kirchhoff's laws to the armature circuit. First, model the solenoid actuator and then model the rate of change of the armature current.

$$\int \frac{di}{dt} dt = i$$

Then the equations of motion for electrical the system that is used for crating Simulink is obtained on the above analysis by rearranging equation 3.67, which is:

$$L_a \frac{di_a}{dt} = -R_a i_a - e_b + V_{in} \rightarrow L_a \frac{di_a}{dt} = -R_a i_a - k_e \frac{dx_a}{dt} + V_{in}$$

$$\frac{di_a}{dt} = \frac{1}{L_a}\left[-R_a i_a - k_e \frac{dx_a}{dt} + V_{in}\right] \qquad (i)$$

To build the simulation model, open MATLAB Simulink and open the pervious saved solenoid actuator model. Then add the electrical equation in place of plunger force (Fp) by following the steps listed below.

- Insert another Integrator block above the previous model integrator and draw lines to and from its input and output terminals.
- Mark the line of input as "d/dt(i)" and the line of output as "i".

From the equation (i), the derivative of current in the armature is equal to $1/L_a$ multiplied by the sum of three terms (one positive, two negative). Proceed with the following steps to continue modeling these equations in Simulink.

- Insert one Gain blocks from the Simulink/Math Operations library above solenoid actuator model, attached to the integrators.
- Change the label "Inductance" and the value of the Gain to "1/L."
- Insert Add blocks from the Simulink/Math Operations library above the actuator model, attached by a line to the Gain block.
- Edit the signs of the Add block to "-+-" to represent the signs of the terms in the electrical equation.

Next, we will add in the magnetic force from the armature.

- Insert a Gain block attached to the positive input of the linear Add block with a line.
- Edit its value to "K_f" to represent the force constant and Label it "Kf".
- Draw the line that connects the current Integrator to the "Kf" block and continue drawing it.

Adding the voltage terms that are shown in the electrical equation will be our next step. The voltage drop across the armature resistance will be added first.

- Over the "Inductance" block, insert a Gain block and flip it from left to right.
- Change the block's name to "Resistance" and set the Gain value to "R".
- Attach a line to the input of the "Resistance" block by tapping off the output of the current integrator.
- Draw a line connecting the output of the "Resistance" block to the current equation's upper negative input. Include a block.

Next, we will add in the back emf from the solenoid actuator.

- Add a Gain block and attach it with a line to the current Add block's other negative input.
- Edit its value to “K_e” to represent the solenoid back emf constant and Label it "K_e".
- Tap a line off the linear Integrator's output and connect it to the “K_e”block.
- Add In1 and Out1 blocks from the Simulink/Ports & Subsystems library and respectively label them “Voltage” and “displacement”

Final design of electrical system and solenoid actuator are shown below;

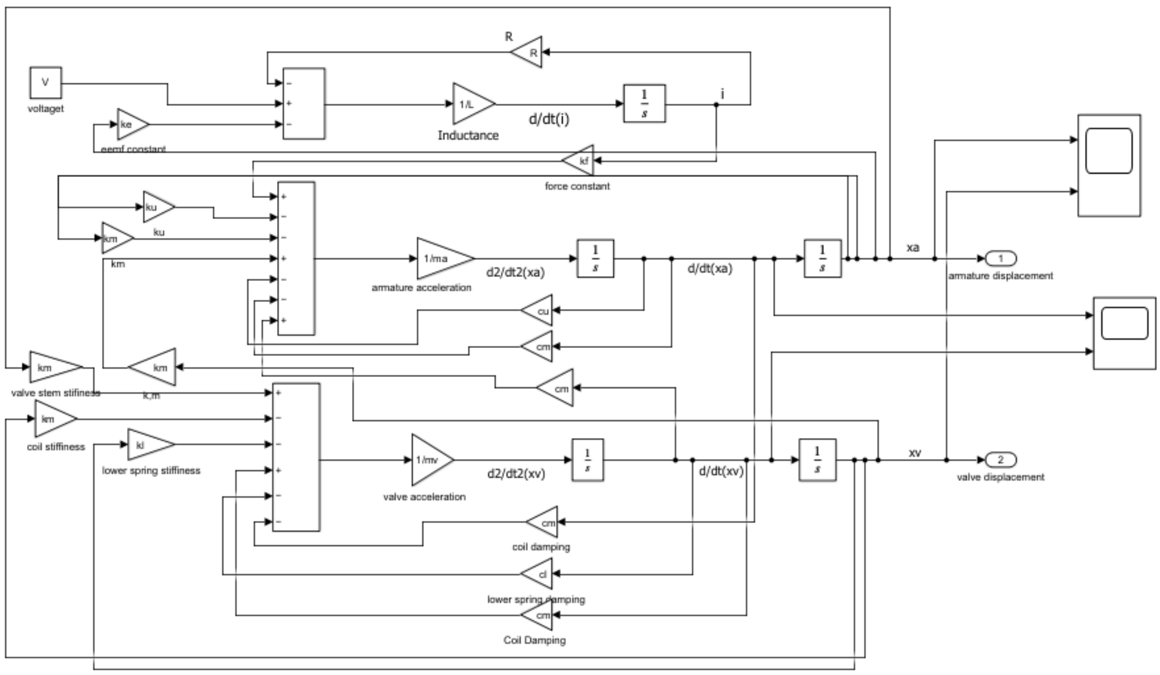

Figure 4.32: Electromechanical Valve Actuator Simulink model

4.4 Control System and Program Design

Due to periodic operation, the closed loop actuator control strategy is going to be described only for valve-closing. The valve is fully open and the armature is being held at the bottom pole face prior to the beginning of the closing event. First, the bottom coil is discharged and the armature starts moving towards the top pole face with the loaded springs. The top coil must be properly energized to ensure that it gently captures the armature due to energy losses. One the one hand, the coils must supply the system with enough energy to ensure that the armature will be caught in the event of losses. Excessive energy is going to result in contacts of moving parts with non-zero kinetic energy. Quiet, dependable, and long-lasting operation requires soft-seating of the armature to each pole face and the valve to the valve head. The goal of the control is to strike a delicate balance between hard-seating the armature/valve and unsuccessful valve operation (V. Utkin, J. Guldner, 2009).

4.4.1 Sensors Communication

The engine speed sensor uses the same sensor as the crankshaft angle sensor (Prof. Ir. Dr. Alias Bin Mohd Noor, 2006). If the sensor detects a hole, the output will generate a high pulse (+5 volt). In order to obtain the current engine speed, the ECU counts the total number of pulses detected by the speed sensor for every one second (Prof. Ir. Dr. Azhar Bin Abdul Aziz, 2006). The engine speed in RPM will be obtained using the following formula:

$$\text{Engine Speed} = \frac{\text{Total number of pulseper second} \times 60}{72} \qquad (4.68)$$

When the Zero TDC sensor detects the zero TDC position, the ECU begins counting pulses and turning on the one-second timer. When the one- second timer stops, the ECU has counted the total pulses (Prof. Ir. Dr. Azhar Bin Abdul Aziz, 2006). 72 is number of teeth on the rotating disk to detect the number of pulses developed in a specific rotating speed, it may be varied as we want.

- **Crank Angle Sensor**

The crankshaft angle sensor also uses a trans-missive optoschmitt Sensor to detect the current crankshaft angle with respect to the zero TDC position.

The trasmissive optoschmitt Sensor consists of an infrared emitting diode facing an optoschmitt detector encased in a black thermoplastic housing.

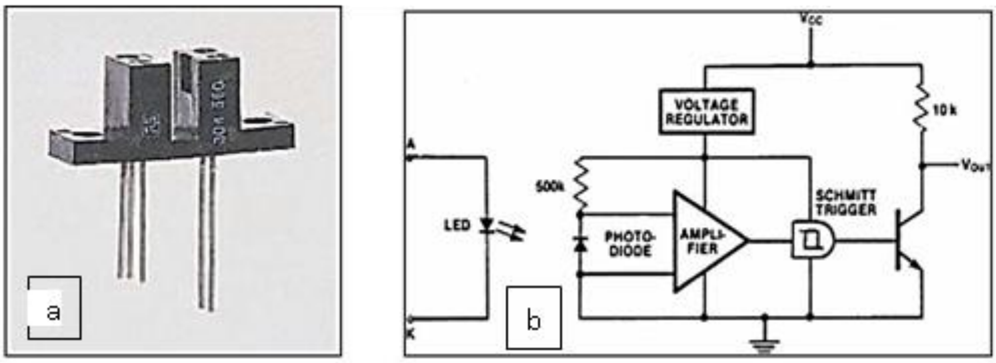

Figure 4.33: a) Transmissive Optoschmitt Sensor b) Schematic diagram (Prof. Ir. Dr. Azhar Bin Abdul Aziz, 2006).

The output of the detector provides a high output (+5 volt) when the optical path is clear, meaning that the hole on the aluminum disc has been detected. The output of the detector gives a low output (0 volt) when the path is interrupted, meaning that the aluminum disc has blocked the path. The output of this TDC sensor is used to inform the Electronic Control Unit (ECU) that the Zero TDC has been detected (Prof. Ir. Dr. Azhar Bin Abdul Aziz, 2006).

In this thesis the design to detect the crankshaft angle, 72- hole equally spaces have been made on the same aluminum disc used for the zero TDC sensors. It indicates that there are five degrees of space between the two holes. The way of the crankshaft angle sensor work is similar to that of the zero TDC sensors. Instead of detecting only one hole, the crankshaft angle sensor detects the certain angle position of the crankshaft by counting the holes that have been detected. If the sensor detects a hole, the output will generate a high pulse (+5 volt). Consequently, it is possible to determine the crankshaft's angle position by counting the output pulses. In this case, one pulse represents angle of 5 degrees. When the zero TDC sensors come into contact with the zero TDC position, the crankshaft angle sensor begins to count. The ECU counts the crankshaft angle position based on the sensor's output. Based on this information, the ECU can determine when to activate the solenoid valve.

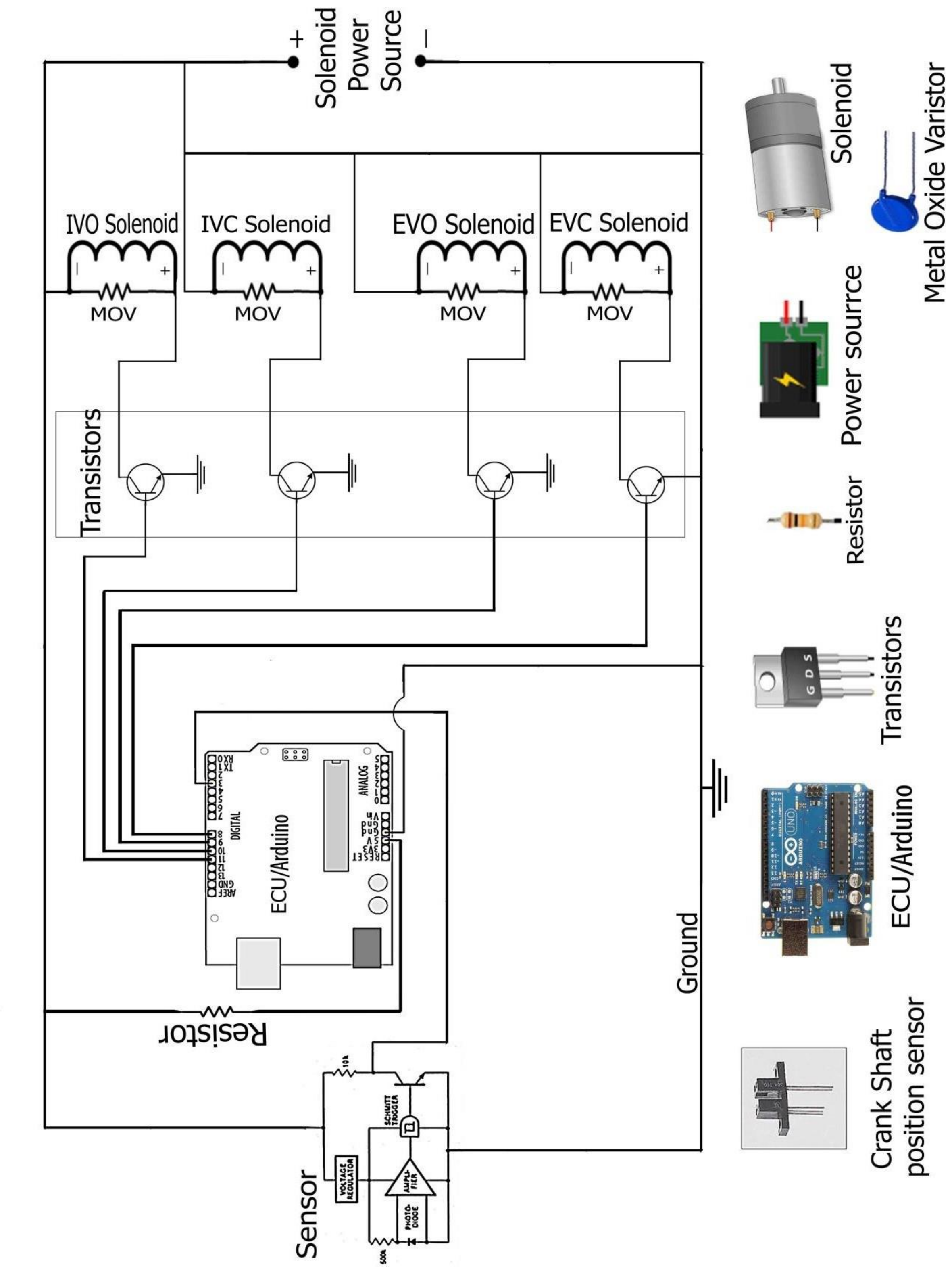

Figure 4.34: General circuit diagram of the designed EMV actuation system

4.4.2 Programming

In the case of this paper the controller is Arduino and the programming is performed on the basis of the output signal of crank shaft position sensor. This is performed by the integrated formula calculation of the three sensors; such that crankshaft position sensor, speed sensor and zero TDC sensor. The relation is described in the above.

The programs that can use to control the system by using Arduino as an ECU is designed (Michael, 2017) and see at the end of the paper in Appendix-B.

Since this program is used for only Arduino for simulation as ECU, it is possible to design the program for original ECU in such way.

4.5 Cost Benefit Analysis

Cost analysis consists many costs but in this case it‘s only considered the cost of materials but not the labor cost, machining and the like costs. The cost of the materials/the designed machine component should be taken in to consideration in a proper design flow. In this case of cost analysis the cost is considered only on the electrical system of the actuator and its support. Thus the components including the four solenoids with the armature unit, the solenoid stand, coupling member ECU/Arduino Uno, sensors, cooling fins, upper springs (two springs), relay and MOV/Diode. The other components are already found in the conventional cam engine, so it does not need any more calculation of the cost.

$$\text{cost of material in \$} = \frac{\$}{kg} \times \text{ mass of material in kg} \tag{4.69}$$

Let us first calculate the mass of the solenoid stand member with fins;

$$Mass = density\ of\ the\ material \times volume$$

$$volume = \ length \times \ width \ \times height$$

This member is already designed and takes the dimension in the design analysis section;

$$volume = 3(0.08m \times 0.045m \times 0.005m) + 2(0.17204m \times 0.045m \times 0.005m)$$
$$+2(0.02m \times 0.045m \times 0.005m) + 2(0.09m \times 0.05004m \times 0.007m)$$

$$volume = 0.000054m^3 + 0.000077418m^3 + 0.000009m^3 + 0.0000630504m^3$$
$$= 0.00002133m^3$$

$$mass\ of\ the\ stand = density\ of\ alumunium\ alloy \times volume$$

$$mass\ of\ the\ stand = \frac{2770kg}{m^3} \times 0.00002133m^3 = 0.591kg$$

Since one kg of aluminum alloy is \$4.9 (Alibaba.com., 2024). So the cost of the solenoid stand with fins is;

$$cost\ of\ stand\ with\ fins = \frac{\$4.9}{kg} \times 0.591kg = \$2.8959$$

The cost of the solenoid with armature and plunger is estimated from the current price of the equivalent solenoid in the market which $20.83 (Alibaba.com, 2024).

Solenoid size (D/H)	Number of units	Unit price
38x18	4	$20.83
Total price = $83.32		

The mass of coupling member:

$$Volume\ of\ coupling\ =\ 2(0.01m \times 0.01m \times 0.038m) - 2(0.0.005m \times \pi \times \frac{0.006^2}{4})$$

$$Volume\ of\ coupling\ =\ 0.000007317m^3$$

Coupling is made of stainless steel which has the density of 7700kg/m^3. Now, price per kg is $5 (Mesotek, 2024). Mass of coupling member is given by:

$$mass\ of\ coupling = \frac{7700kg}{m^3} \times\ 0.000007317m^3 = 0.0563409kg$$

$$cost\ of\ coupling\ = \frac{\$5}{kg} \times 0.0563409kg = \$2.817$$

Arduino Uno uses as ECU, its price is $20. Other components like relay, sensors, wires, MOV and other accessories cost about $136.

The cost of the spring is also estimated in the same way (Focus Technology Co., 2024);

$$volume\ of\ spring = 2\left(\frac{\pi}{4} \times (0.001829m)^2 \times 0.202m\right) = 0.0000010614m^3$$

$$mass\ of\ spring = 7800kg/m^3 \times 0.0000010614m^3 = 0.00828kg$$

$$cost\ of\ spring\ = \frac{\$1.2}{kg} \times 0.00828kg = \$0.0099$$

Mass of bolt is density time's volume of bolt. Volume is given by;

$$volume\ of\ bolt = 4\left(\frac{\pi}{4} \times (0.003m)^2 \times 0.0645m\right) + 2\left(\frac{\pi}{4} \times (0.003m)^2 \times 0.007m\right)$$

$$= 0.0000072944m^3 + 0.00000009896m^3 = 0.0000073933m^3$$

$$mass\ of\ bolt = \frac{7860kg}{m^3} \times 0.0000073933m^3 = 0.0581kg$$

$$cost\ of\ spring\ = \frac{\$16}{kg} \times 0.0581kg = \$0.9296$$

Nuts which ranges from M1- M30 is $1. System has 6 nuts then total price is 6*$1=$6.

The total cost of the valve actuation system component is the sum of all in the above.

Total cost = $ 251.97

This is the total estimated cost required to build the system in current material price of the market. But cost used for conventional camshaft engine is expensive which has $528.33. Therefore the designing electromechanical valve actuator camless engine is beneficial in terms of cost because it is so cheap as compared to conventional one.

CHAPTER FIVE

5. RESULT AND DISCUSSION

5.1 Simulation and Stress Testing Analysis Using Software

A. Electrical system simulation

The simulation of electrical system is done by using electrical design software which is PROTEUS DESIGN SUIT PROFESSIONAL 8.6 SP3 and Arduino IDE 2.3.2 version. This system uses Arduino Uno as controller, LED as a valve and there are also other colored LED‘s as a solenoid valves. In addition to this digital oscilloscope is used to observe the pulse width as the speed varies. The system uses two green LEDs and two red LEDs to show opening and closing solenoid valve is activated and uses two LED-BIBYs which displays yellow and blue color. The yellow indicates valve is opening and blue shows valve is in closed position. The system operation is described as follows.

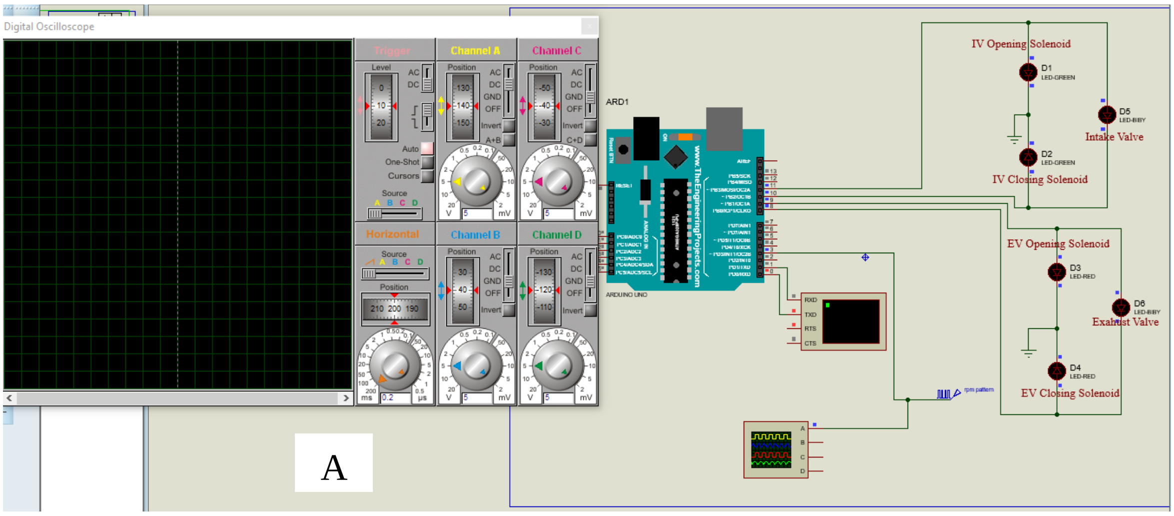

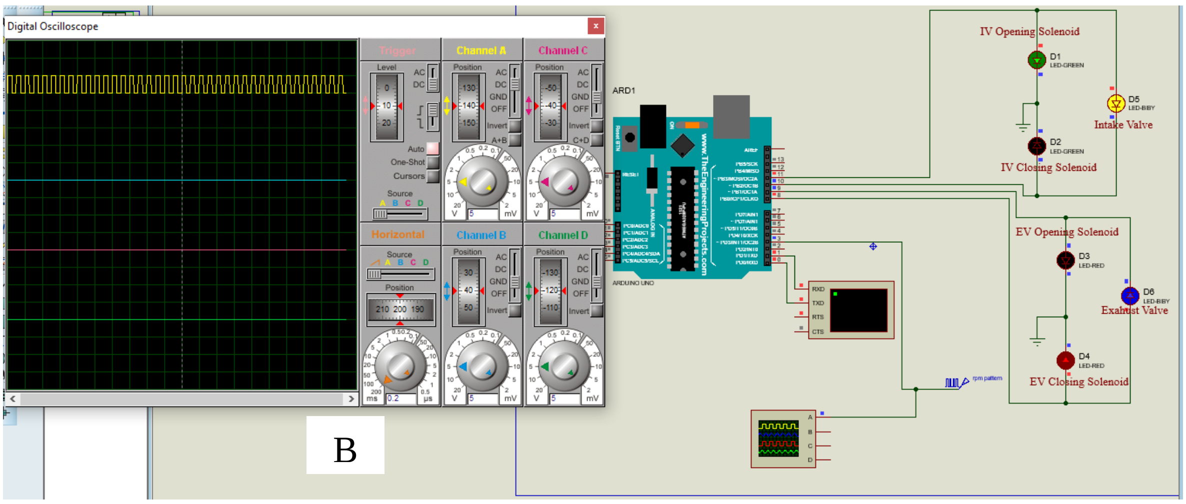

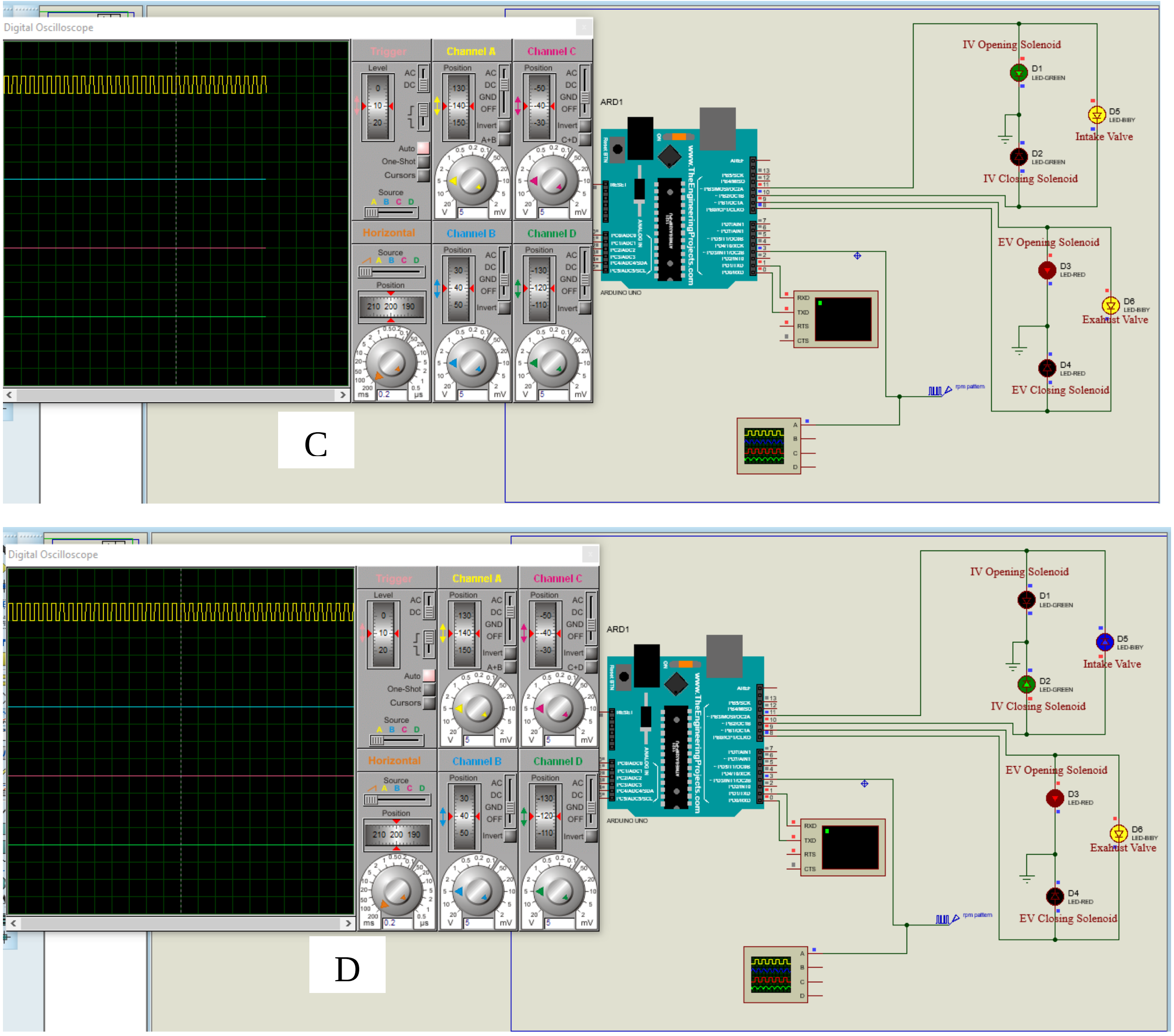

Figure 5.1: Electrical system simulation of the actuators.

Figure 5.1 describes the electrical system simulation; initially the figure (A) shown the system has non-operational condition. In figure (B), the yellow color (D5) shows the intake valve is open and the green color (D1 (IV opening solenoid)) that have connection with the D5 (LED BIBY) is activated and at same time EV closing solenoid is activated which is controlled by ECU. In the same way the blue color (D6) is indicates as the exhaust valve is closed and the red one (D4) is the exhaust valve closing solenoid is activated. In figure (C), yellow color (D5 and D6) shows both intake and exhaust valve is in opening position and green color (D1 (IV opening solenoid)) and red color (D3(EV opening solenoid) that has connection with D5(LED BIBY) and D6(LED BIBY) are activated which is also known as valve overlapping state. In figure (D) the yellow color D6 shows exhaust valve is open and red LED D3(EV opening solenoid) that have connection with the D6 is activated, similarly at the same time IV closing solenoid (D2) is activated to close intake valve. And In the same way the blue color (D5) is indicates as the intake valve is closed and the red one (D2) is the intake valve closing solenoid is activated. In the same way the valves are actuated infinitely with in a verity of speed ranges and valve timings. As it is described in the figure 5.1 there is a pulse generated by the digital oscilloscope and opening degrees with related engine speed, but it must be taken in to consideration that the software is help to understand what it looks like because when the speed goes maximum the system software cannot recognize/out of expected vale/. And also electromagnetic valve actuation system has an implementation on proper valve overlapping time. See the above figure 4.1; from the figure the Arduino Uno is as electronic control unit with related programing.

B. Solenoid actuator simulation analysis

Enhancing efficiency is possible if the valve opens and shuts quickly enough to eliminate the current restriction. As a result, it is critical that the valve achieves full lift as quickly as feasible

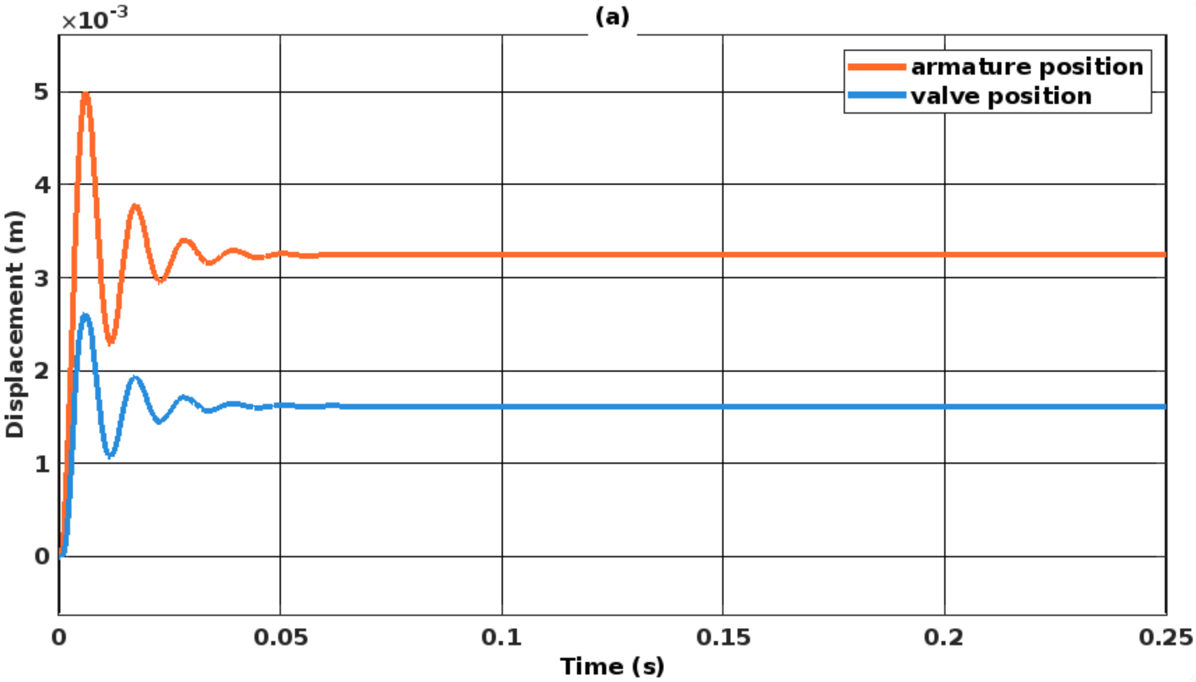

(a) Illustrates the displacement response of the armature and valve.

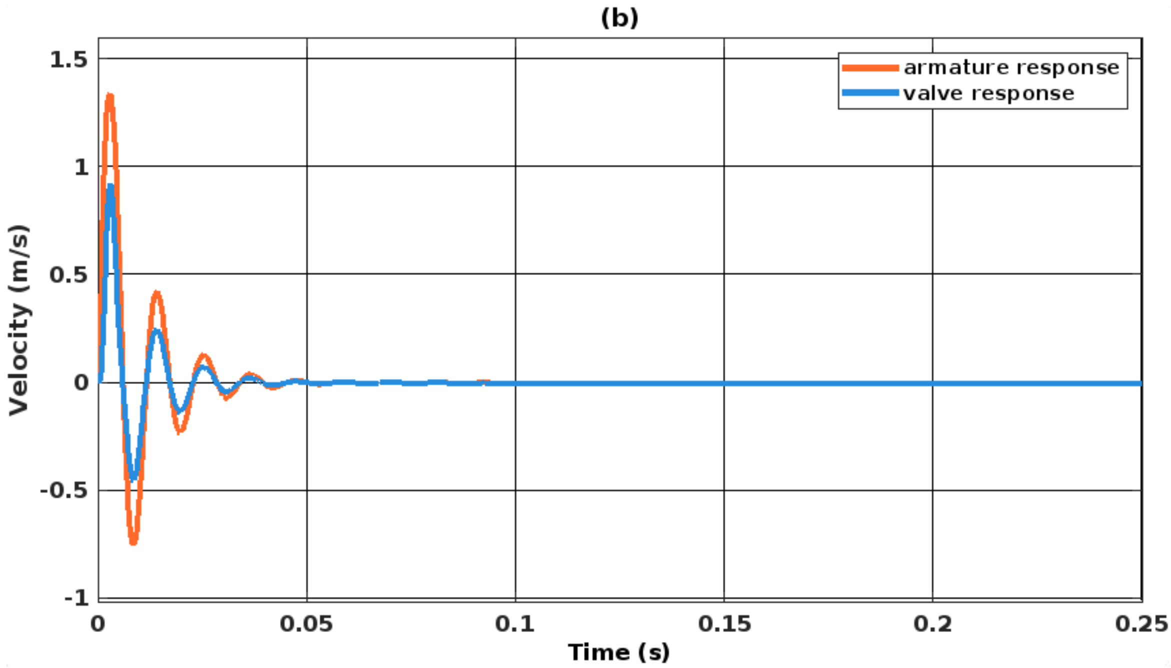

(b) Displays the velocity response for both the armature (blue) and the valve (orange).

Figure 5.2: EMVA System response in time domain for zero current

Figure 5.2 shows the EMVA system response in time domain. Figure 5.2(a) illustrates the displacement response of the armature and valve. The blue and orange curves indicate armature and valve displacement, respectively. The results indicate that the armature and valve are dampened after 0.1 seconds, with the armature having a greater rising domain. Figure (5.2b) displays the velocity response for both the armature (blue) and the valve (orange). The armature and poppet valve increase at the same rate of 0.8 m/s and reach the dampened value within 0.1 seconds.

Figure 5.3 shows variable armature lift profile of a solenoid, likely measured in millimeters (mm), for different actuation currents.

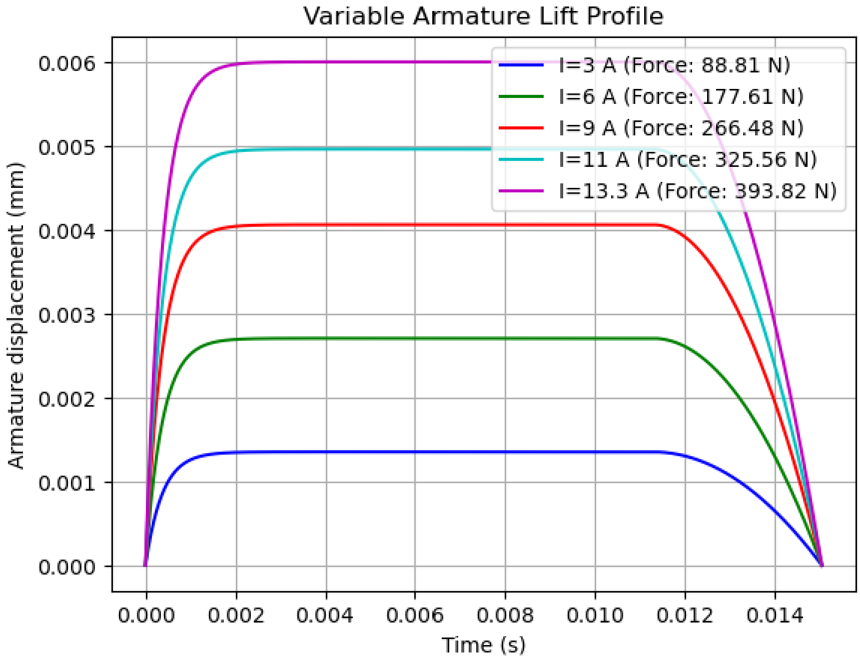

Figure 5.3: Variable armature lift

Figure 5.3 demonstrates how the current supplied to the actuator directly influences the lift (displacement) of the valve/armature. The different lines on the graph likely represent various actuation currents applied to the solenoid coil. Higher currents generate a stronger magnetic field within the solenoid, resulting in a greater pulling force exerted on the armature and armature displacement (opening) over time for each current level, higher current lines will generally show a larger peak displacement on the Y-axis, indicating a greater valve opening. By varying the current, the engine can achieve different lift profiles, optimizing performance across various operating conditions. In general, solenoid actuator uses electromagnetism to create force. The current supplied to the solenoid's armature windings determines the strength of the magnetic field generated by the armature, which in turn affects the force produced by the solenoid. The graph likely shows how varying the current supplied to the solenoid's armature coil affects the position (displacement) of the armature over time.

C. Finite Element Analysis

For analysis purpose, ANSYS software is used. The ANSYS space claim model is imported to ANSYS workbench. Finite element model of each supporting components of the system and solenoid armatures used in numerical analysis were generated in order to estimate the stress distribution and structural displacements. FEA will provide results that may be used to evaluate the strength of design based on the Von-Misses criterion, deformation criterion, principal elastic strain criterion, and fatigue strength to identify the areas that require improvement.

- **Static structural analysis:**

The mechanical system components stress, deflections and strain are analyzed by using ANSYS 2023 R2 workbench software as shown in figure 5.4. This section investigates the stress distribution in an aluminum member (lower, middle and upper) subjected to a static load of 393.82 N using ANSYS workbench software. The material properties used for the aluminum alloy are: Young's modulus (E) = 70GPa and Poisson's ratio (ν) = 0.33. Both ends of the member are fixed.

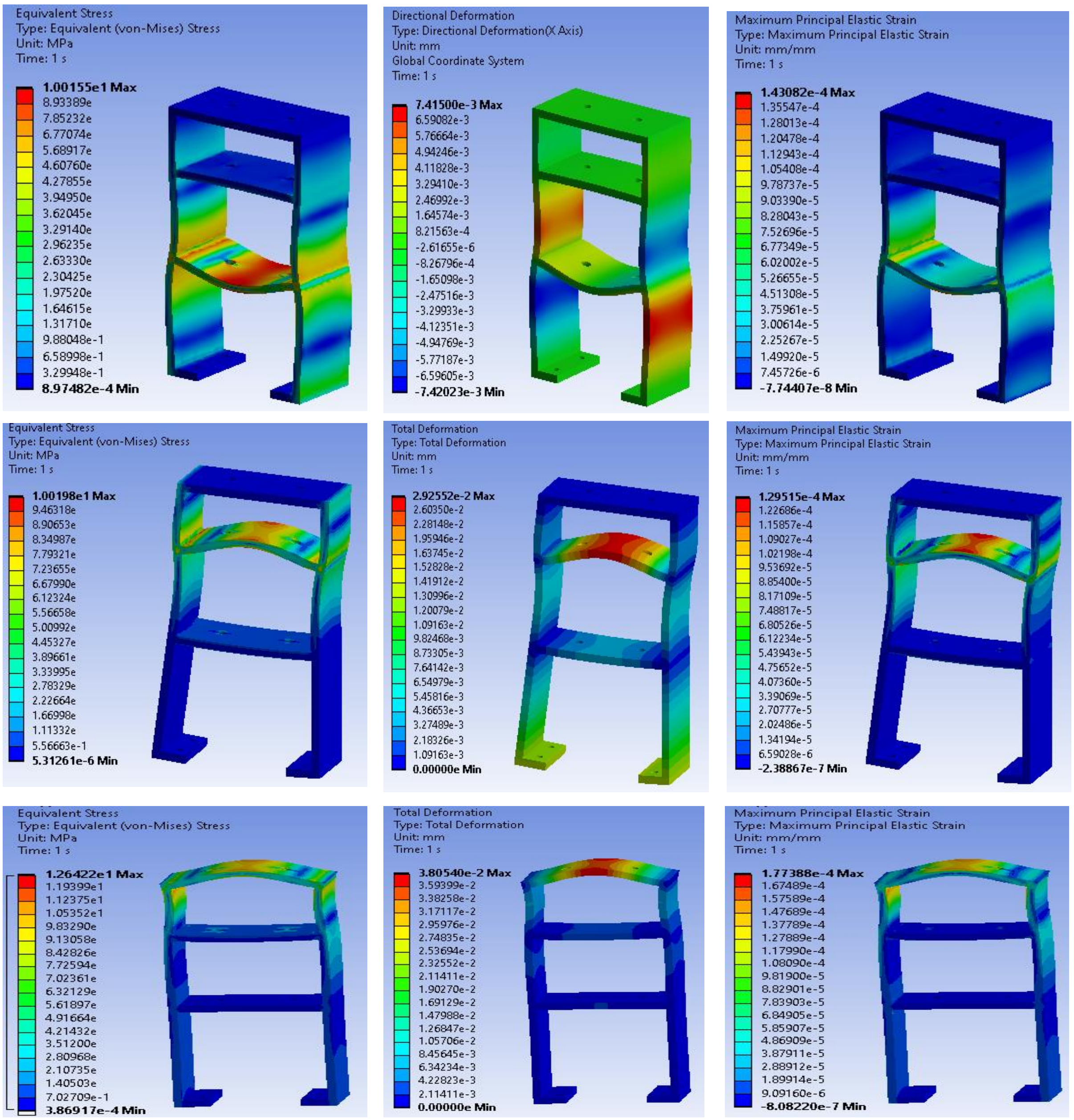

Figure 5.4: Simulation of the solenoid stand/stress analysis of a horizontal members/.

From the figure 5.4 above shows that the ANSYS simulation of the aluminum member reveals key findings regarding its stress and deformation. The low equivalent elastic strain (0.000146) and equivalent stress (10.279MPa) suggest the member is likely experiencing elastic deformation and hasn't reached its yield point. This aligns with the analytical solution, which indicates the member remains within the elastic regime.

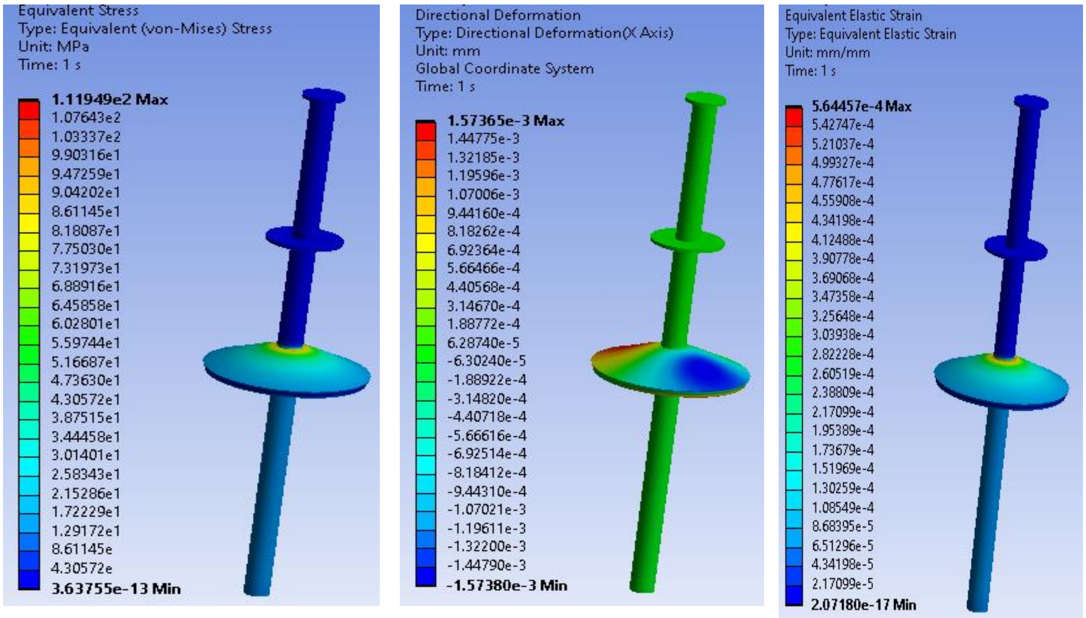

Figure 5.5: Stress analysis and simulation of the armature with plunger.

Figure 5.5 shows the stress distribution and simulation of armature with plunger subjected to a static load of 393.82 N using ANSYS software. The material properties used for the cast iron are: Young's modulus (E) = 66.2GPa and Poisson's ratio (ν) = 0.26. Boundary condition: One ends of the plunger is fixed.

The ANSYS simulation resulted in an equivalent (von-miss) stress of 111.949 N/mm² and a maximum directional deformation is 0.00157365 mm. The stress distribution plot (Figure 5.5) illustrates these findings. The highest von-miss stress is concentrated around the center of the armature. The low equivalent elastic strain (0.000564457mm) and equivalent stress (111.949MPa) suggest the armature with plunger is likely experiencing elastic deformation and hasn't reached its yield point, which indicates the member remains within the elastic regime.

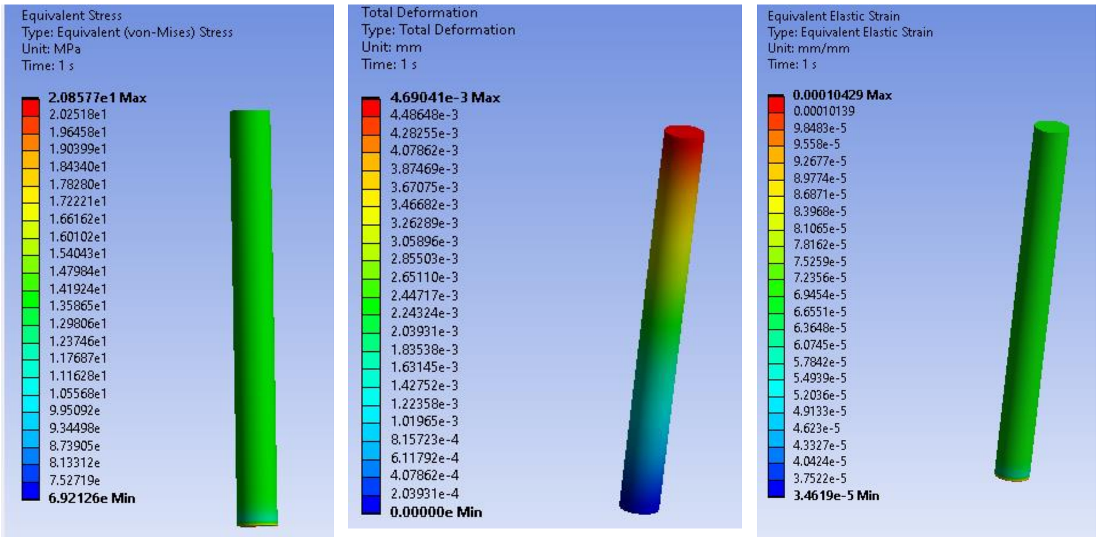

Figure 5.6: Stress analysis and simulation of the half of plunger unit.

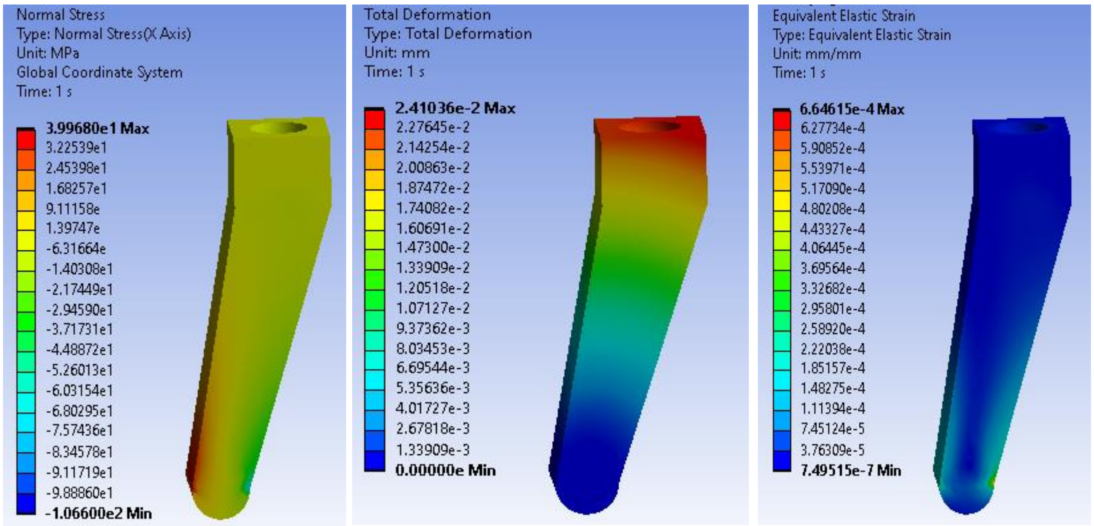

Figure 5.7: Stress analysis and simulation of coupling member.

Figure 5.6 and 5.7 shows the stress distribution and simulation of half plunger unit and coupling member subjected to a static load of 393.82 N using ANSYS software respectively. The material properties used for the stainless steel for both are: Young's modulus (E) = 193GPa and Poisson's ratio (ν) = 0.31. Boundary condition: One ends (lower end) of the half plunger and coupling member is fixed.

The simulation resulted in an equivalent (von-miss) stress of 20.8577N/mm² and 39.968N/mm² and a maximum deformation is0.00241036mm and 0.002410mm respectively. The stress distribution plot (Figure 4.4) illustrates these findings. The highest von-miss stress is concentrated around the tip of the half plunger and coupling member. The low equivalent elastic strain (0.000466461 and 0.000564457) and von-miss stress (20.8577MPa and 39.968MPa) respectively suggests that the coupling is likely experiencing elastic deformation and hasn't reached its yield point of material (151MPa), which indicates the member remains within the elastic regime.

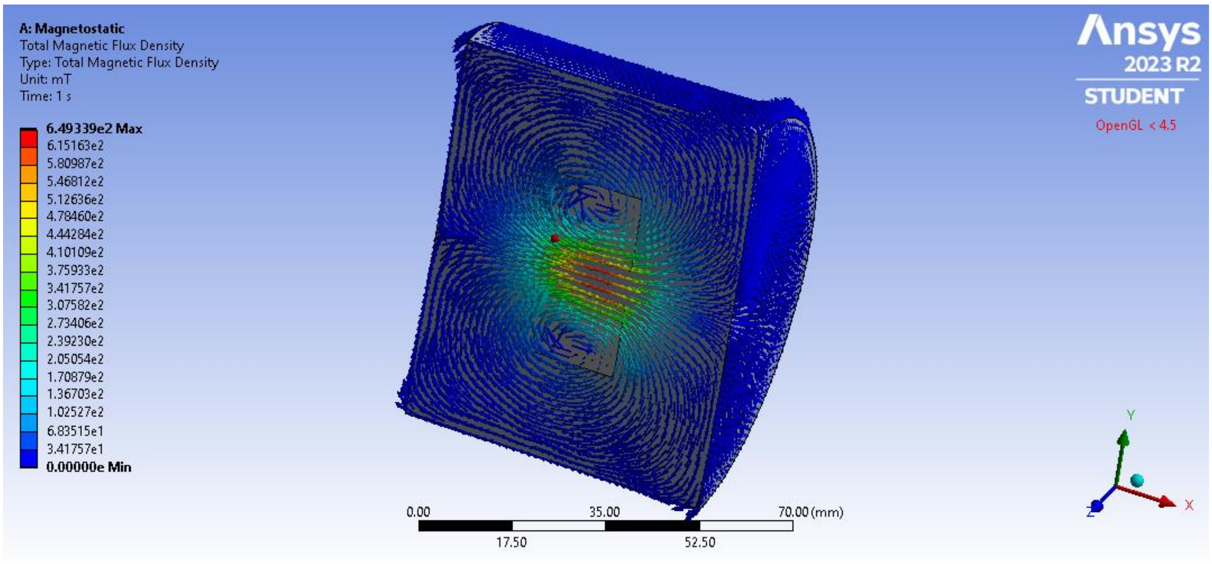

Figure 5.8: Magnetic field lines through cut section of the solenoid simulation in ANSYS

Figure 5.8 shows the simulation result of half section of solenoid coil in ANSYS magneto-static analysis. Figure illustrates the coil's magnetic field behavior; the magnetic field lines point downwards through the middle of the solenoid and curve around the bottom of the coil and circle back upwards to the top of the coil. Both the size and color of the arrow scales to the magnitude of the magnetic flux density, therefore the magnetic field is strongest and uniform inside the middle of the coil and decrease significantly in magnitude outside the coil. By Comparing the analytical calculation of magnetic flux density (B=0.69mT) and the maximum simulation ANSYS magneto-static analysis result (0.649mT) are numerically very close to each other. In fact, they are practically identical. Based on this comparison, the theoretical calculation and the ANSYS magneto-statics analysis are excellent agreement. This consistency reinforces the confidence in the accuracy of both approaches and suggests that the magnetic flux density result of approximately 690MT is reliable.

The research conducted on the electromechanical valve actuation system compared to conventional valve actuation components in Honda CG 125 engines yielded the following results:

- The total weight of the analyzed electromechanical valve actuation system was approximately 2.729 kilograms, which is a reduction of 0.671 kilograms (about 20%) compared to the 3.4 kilograms of the conventional valve actuation components. This weight reduction was achieved through the reduction of valve train components and the camshaft itself.

- The reduction in engine weight contributes to improved engine efficiency. A lighter engine requires less energy to operate, resulting in improved fuel economy and reduced fuel consumption.
- The implementation of variable valve timing in the electromechanical valve actuation system allows for the efficient control of valve lift and timing. The maximum valve lift achieved in the system was approximately 6mm, which is comparable to conventional valve lift mechanisms. The PROTUES simulation demonstrated that the valve timing can be infinitely varied based on control programming, enabling the decoupling of valve lift, timing, and actuation speed from the crankshaft position.
- The cost analysis revealed that the design of the electromechanical valve actuation system is cost-effective compared to conventional camshaft engines in the current market. This means that the electromechanical system offers a more affordable option without compromising performance.

Based on these research findings, it can be concluded that the analyzed electromechanical valve actuation system shows great potential for practical implementation in real engines with some technical adjustments. The system offers weight reduction, improved engine efficiency, reduced fuel consumption, and cost-effectiveness compared to conventional camshaft engines.

6. CONCLUSION AND RECOMMENDATIONS

6.1 Conclusion

This thesis presented the expected design of electromechanical valve actuation system to Honda 125 CG engine model. Mechanical and electrical analysis and simulation were made, and this development has proven the concept of replacing an internal combustion engines camshaft with an electromagnetic actuated electronically controlled valves, is possible. In this research study;

- The design of valves and valve springs was carried out, ensuring appropriate dimensions, force required for designing and characteristics to enable effective valve operations.
- An electromechanical actuation system was designed, comprising solenoid actuators and associated electronic control components, to provide independent control over valve timing, lift and duration.
- The electronic control system was programed to manage the actuation of the valves, enabling real-time adjustments to optimize engine performance and efficiency.
- The total weight of the analyzed electromechanical valve actuation system was 2.729 kilograms, which is a reduction of 0.671 kilograms (about 20%) compared to the 3.4 kilograms of the conventional valve actuation components. This weight reduction was achieved through the reduction of valve train components and the camshaft itself. The reduction in engine weight contributes to improved engine efficiency. A lighter engine requires less energy to operate, resulting in improved fuel economy and reduced fuel consumption.
- Computer simulations using ANSYS 2023R2 workbench, MAT LAB/Simulink and PROTEUS design software were conducted to evaluate the design is safe, functionality and performance of the electromechanical valve actuation system. The results demonstrated the feasibility and potential benefits of the proposed camless engine design.

The implementation of the camless engine with electromechanical valve actuation system has the potential to enhance fuel economy, increase torque, reduce emissions, and optimize engine performance across the operating range.

The elimination of the camshaft and associated mechanical components leads to a reduction in the overall engine weighted, contributing to improve fuel efficiency and reduced energy losses. The soft landing capability of the valve actuation system ensures minimal wear on the engine valves, improving durability and reliability. This initial development has also confirmed its functional ability to control the valve timing, lift, velocity, and event durations in a completely controlled manner. Regardless of the research takes this phase can be considered successful. The working unit has seen the capable of doing the expected job on the software and has proven the camless engine based on electromagnetic control is feasible. This phase alone makes a great leads into the automotive and valve technology of the future. Generally, from this finding the EMVA system is feasible system for internal combustion engines.

6.2 Recommendations

Based on the finding of this research, it has some limitation related to the valve velocity comparing with the previous research work. However, this limitation provides the inspiration for continued development and discovery.

Based on the finding of this research, the following recommendations are made:

- This system needs a further study to be conducted on the soft landing control of valve and its velocity because this EMVA system has little soft landing problem, and this design is performs for single cylinder engine, also improving this development to install for multi-cylinder engines is recommended to widen the technology application.
- Other phase is new approach to the overall system; one of the prime concerns is reduction of size and power consumption of the solenoid. Although this research achieved the weight reduction on this thesis, it needs to be reduced further. This can be achieved through a new design of solenoid, if the size of the solenoid is reduced (i.e. by keeping the same magnetic force production) there will be unnecessary part to be removed, this leads to further improved size.
- Since this work is performs using computer simulation and manual analysis for validation, further experimental validation needed for Conducting experimental tests and measurements on a physical prototype of the camless engine cylinder head with the electromechanical valve actuation system would provide practical validation of the design and simulation results. This will help in assessing the performance, efficiency, and emissions characteristics of the system under real-world operating conditions.

- This work is used Arduino Uno for controlling of EMVA system independently but Integration with advanced control algorithms and explore the integration of advanced control algorithms, such as model predictive control or adaptive control, to further enhance the dynamic response and precision of the valve actuation system. These algorithms can adapt to changing operating conditions and optimize valve timing and lift for improved engine performance and fuel efficiency.

By addressing these recommendations and further advancing research in the field of camless engine technology, it is possible to overcome the limitations of conventional valve actuation systems and achieve improved engine performance, fuel efficiency, and emissions control in internal combustion engines.

REFERENCES

Alibaba.com. (2024). *aluminum plate 7075 t6 price per kg*. https://www.alibaba.com/product-detail/aluminum-plate-7075-t6-price-per_60739108289.html?spm=a2700.galleryofferlist.normal_offer.d_title.7cef376e61beA9

Alibaba.com. (2024). *18mm long stroke solenoid U1253S Push-pull linear solenoid*. https://www.alibaba.com/product-detail/18mm-long-stroke-solenoid-U1253S-Push_1600941282144.html?spm=a2700.galleryofferlist.normal_offer.d_title.1ffd387f516VqS

ANAN*, A. (2015). *CAMLESS ENGINE*. https://es.scribd.com/document/307081400/Camless-Engine-Report

Ashby, M. F. (2005). *MATERIALS SELECTION SECOND EDITION MECHANICAL DESIGN* (Third Edit).

Bansal, D. R. K. (2009). *A Text Book of Strength of Materials* (Fouth edit). LAXMI PUPLICATIONS (P) LTD 113.

Bhattacharyya, S. (2023). *Thermohydraulic characteristics of magnetic nanofluid in mini channels under the influence of an external magnetic field*. *Volume 55*, 89–119. https://doi.org/https://doi.org/10.1016/bs.aiht.2023.02.001

BL Theraja. (1959). *A Textbook of Electrical Technology* (Volume I (). https://books.google.com.et/books?hl=en&lr=&id=KfWpQf5zFDEC&oi=fnd&pg=PP1&dq=textbook+of+electrical+technology+(+theraja)&ots=P178eEhZA4&sig=0LysEPl9vZmWIF-3Gc0wm2LcUOg&redir_esc=y#v=onepage&q&f=false

Blech, I. A. (1976). *Principles of Electronic Materials and Devices*. https://doi.org/10.1201/9781482292138-16

Brader, J. S. (2001). *Development of a Piezoelectric Controlled Hydraulic Actuator for a Camless Engine*. 94. http://www.me.sc.edu/Research/aarg/Thesis Final.pdf

BSB.Progeny. (2024). *Back EMF Suppression*. https://progeny.co.uk/back-emf-suppression/

BSB, P. L. (2024). *Back EMF Suppression*. https://progeny.co.uk/back-emf-suppression/

Chukwuneke, J. L., 1 Achebe, C. H. ., Okolie, P. C. ., & Anisiji, O. E. . (2013). Modelling of Electromechanical Control of Camless Internal Combustion Engine Valve Actuator. *International Journal of Science and Engineering Investigations*, *2*(15, April 2013). https://dokumen.tips/documents/modelling-of-electromechanical-control-of-camless-internal-modelling-of.html?page=1

Co, Industrial Hartford., L. (1999). *Service manual part Engine for CG-125/150*.

Darwin, C. (1895). This is a reproduction of a library book that was digitized by Google as part of an ongoing effort to preserve the information in books and make it universally accessible. https://books.google.com. *Oxford University*, *XXX*, 60.

Deokar, A. (2016). *Working of Piezoelectric Controlled Hydraulic actuator for Camless Engines - A Seminar Report on Working of Piezoelectric controlled Hydraulic actuator for Camless Engines By Under the guidance of : Mr . Vinayak Bhosale*. *January 2013*. https://doi.org/10.13140/RG.2.2.23139.96805

Deshmukh, G., Gawade, V., Godse, V., Londhe, N., & Gawari, D. (2018). Smart Navigational Shoes for Bikers/Cyclists. *International Journal of Computer Applications*, *180*(41), 6–10. https://doi.org/10.5120/ijca2018917062

Di Gaeta, A., Hoyos Velasco, C. I., & Giglio, V. (2021). Modelling of an electro-hydraulic variable valve actuator for camless engines aimed at controlling valve lift parameters. *International Journal of Control*, *94*(10), 2857–2873. https://doi.org/10.1080/00207179.2020.1737333

EETech Media, L. (2024). *Factors Affecting Inductance*. https://www.allaboutcircuits.com/textbook/direct-current/chpt-15/factors-affecting-inductance/

Electrical Engineering Stack Exchange. (2024). *With what force can a solenoid pull?* https://electronics.stackexchange.com/questions/472622/with-what-force-can-a-solenoid-pull

Elprocus. (2013). *Arduino UNO R3, Pin Diagram, Specification and Applications*. https://www.elprocus.com/what-is-arduino-uno-r3-pin-diagram-specification-and-applications/

Focus Technology Co., L. (2024). *Oil Tempered Wire 1800-2300MPa B60 Metal Spool/Coil Steel Wire for Brush*. https://geron-wire.en.made-in-china.com/product/mdKaYAJjVURz/China-plusmn-0-01mm-Oil-Tempered-Wire-1800-2300MPa-B60-Metal-Spool-Coil-Steel-Wire-for-Brush.html

Giglio, V., Iorio, B., Police, G., & Di Gaeta, A. (2001). Preliminary experiences in the design of an electromechanical valve actuator. *SAE Technical Papers*, *2001-Septe*(September). https://doi.org/10.4271/2001-24-0016

Gillella, P., & Sun, Z. (2009). Modeling and control design of a camless valve actuation system. *Proceedings of the American Control Conference*, 2696–2701. https://doi.org/10.1109/ACC.2009.5160296

Goss. (2018). *CAM & CRANK SENSORS*. https://www.goss.com.au/products/auxillary-sensors-switches-and-valves/cam-and-crank-sensors/

Gould, L. A., Richeson, W. E., & Erickson, F. L. (1991). *SA E TECHNICAL Performance Evaluation of a Camless Engine Using Valve Actuators with Programmable Timing*.

Gross, C. A. (2006). Electric Machines. In *Electric Machines*. https://doi.org/10.1201/9780429464997-4

Guelph, C. (2000). *Inductance of a Solenoid*. http://hyperphysics.phy-astr.gsu.edu/hbase/electric/indsol.html

Had2Know. (2010). *How to Calculate Wire for Solenoid Coils*. https://www.had2know.org/technology/solenoid-coil-wire-calculator.html

Hedges, G. L. (2013). Solenoid and electromagnet windings. *Proceedings of the American Institute of Electrical Engineers*, *34*(11), 2595–2614. https://doi.org/10.1109/paiee.1915.6590492

Hoffmann, W., Stefanopoulou, A. G., & Ag, S. (2001). Valve Position Tracking for Soft Landing of Electromechanical Camless Valvetrain. *IFAC Proceedings Volumes, 34*(1), 295–300. https://doi.org/10.1016/S1474-6670(17)34413-0

Howe, A. (2022). Electrical and Electronic Systems. In *Introduction to Mechanical Engineering: Part 1*. https://doi.org/10.1201/9780429319167-5

Ibex UK. (2024). *Supressing back EMF*. https://ibex.tech/resources/geek-area/electronics/back-emf/supressing-back-emf

Iii, S.-. (2020). *Magneto motive Force (MMF) - Definition of Magnetic Field Definition of Magnetic Flux Differences between Magnetic Field and Magnetic Flux*.

Ingenieria Y Mecanica Automotriz. (2019). *VALVE TIMING DIAGRAM OF TWO STROKE AND FOUR STROKE ENGINES: THEORETICAL AND ACTUAL*. https://www.ingenieriaymecanicaautomotriz.com/valve-timing-diagram-of-two-stroke-and-four-stroke-engines-theoretical-and-actual/

Izumida, H., Kontani, H., & Natsumeda, Y. (2023). *Fatigue Properties and Improvement Mechanisms of 1500 MPa-Class-High Strength Oil Tempered Wire*. *96*, 116–122.

Jalees Abro, M. A., Samo, S., Pathan, D. M., & Halepoto, I. A. (2019). Novel Design and Modeling of Shutter Valves for Camless Engines. *3C Tecnología_Glosas de Innovación Aplicadas a La Pyme*, *May*, 518–533.

https://doi.org/10.17993/3ctecno.2019.specialissue2.518-533

Jr, J. H. L., Iv, W. V. D., & Donaldson, J. (2016). *The Design And Simulation Of A High Force Low Power Actuation System For Camless Engines*. 1–9.

JU'S. (2024). *What is Resistor?* https://byjus.com/physics/resistor/

Kahan Acadamy. (2024). *What is magnetic flux?* https://www.khanacademy.org/science/physics/magnetic-forces-and-magnetic-fields/magnetic-flux-faradays-law/a/what-is-magnetic-flux

Kesav. (2013). *Mechanical Engineering: CAMLESS ENGINE - Blogger*. https://dasmechanical.blogspot.com/2013/02/v-behaviorurldefaultvmlo.html

Khayal, O. (2020). *Sensors in Autombiles Internal Combusion engines*. *July*.

Khurmi, R. S., & Gupta, J. K. (2005). A Textbook of Machine Design by R.S.KHURMI AND J.K.GUPTA. *Garden*, *I*, 1087–1088.

Kumar, S. (2020). *Work, Energy and Power*. SANJAY KUMAR. https://www.google.com.et/books/edition/Work_Energy_and_Power/phT9DwAAQBAJ?hl=en&gbpv=0

Kuphaldt, T. (2002). *Lesson in Electric Circuit volume I: Vol. volume I* (Fifth edit). https://www.ibiblio.org/kuphaldt/electricCircuits/DC/DC.pdf

Lanusse, P., Moreau, X., Tari, M., Lanusse, P., & Aioun, F. (2019). Development and Control of a Camless Engine Valvetrain. *IFAC-PapersOnLine*, *52*(5), 399–404. https://doi.org/10.1016/j.ifacol.2019.09.064

Leela Prasad. (2022). *What is Relay? How it Works? Types, Applications, Testing*. https://www.electronicshub.org/what-is-relay-and-how-it-works/

Magnetic Sensor, S. (1998). *Minimizing Unnecessary Energy Consumption*. https://www.magneticsensorsystems.com/solenoid/manual/minimizingenergy/minimizingenergy.asp

McGraw, C. (2018). *hydra force solenoid-training-manual*. https://www.hydraforce.com/globalassets/forms/solenoid-training-manual.pdf

Mesotek. (2024). *SS 304 Suppliers In India, 304 Stainless Steel Price Per Kg*. https://www.fastwell.in/304-stainless-steel-supplier-manufacturer.html

Michael, M. (2017). Опыт аудита обеспечения качества и безопасности медицинской деятельности в медицинской организации по разделу «Эпидемиологическая безопасность. In *Вестник Росздравнадзора* (Vol. 4, Issue 1).

Nam, K., Cho, K., Park, S., & Choi, S. B. (2017). *Design and Performance Evaluation of* *an Electro-Hydraulic Camless Engine Valve Actuator for Future Vehicle Applications*. https://doi.org/10.3390/s17122940

Norman. (2019). *Parts of a Solenoid Valve and their Functions*. https://startersolenoid.net/solenoid-valve-parts-and-their-functions/

Numayer. (2021). *Arduino UNO: A Short Review*. https://www.edugonist.com/arduino-uno/

Patel, T. (2015). *Select the Right Varistors for Overvoltage Circuit Protection*. https://www.electronicdesign.com/technologies/power/article/21800530/select-the-right-varistors-for-overvoltage-circuit-protection

Patil, P. A. M., Tarwade, P. K. K., Irfan, P., & Sayyad, K. (2023). *Redesign of Stationary I . C . Engine Valve using Optimization and FEM*. 324–332. https://doi.org/10.48175/IJARSCT-11554

Performance, T. I. (1986). *Cylinder Pressure*. https://www.performancetrends.com/Definitions/Cylinder-Pressure.htm

Peterson, K. S., & Stefanopoulou, A. G. (2004). Extremum seeking control for soft landing of an electromechanical valve actuator. *Automatica*, *40*(6), 1063–1069. https://doi.org/10.1016/j.automatica.2004.01.027

Point Team @ Tutorials. (2024). *Basic Electronics - Transistors*. https://www.tutorialspoint.com/basic_electronics/basic_electronics_transistors.htm

Prof. Ir. Dr. Alias Bin Mohd Noor. (2006). *A Technical Report On Design And Development Of Auxiliary Components For A New Two-Stroke , Gasoline Engine*. *November*.

Prof. Ir. Dr. Azhar Bin Abdul Aziz. (2006). *A TECHNICAL REPORT ON THE DESIGN AND DEVELOPMENT OF A NEW TWO- AIR-COOLED ENGINE BY PROF . Ir . Dr . AZHAR BIN ABDUL AZIZ AUTOMOTIVE DEVELOPMENT CENTRE (ADC) FACULTY OF MECHANICAL ENGINEERING JANUARY 2006*. *JANUARY*.

Rick Kertes. (2016). *Valve Timing Events And The Order Of Importance*. https://www.underhoodservice.com/valve-timing-events-and-the-order-of-importance/#:~:text=To calculate the duration of,timing event is 232°.

S.A.Annestrand. (2003). Power Transmission, High-Voltage. *Encyclopedia of Physical Science and Technology, Third edition,* 35–55. https://doi.org/https://doi.org/10.1016/B0-12-227410-5/00608-6

Schechter, M. M., & Levin, M. B. (1996). Camless engine. *SAE Technical Papers*.

https://doi.org/10.4271/960581

Scott, P. W. L. (2024). *The Resistance Of Wire Explained*. https://www.scottprecisionwire.com/the-resistance-of-wire-explained/

Shewale, A. P., Thosar, A. S., & Sawant, P. A. (2017). Review on Camless Engine Development. *International Jurnal of Creative Research Thoughts*, *5*(3), 1–6.

Shoemark, P., & Churchill, J. (1994). *Honda CG125 owners workshop manual*.

Shrushti B Walvekar. (2021). IRJET- Development of Internet of Things (IoT) based Data Acquisition System using Arduino Uno. *Irjet*, *8*(1), 834–844.

Soares Machado, C. A., Lincoln, C., Yamamura, K., Patrick, N., De Salles Hue, M., Berssaneti, F. T., & Quintanilha, A. (2019). Innovative Vehicular Technologies for Urban Mobility: A Smart City Perspective. *International Journal of Science and Engineering Investigations*, *8*(October), 93. www.IJSEI.com

Stock, R. (2024). *Bourns, MOV-14D Metal Oxide Varistor 460pF 50A, Clamping 710V, Varistor 430V*. https://my.rs-online.com/web/p/varistors/1739269

Suresh, R., Narayan, K. L., & Poornima, C. L. (2014). *Design and Analysis of Cylinder Fins*. *3*(1), 2568–2575.

V. Utkin, J. Guldner, J. S. (2009). *Sliding Modes in Electromechanical Systems*.

Velasco, C. I. H. (2011). *Modelling, Analysis, Control andExperimental Validation ofElectromechanical Valve Actuators inAutomotive Systems*. 148. https://docplayer.net/62103843-Modelling-analysis-control-and-experimental-validation-of-electromechanical-valve-actuators-in-automotive-systems.html

Venkatesh, D., & Selvakumar, A. (2016). *A Novel Design of Pneumatic Actuator for Camless Engines*. https://doi.org/10.4271/2016-01-0099.Copyright

Wikimedia Foundation, I. (2023). *Crankshaft position sensor*. https://en.wikipedia.org/wiki/Crankshaft_position_sensor

Wikimedia Foundation, I. (2024). *American wire gauge of wire of solenoid*. https://en.wikipedia.org/wiki/American_wire_gauge#

Zibani, I., Marumo, R., Chuma, J., Ngebani, I., & Tsamaase, K. (2020). Variable Valve Timing for a Camless Stepping Valve Engine. *Procedia Manufacturing*, *43*, 590–597. https://doi.org/10.1016/j.promfg.2020.02.154

APPENDIX

Appendix-A: Data Source Tables

Table A-1: Temperature coefficient (α) per degree C:

Material	Element/Alloy	Temp. coefficient
Nickel	Element	0.005866
Iron	Element	0.005671
Molybdenum	Element	0.004579
Tungsten	Element	0.004403
Aluminum	Element	0.004308
Copper	Element	0.004041
Silver	Element	0.003819
Platinum	Element	0.003729
Gold	Element	0.003715
Zinc	Element	0.003847
Steel*	Alloy	0.003
Nichrome	Alloy	0.00017
Nichrome V	Alloy	0.00013
Manganin	Alloy	0.000015
Constantan	Alloy	±0.000074
* = Steel alloy at 99.5% iron, 0.5% carbon		

Table A-2: Standard wire gauge (SWG) number and corresponding diameter of spring wire (Khurmi & Gupta, 2005).

SWG	*Diameter (mm)*	*SWG*	*Diameter (mm)*	*SWG*	*Diameter (mm)*	*SWG*	*Diameter (mm)*
7/0	12.70	7	4.470	20	0.914	33	0.2540
6/0	11.785	8	4.064	21	0.813	34	0.2337
5/0	10.973	9	3.658	22	0.711	35	0.2134
4/0	10.160	10	3.251	23	0.610	36	0.1930
3/0	9.490	11	2.946	24	0.559	37	0.1727
2/0	8.839	12	2.642	25	0.508	38	0.1524
0	8.229	13	2.337	26	0.457	39	0.1321
1	7.620	14	2.032	27	0.4166	40	0.1219
2	7.010	15	1.829	28	0.3759	41	0.1118
3	6.401	16	1.626	29	0.3454	42	0.1016
4	5.893	17	1.422	30	0.3150	43	0.0914
5	5.385	18	1.219	31	0.2946	44	0.0813
6	4.877	19	1.016	32	0.2743	45	0.0711

Table **A**-3: Tables of AWG wire sizes for solenoid coil (Darwin, 1895)

A.W. G.	DIAMETER	AREA	WEIGHT		LENGTH		RESISTANCE	
B. & S.	Mm.	Sq. Mm.	Kg. per M.	Kg. per Ohm	M. per Kg.	M. per Ohm	Ohms per Kg.	Ohms per M.
0000	11.7	107.2	.953	5940	1.05	62,300	.000168	.0000161
000	10.4	85.0	.756	3730	1.32	49,400	.000268	.0000202
00	9.27	67.4	.599	2350	1.67	30,200	.000426	.0000255
0	8.25	53.5	.475	1480	2.10	31,100	.000677	.0000322
1	7.35	42.4	.377	929	2.65	24,600	.00108	.0000406
2	6.54	33.6	.299	584	3.35	19,500	.00171	.0000512
3	5.83	26.7	.237	367	4.22	15,500	.00272	.0000645
4	5.19	21.2	.188	231	5.32	12,300	.00433	.0000814
5	4.62	16.8	.149	145	6.71	9,750	.00688	.000103
6	4.11	13.3	.118	91.4	8.46	7,730	.0109	.000129
7	3.67	10.6	.0938	57.5	10.7	6,130	.0174	.000163
8	3.26	8.37	.0744	36.2	13.5	4,860	.0277	.000206
9	2.91	6.63	.0590	22.7	17.0	3,860	.0440	.000259
10	2.59	5.26	.0468	14.3	21.4	3,060	.0699	.000327
11	2.31	4.17	.0371	8.99	27.0	2,420	.111	.000413
12	2.05	3.31	.0294	5.66	34.0	1,920	.177	.000520
13	1.83	2.62	.0234	3.56	42.9	1,530	.281	.000656
14	1.63	2.08	.0185	2.24	54.1	1,210	.447	.000827
15	1.45	1.65	.0147	1.41	68.2	959	.711	.00104
16	1.29	1.31	.0116	.885	86.0	760	1.13	.00132
17	1.15	1.04	.00922	.556	108	603	1.80	.00166
18	1.02	.823	.00732	.350	136	478	2.86	.00209
19	.912	.653	.00580	.220	172	379	4.54	.00264
20	.812	.518	.00460	.138	217	301	7.23	.00333
21	.723	.410	.00365	.0871	274	239	11.5	.00419
22	.644	.326	.00289	.0548	346	189	18.3	.00529
23	.573	.258	.00229	.0344	436	150	29.1	.00667
24	.511	.205	.00182	.0217	550	119	46.2	.00841
25	.455	.162	.00144	.0136	693	94.3	73.4	.0106
26	.405	.129	.00114	.00856	874	74.8	117	.0134
27	.361	.102	.000908	.00538	1,100	59.3	186	.0169
28	.321	.081	.000720	.00339	1,390	47.0	295	.0213
29	.286	.0642	.000571	.00213	1,750	37.3	470	.0268
30	.255	.0510	.000453	.00134	2,210	29.6	747	.0338
31	.227	.0404	.000359	.000842	2,790	23.5	1,190	.0426
32	.202	.0320	.000285	.000530	3,510	18.6	1,890	.0537
33	.180	.0254	.000226	.000333	4,430	14.8	3,000	.0678
34	.160	.0201	.000179	.000210	5,590	11.7	4,770	.0855
35	.143	.0160	.000142	.000132	7,040	9.28	7,590	.108
36	.127	.0127	.000113	.0000829	8,880	7.36	12,100	.136
37	.113	.0101	.0000893	.0000521	11,200	5.84	19,200	.171
38	.101	.00797	.0000708	.0000327	14,100	4.63	30,600	.216
39	.0897	.00632	.0000562	.0000206	17,800	3.67	48,500	.273
40	.0799	.00501	.0000445	.0000130	22,500	2.91	77,100	.344

Appendix B: Design of the Program Using Arduino IDE 2.3.2

```
const byte SENSORpin = 3;
const byte IVOpin = 11;
const byte IVCpin = 10;
const byte EVOpin = 9;
const byte EVCpin = 8;
byte engine_cylinders = 1;
byte engine_cycles = 4;
byte No_Teeth = 72;
int refresh_interval = 750;
unsigned long privious_millis = 0;
volatile int RPMpulse = 0;
volatile int count=0;
int current_position;
int IVOBTDC=10;
int IVCABDC=20;
int EVOBBDC=25;
int EVCATDC=5;
static volatile unsigned long shortpulse = 0;
static volatile unsigned long lastpulse = 0;
boolean INTAKE_STROCK = false;

void setup() {
// put your setup code here, to run once:
pinMode(SENSORpin, INPUT_PULLUP);
pinMode(IVOpin, OUTPUT);
pinMode(IVCpin, OUTPUT);
pinMode(EVOpin, OUTPUT);
pinMode(EVCpin, OUTPUT);
attachInterrupt(1, countRPM, FALLING);
Serial.begin(9600);
}

void loop() {
 // put your main code here, to run repeatedly:
 getRPM();
 getPOSITION();
 openINTAKEVALVE();
 openEXHOSTVALVE();
}

void countRPM() {
unsigned long now = micros();
 unsigned long nowpulse = now - lastpulse;
 lastpulse = now;
 if ((nowpulse >> 1) > shortpulse) {
 RPMpulse ++;
```

```
 shortpulse = nowpulse;
 count = 1;
 INTAKE_STROCK = !INTAKE_STROCK;
 }
 else {
 shortpulse = nowpulse;
 count ++;
 Serial.println(current_position);
 }
}

int getRPM() {
 if (millis() - privious_millis >= refresh_interval) {
 privious_millis = millis();
 int RPM =int(RPMpulse* (60000.0/float(refresh_interval))* engine_cycles /
engine_cylinders /1.0);
 RPMpulse = 0;
 RPM = min(9999, RPM);
 Serial.print("RPM= ");
 Serial.println(RPM);
 return RPM;
 IVCABDC=int( RPM*20/2200);
 EVOBBDC=int( RPM*25/3100);
 EVCATDC=int( RPM*5/1375);
 }
}

int getPOSITION(){
 if (INTAKE_STROCK){
 current_position=map(count,0,No_Teeth,0,360);
 }
 else{
 current_position=map(count,0,No_Teeth,-360,0);
 }
}

void openINTAKEVALVE(){
 if (current_position > -IVOBTDC && current_position <
(180+IVCABDC)){
 digitalWrite(IVOpin,HIGH);
 digitalWrite(IVCpin,LOW);
 }
 else{
digitalWrite(IVOpin,LOW);
 digitalWrite(IVCpin,HIGH);
 }
}
```

```
void openEXHOSTVALVE(){
 if (current_position > -(180-EVOBBDC) && current_position <
EVCATDC){
 digitalWrite(EVOpin,HIGH);
 digitalWrite(EVCpin,LOW);
 }
else{
 digitalWrite(EVOpin,LOW);
 digitalWrite(EVCpin,HIGH);
 }
}
```

Appendix-C: Part drawing

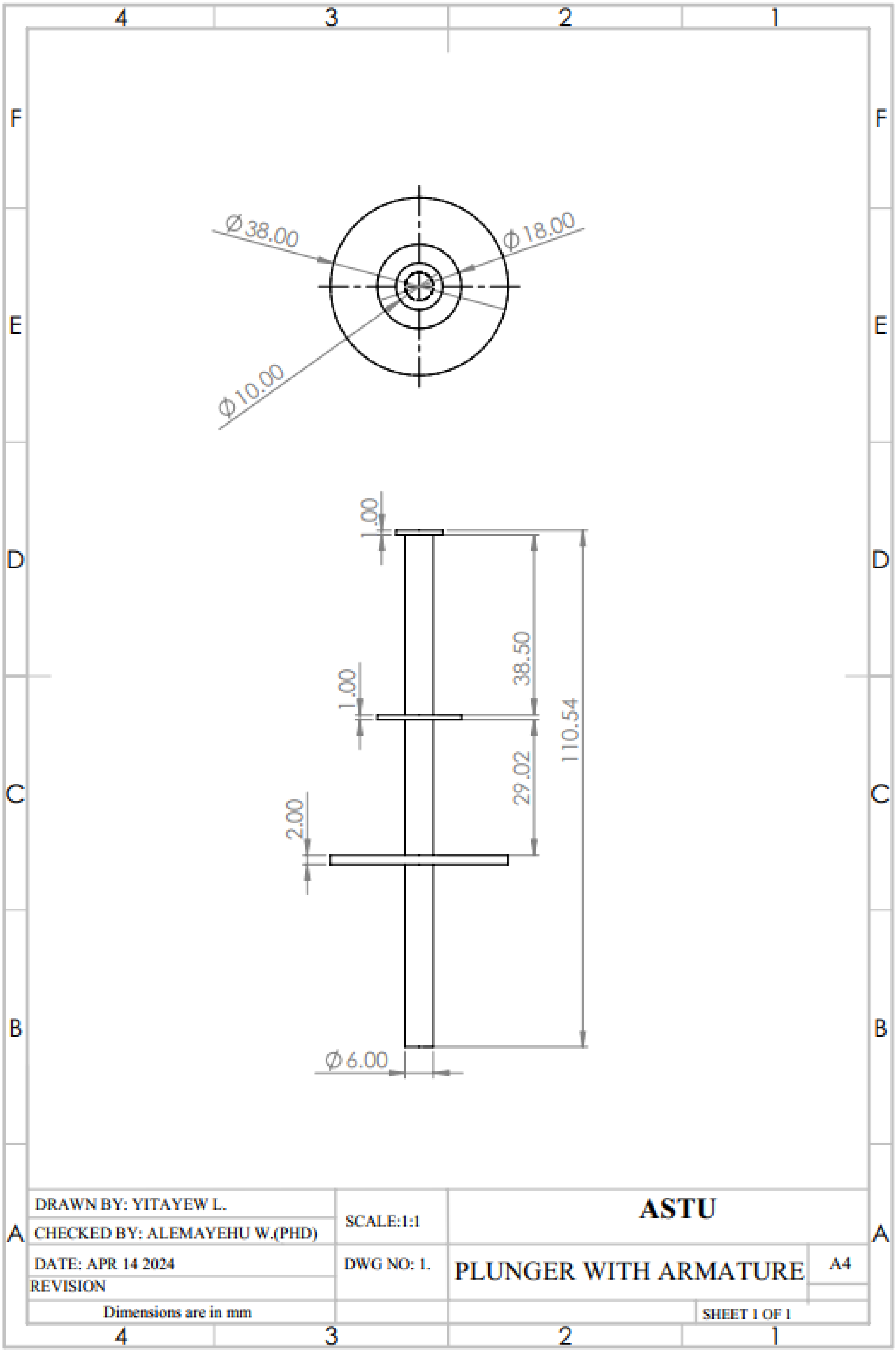

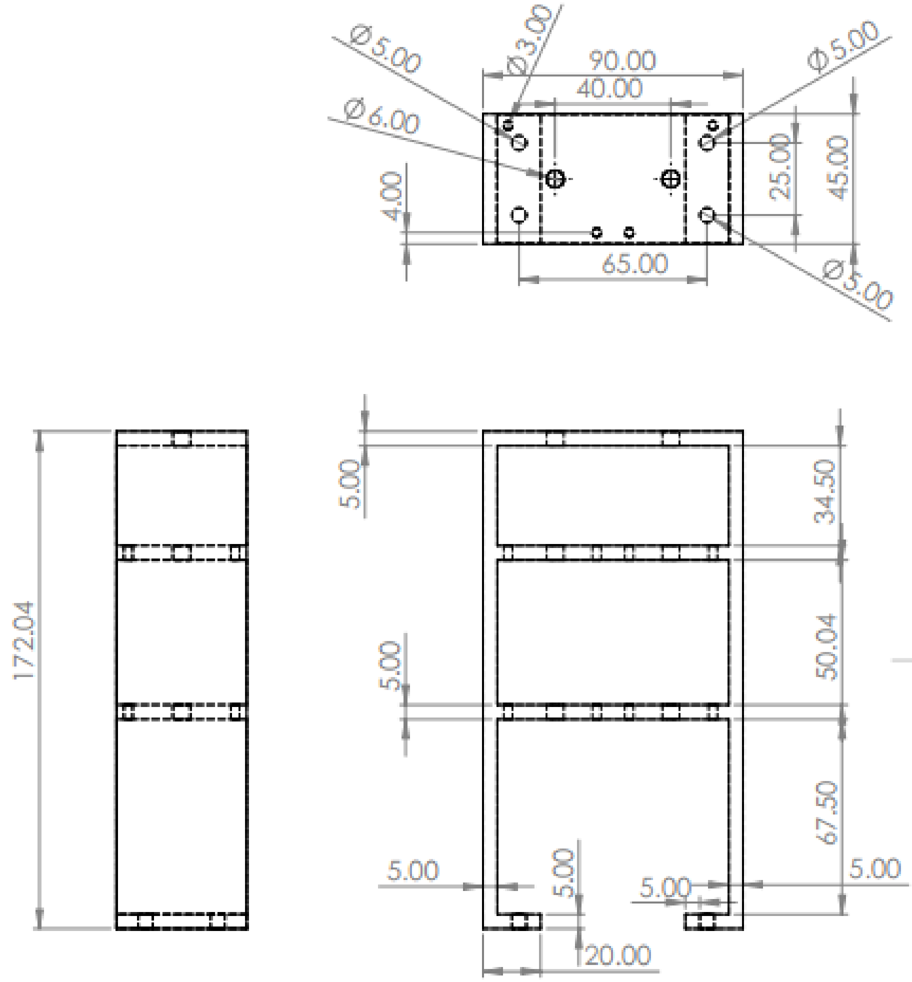

DRAWN BY: YITAYEW L.

CHECKED BY: ALEMAYEHU W.(PHD

DATE APR 14 2024

REVISION

Dimensions are in mm

SCALE:1:2

DWG NO:2

ASTU

SOLENOID STAND

A4

SHEET 1 OF 1

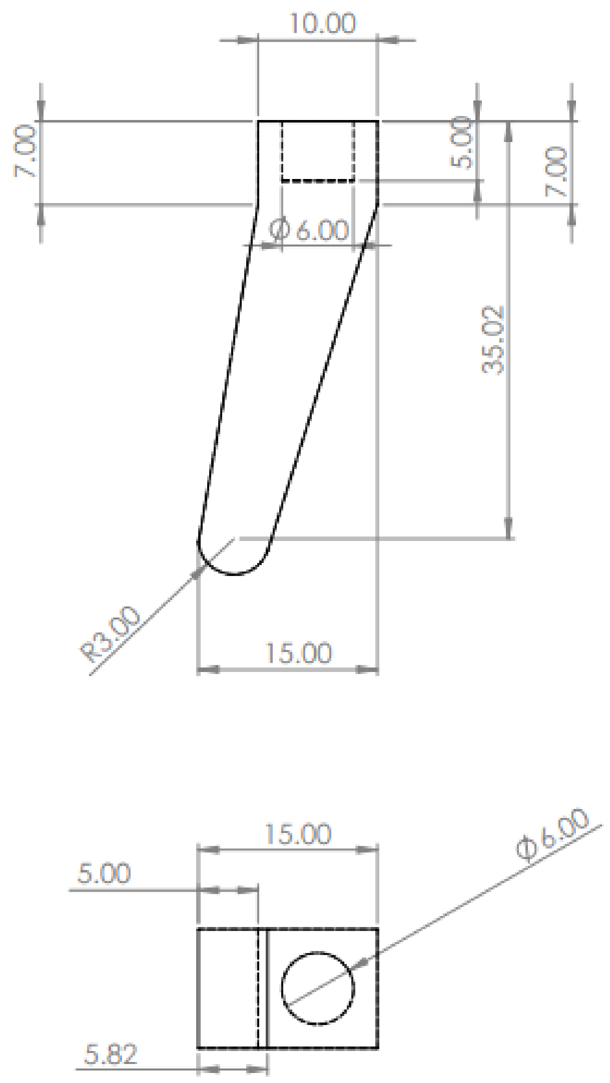

DRAWN BY: YITAYEW L.	SCALE:2:1	ASTU
CHECKED BY: ALEMAYEHU W.(PHD)		
DATE: APR 14 2024	DWG NO: 3.	COUPLING MEMBER — A4
REVISION		
Dimensions are in mm		SHEET 1 OF 1

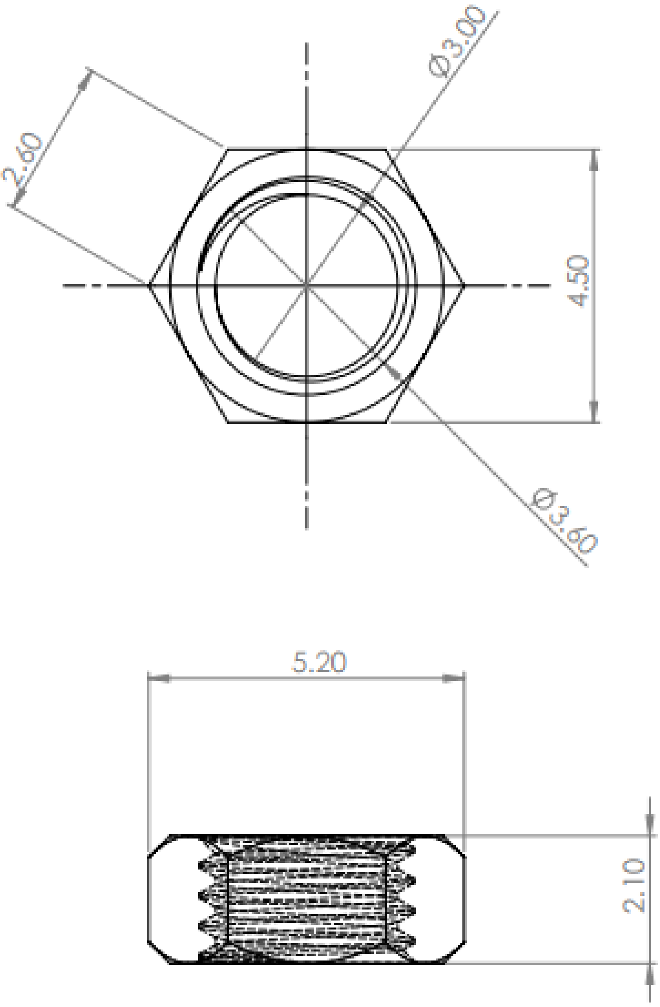

DRAWN BY: YITAYEW L. CHECKED BY: ALEMAYEHU W.(PHD)	SCALE:10:1	ASTU	
DATE APR 14 2024			
REVISION	DWG NO.4	NUT	A4
Dimensions are in mm		SHEET 1 OF 1	

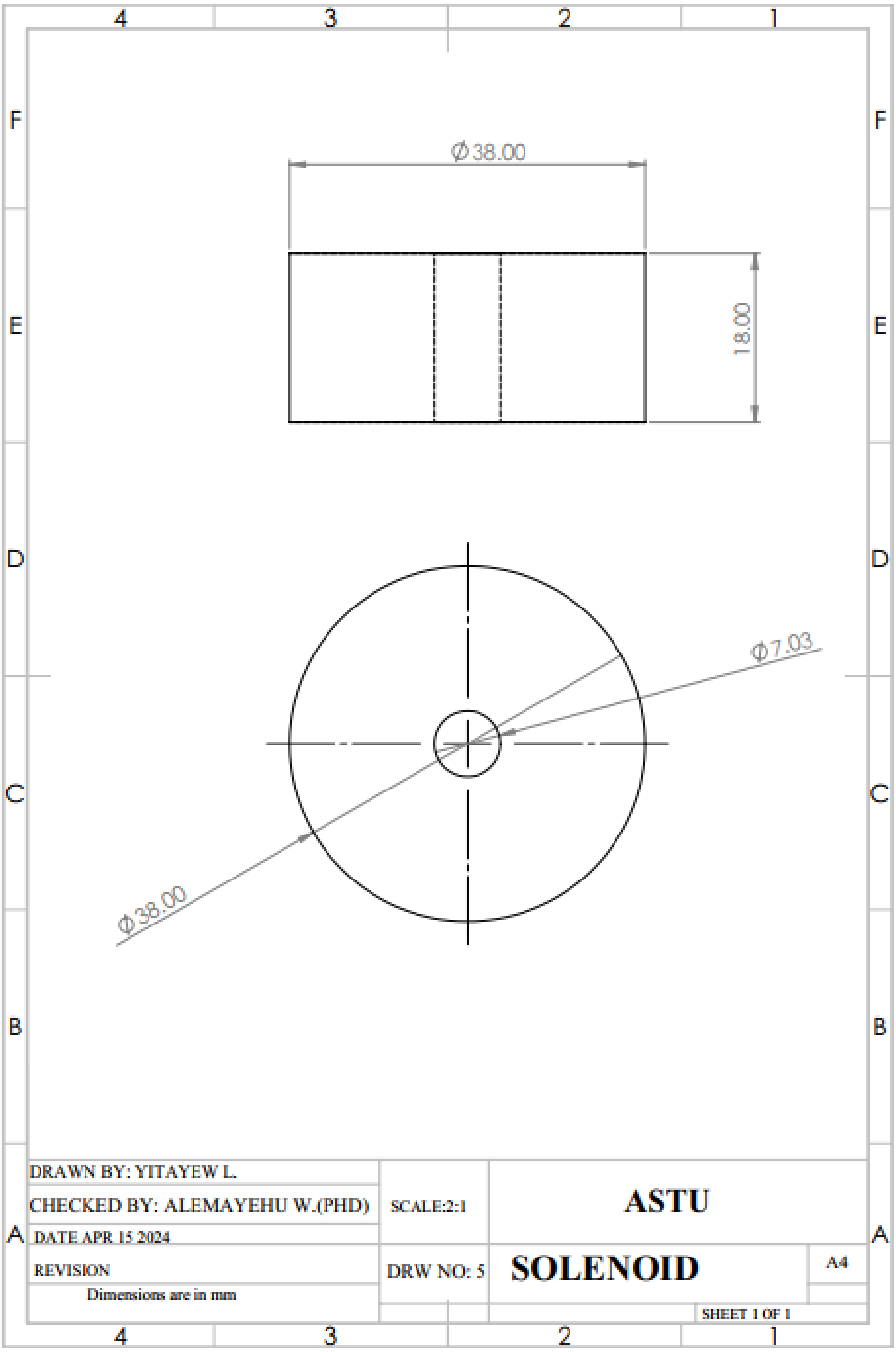
Ø38.00
18.00
Ø7.03
Ø38.00
DRAWN BY: YITAYEW L.
CHECKED BY: ALEMAYEHU W.(PHD)
DATE APR 15 2024
REVISION
Dimensions are in mm
SCALE:2:1
DRW NO: 5
ASTU
SOLENOID
A4
SHEET 1 OF 1

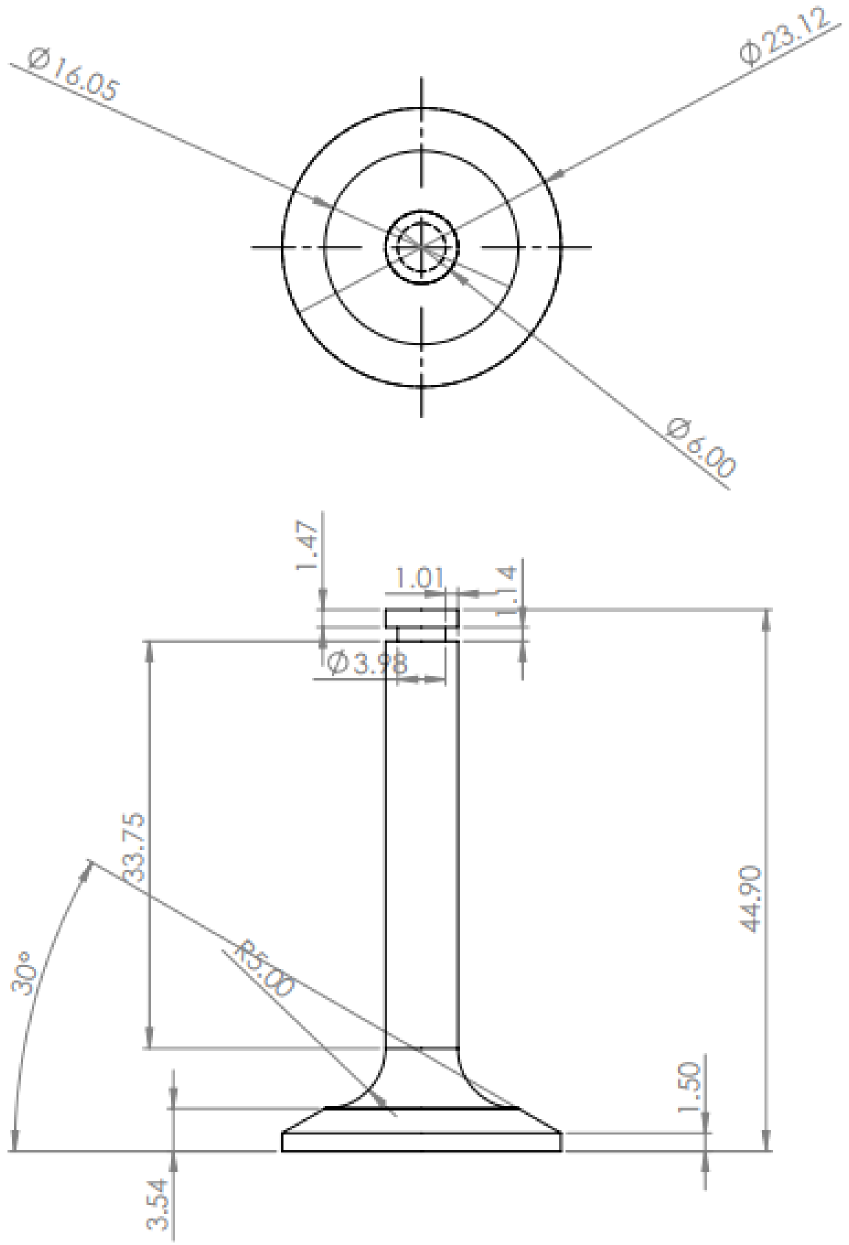

DRAWN BY: YITAYEW L.	SCALE:2:1	ASTU	
CHECKED BY: ALEMAYEHU W.(PHD)			
DATE: APR 16 2024	DWG NO. 6	INTAKE VALVE	A4
REVISION			
Dimensions are in mm		SHEET 1 OF 1	

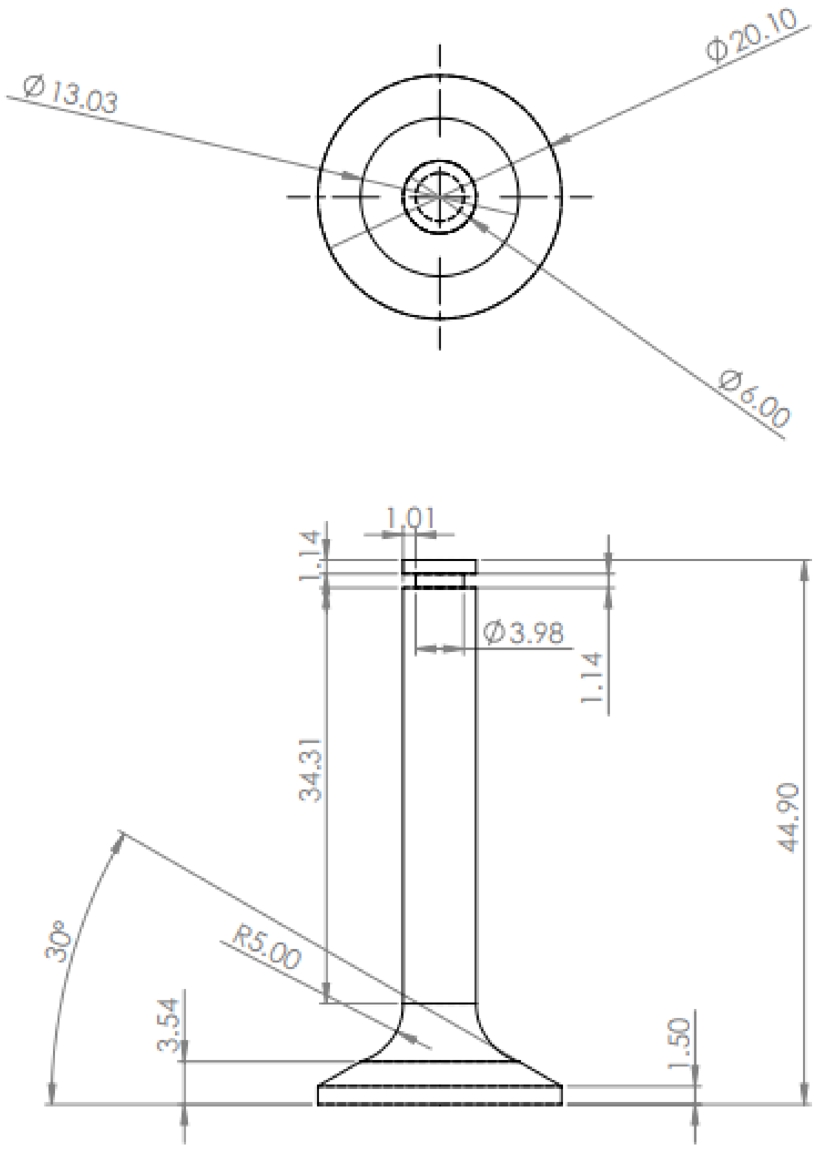

DRAWN BY: YITAYEW L.	SCALE:2:1	ASTU	
CHECKED BY: ALEMAYEHU W.(PHD)			
DATE: APR 15 2024	DWG NO.7	EXHAUST VALVE	A4
REVISION			
Dimensions are in mm		SHEET 1 OF 1	

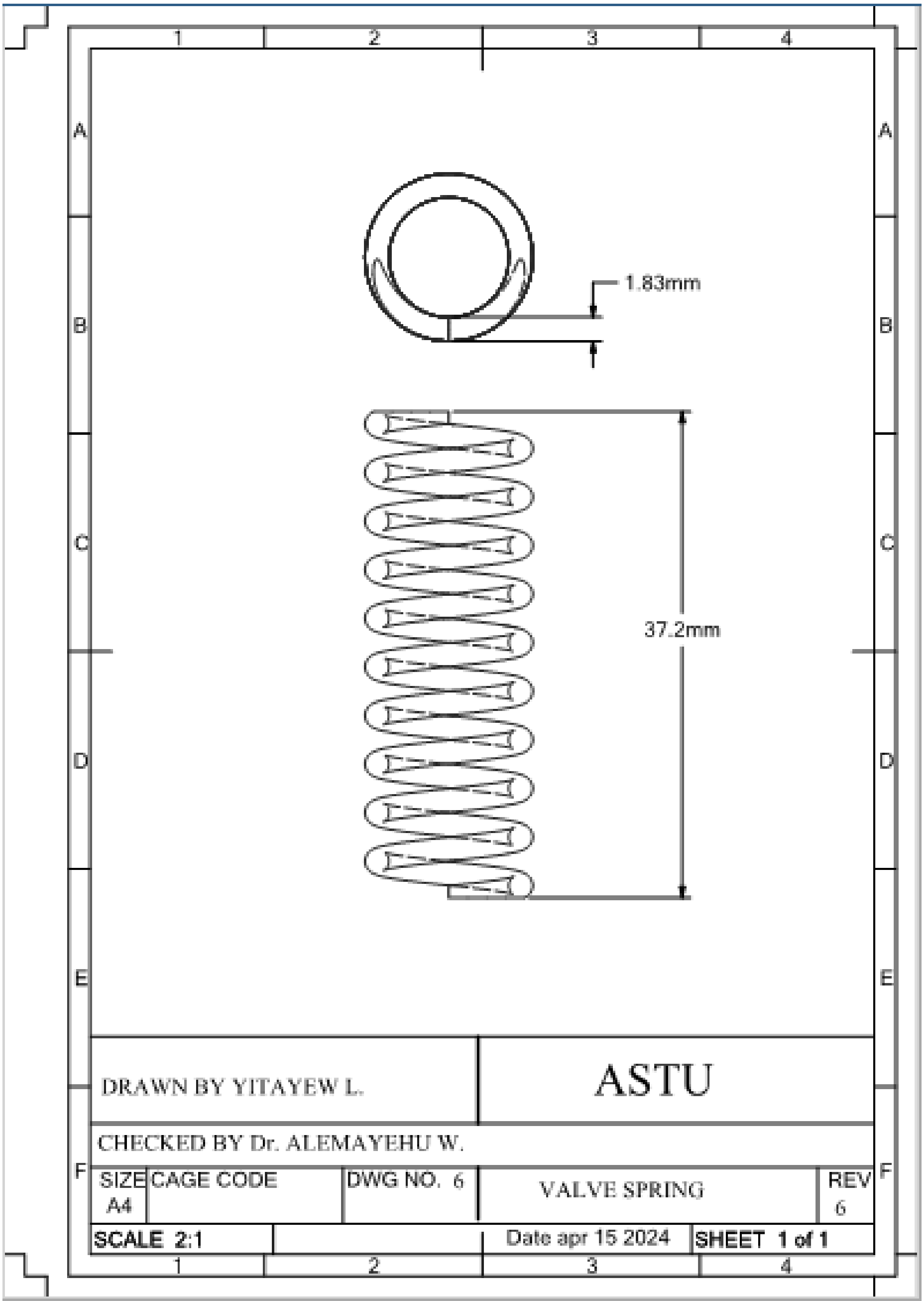
1.83mm
37.2mm
DRAWN BY YITAYEW L.
ASTU
CHECKED BY Dr. ALEMAYEHU W.
SIZE A4
CAGE CODE
DWG NO. 6
VALVE SPRING
REV 6
SCALE 2:1
Date apr 15 2024
SHEET 1 of 1

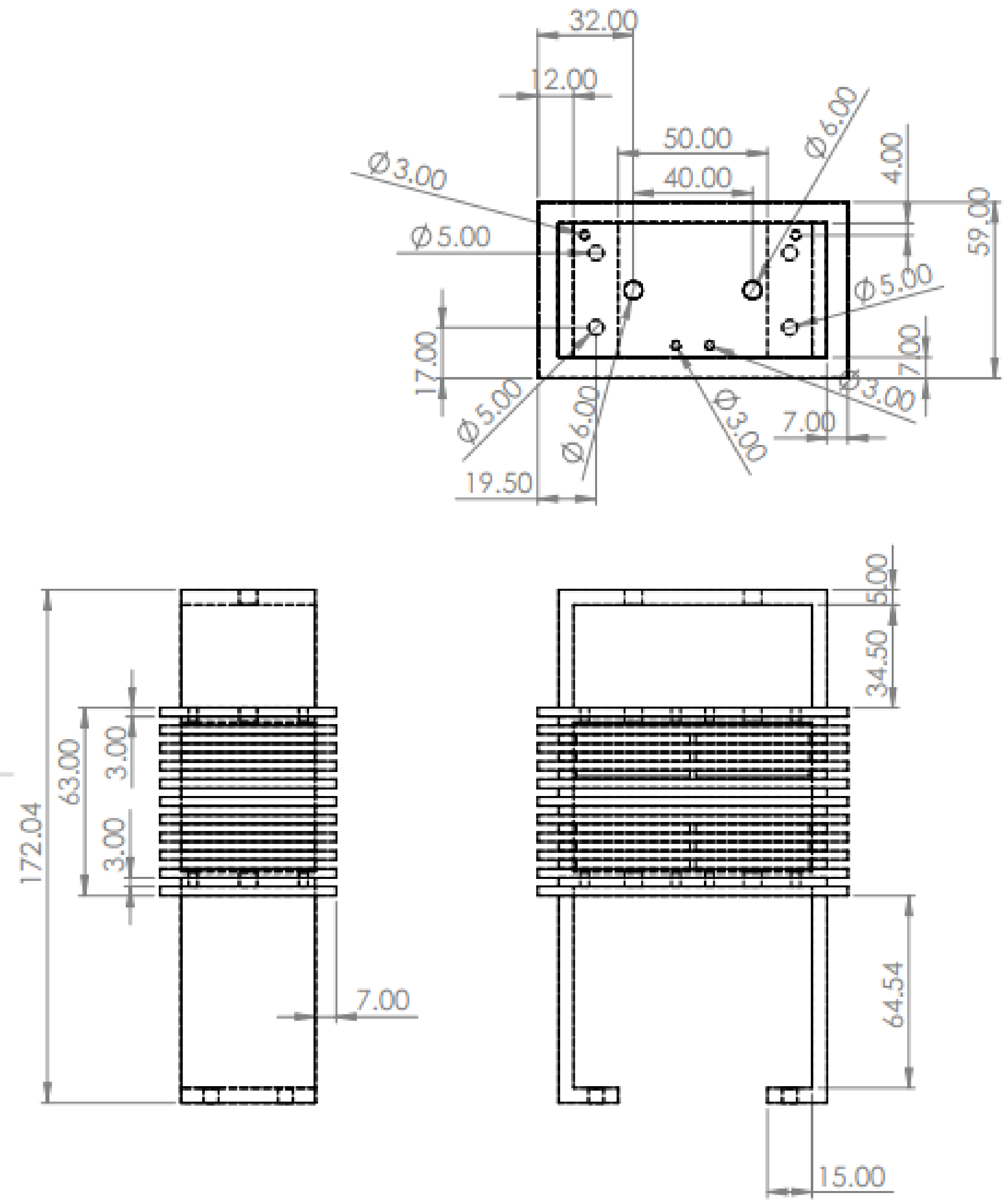

DRAWN BY: YITAYEW L.	**SCALE:1:2**	**ASTU**	
CHECKED BY: ALEMAYEHU W.(PHD)			
DATE: APR 16 2024	DWG NO.9	SOLENOID STAND WITH FINS	**A4**
REVISION			
Dimensions are in mm			SHEET 1 OF 1

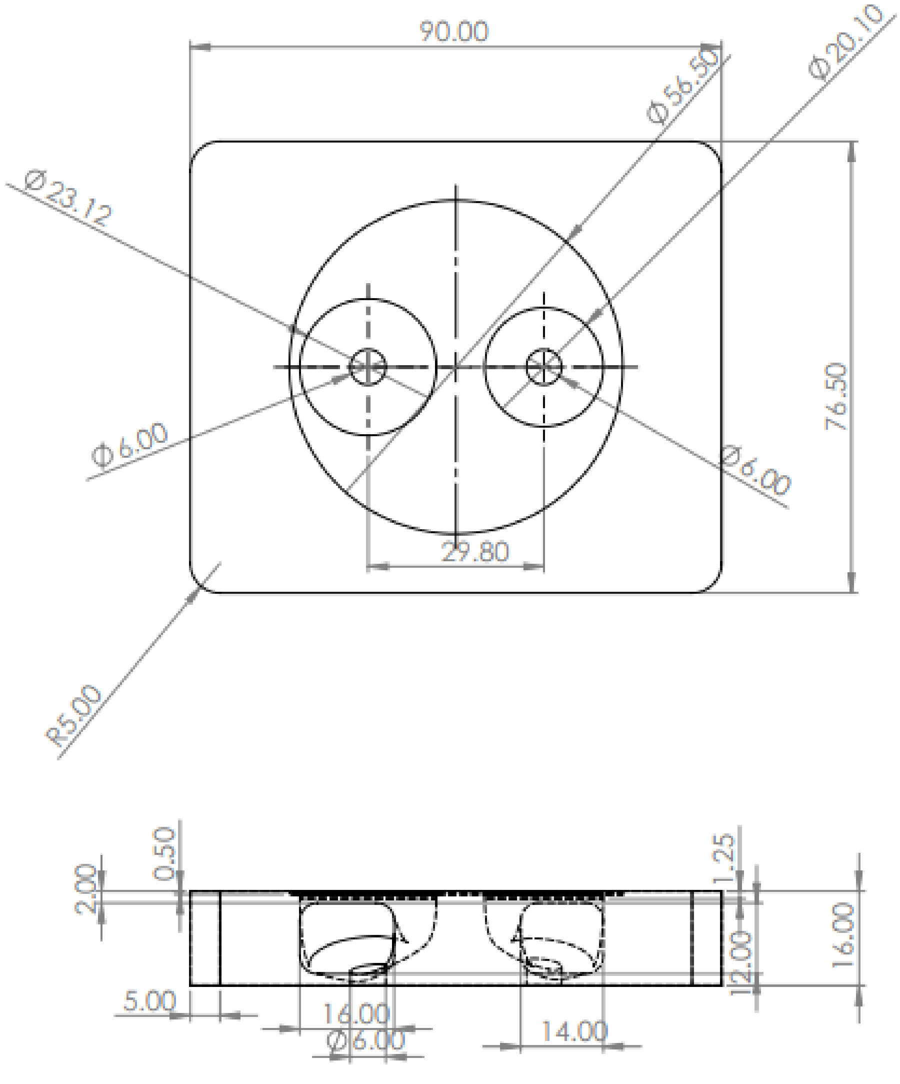

DRAWN BY: YITAYEW L.	SCALE:1:1	ASTU	
CHECKED BY: ALEMAYEHU W.(PHD)			
DATE: APR 17 2024 REVISION	DWG NO.10	CYLINDER HEAD	A4
Dimensions are in mm		SHEET 1 OF 1	

Appendix-D: Assembly Drawing